

INTRAVASCULAR PHOTOACOUSTICS

Krista Jansen

2013

This work was funded by the Dutch Technology Foundation (STW) through the 2007 Simon Stevin Meester grant (STW 10040) to A.F.W. van der Steen. Financial support for the printing of this thesis was provided by the Dutch Heart Foundation. We kindly acknowledge funding from ACIST Medical Systems and Cardialysis BV.

We thank Geert Springeling (Department of Experimental Medical Instrumentation, Erasmus MC) for catheter assembly and setup design, Gerrit van Dijk and Koen W.A. van Dongen (Laboratory of Acoustical Wavefield Imaging, Delft University of Technology) for assistance in catheter fabrication and Xiang Li and Teng Ma (Department of Biomedical Engineering, University of Southern California) for providing ultrasound transducers. We thank Ariadne Ooms, Fiebo ten Kate, Britt Blokker, Duc Nguyen, Eva Krpelanova, Nelleke van der Graaf, Sarah Roshani, José Gaal and Germaine Liebrechts-Akkerman (Department of Pathology, Erasmus MC) for collection of human coronary arteries and Rorry van Haeren (Unit Experimental Cardiology, Erasmus MC) and Kim Kuijt-van Gaalen (Department of Biomedical Engineering, Thorax Center, Erasmus MC) for assistance in histopathology. We also thank Charles Lancée, Robert Beurskens, Frits Mastik and Jan Honkoop for their technical support and David Maresca, Pieter Kruizinga and Marcia Emmer (Department of Biomedical Engineering, Erasmus MC) for helpful discussion on the experimental design and results.

Layout by Arwen Ronner.

Printed by NetzoDruk Groningen BV.

ISBN 978-94-91715-02-0 (print edition)

ISBN 978-94-91715-03-7 (ebook)

Intravascular Photoacoustics

Intravasculaire fotoakoestiek

Proefschrift

ter verkrijging van
de graad van doctor aan de Erasmus Universiteit
Rotterdam op gezag van de
rector magnificus

Prof.dr. H.A.P. Pols

en volgens besluit van het College voor Promoties.

De openbare verdediging zal plaatsvinden op
woensdag 18 december 2013 om 13:30 uur door

Krista Jansen

geboren te Sint-Oedenrode



Promotiecommissie

Promotor: Prof.dr.ir. A.F.W. van der Steen

Overige Leden: Dr. E.S. Regar
Prof.dr. A. van der Lugt
Prof.dr. P. Beard

Copromotor: Dr. G. van Soest

Table of Contents

Introduction	7
Intravascular photoacoustic imaging: a new tool for vulnerable plaque identification	19
Development of an integrated photoacoustic and ultrasonic catheter	29
Intravascular photoacoustic imaging of human coronary atherosclerosis	43
Spectroscopic imaging of lipids in an atherosclerotic plaque	51
Using spectral contrast for lipid detection in coronary atherosclerosis	69
Photoacoustic imaging of human coronary atherosclerosis in two spectral bands	87
Overview and perspectives	103
References	111
Summary	121
Samenvatting	124
Acknowledgements	127
Curriculum Vitae	132
Publications	133
PhD Portfolio	138

Chapter 1

Introduction

Coronary atherosclerosis and the vulnerable plaque

Of the 57 million global deaths in 2008, 17.3 million (30%) were due to cardiovascular disease, of which heart attacks were responsible for 7.3 million deaths¹. This high mortality poses a great burden to society, both in terms of mortality and morbidity. The rupture of vulnerable atherosclerotic plaques is a major contributor to acute cardiovascular events and sudden cardiac deaths². The vulnerability of an atherosclerotic plaque – its susceptibility to rupture – is known to be related to the composition of the plaque, the distribution of mechanical stress within it, and the presence and extent of associated inflammation³⁻⁵. One of the most common types of vulnerable plaques is the thin-cap fibroatheroma (TCFA). These lesions are characterized by a thin fibrous cap, weakened by the presence of macrophages, covering a lipid-rich necrotic core³. These and other known markers of plaque vulnerability are depicted in the schematic in Figure 1a. Figure 1b shows the gross morphology of a ruptured TCFA.

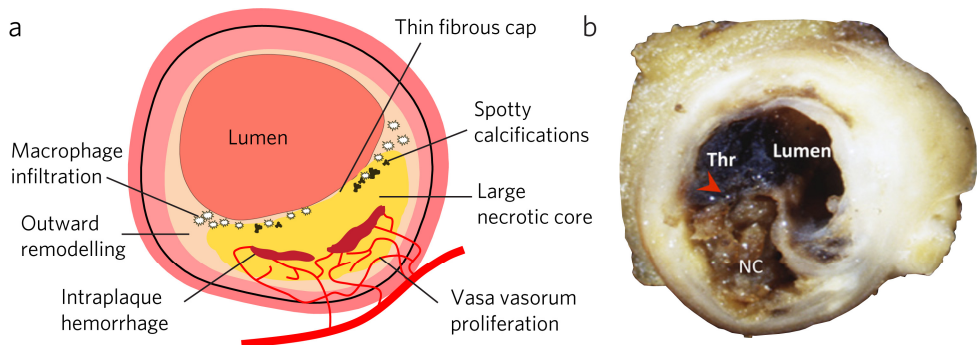


Figure 1. The vulnerable plaque. a) Typical morphological traits associated with plaque vulnerability. b) Gross morphology of human coronary artery. Ruptured vulnerable plaque, showing disruption of fibrous cap at the shoulder region of the plaque (red arrowhead) and thrombus (Thr) superimposed. NC = necrotic core⁶.

Most of our knowledge about vulnerable coronary plaques originates from histological studies of ex vivo material, which consist of sectioning and staining of cells and tissues, after which they are examined under a light microscope. Histology is often used as the gold standard to evaluate the performance of new imaging modalities, particularly for those techniques that aim to image tissue composition. The histology sections of a coronary TCFA, shown in Figure 2, reveal several important hallmarks of the vulnerable plaque. The low power (20x) view of the Movat pentachrome overview stain (Figure 2a) shows an eccentric plaque with a relatively large necrotic core covered by a thin cap.

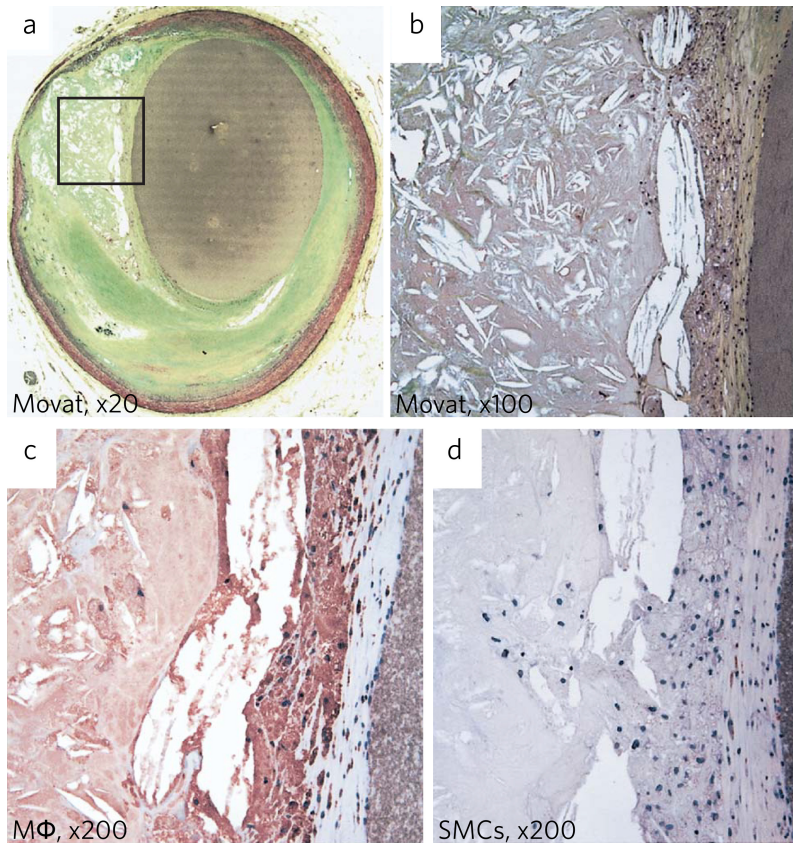


Figure 2. Thin-cap fibroatheroma (TCFA). a) Coronary artery cross-section with an eccentric plaque showing a thin fibrous cap overlying a relatively large necrotic core; greyish material in lumen is barium gelatin (Movat Pentachrome). b) Magnification (5x) of the boxed area in a shows an advanced necrotic containing numerous cholesterol clefts and cellular debris covered by a thin, cellular-rich fibrous cap. c) Immunohistochemical staining reveals numerous CD68-positive macrophages ($M\Phi$) within the fibrous cap (rose-red reaction product). d) Few alpha-actin positive smooth muscle cells (SMCs) are found within the fibrous cap. Adapted from⁷.

Rupture of the thin fibrous cap due to high mechanical stress will release the lipid-rich thrombogenic contents of the necrotic core into the bloodstream. The subsequent formation of a platelet-rich thrombus may result in occlusion, either at the location of the rupture or downstream from the lesion site. If this occlusion takes place in one of the coronary arteries, the vessels that deliver oxygen-rich blood to the myocardium, the result may be unstable angina or a myocardial infarction. The location, size and anatomy of the coronary arteries pose specific challenges for imaging and treatment. They are small, lie relatively deep in the body and curl around the heart, which limits their

accessibility. The motion of the beating heart presents an additional difficulty. The main branches of the coronary arteries are shown in Figure 3.

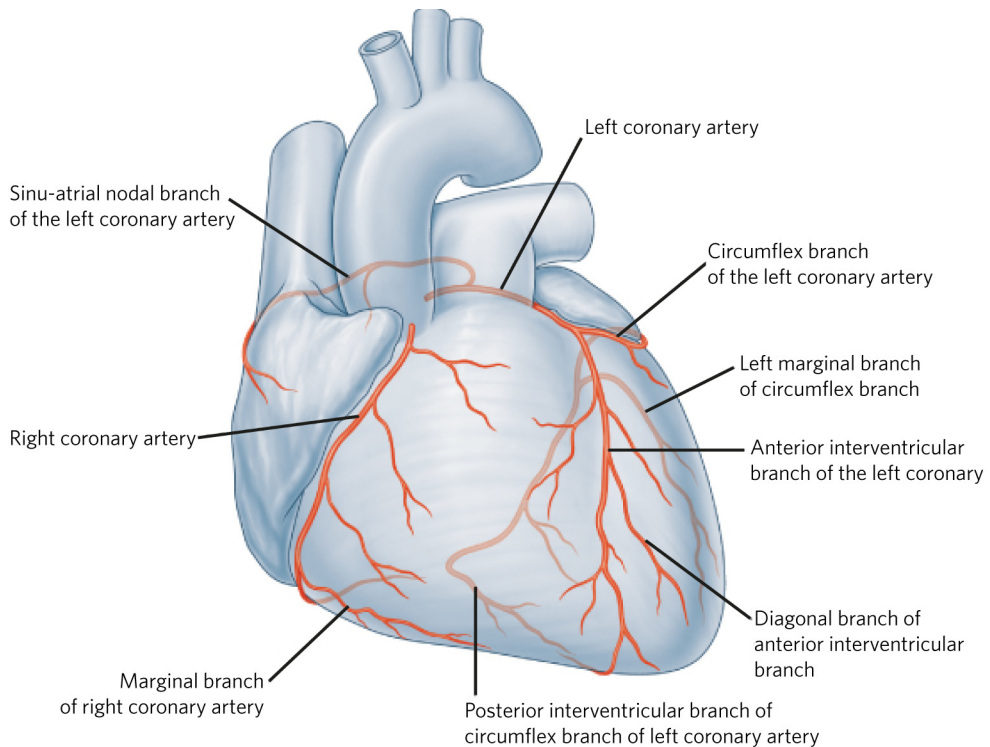


Figure 3. Anatomy of the main coronary arteries. The left and right coronary arteries both originate from the root of the aorta. The left coronary artery (LCA) branches off into the left circumflex coronary artery (LCX) that supplies oxygen and nutrients to the left ventricle, and the left ascending coronary artery (LAD) that supplies two thirds of the anterior heart surface. The right coronary artery (RCA) supplies the right ventricle muscle⁸.

Treatment of symptomatic myocardial disease

A person experiencing myocardial ischemia or a myocardial infarction is often treated with a percutaneous coronary intervention (PCI, see Figure 4). During this non-surgical procedure, an intervention cardiologist feeds a catheter from the femoral or radial artery up through the aorta up to the site of occlusion in the coronary artery. At the occlusion site, the artery is opened up by balloon inflation. A stent is placed to permanently keep

the artery open. Recently, bioabsorbable drug-eluting coronary stents (scaffolds) were developed to prevent restenosis through late stent thrombosis⁹.

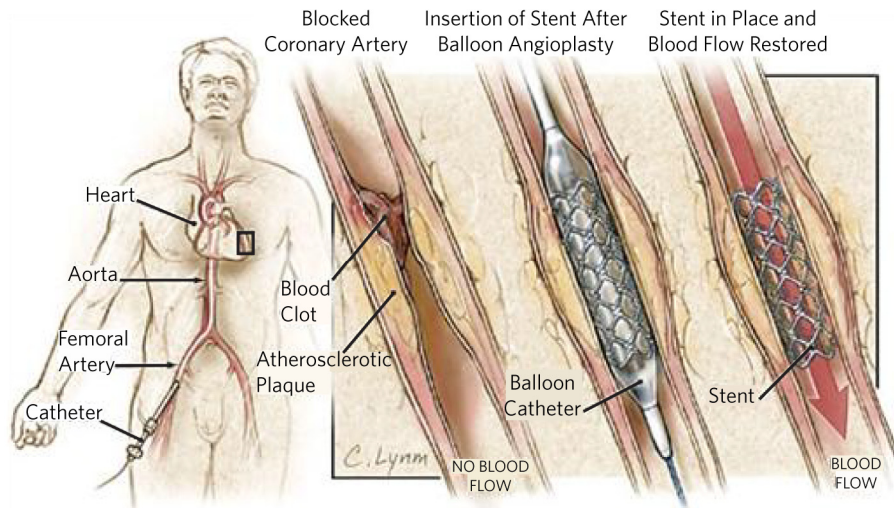


Figure 4. Percutaneous coronary intervention (PCI). A catheter is fed from the femoral (depicted here) or radial artery through the aorta into the coronary artery up to the site of the occlusion (blood clot). After opening the artery through balloon angioplasty, a stent is placed (<http://jama.jamanetwork.com/article.aspx?articleid=198185>).

Visualization of coronary atherosclerosis

To guide the catheter threading during PCI, coronary angiography is used: after injection of a radio-opaque contrast agent via the guiding catheter, real-time X-ray images of the coronary arteries are made. Angiography provides 2D projections of the lumen geometry (angiograms) with a spatial resolution of $200\ \mu\text{m}^{10}$ of the arteries that are used to determine the degree of stenosis. Since atherosclerotic plaques are often characterized by outward remodeling, an angiogram can sometimes show an adequate or even normal luminal cross-section in the presence of advanced atherosclerosis, as is illustrated in Figure 5.

Non-invasive imaging techniques

Computed tomography (CT) coronary angiography has seen rapid advances over the last few years. Multidetector CT (MDCT) using a 64-slice scanner has an improved spatial resolution of 0.4 mm and a faster rotation time (330 ms) compared to prior

MSDT scanners. The most important distinguishing feature of MDCT for coronary imaging is its high negative predictive value, making it a useful tool for screening in an emergency room setting¹¹. MDCT shows good correlation with intravascular ultrasound (IVUS, see below) for measuring plaque burden, plaque volume, and remodeling index¹², where accuracy of this measurement benefits strongly from the improved resolution offered by 64-slice scanners. Vulnerable plaque features have been identified using MDCT, but only in retrospective or observational studies¹³⁻¹⁵. Necrotic core plaques are detected using an attenuation threshold of 30 Hounsfield units (HU), which is subject to blooming and resolution artifacts and large overlap in HU is found between tissue types. This is a problem particularly in the presence of spotty calcification, which is recognized as one of the hallmarks of a vulnerable plaque. Vulnerable plaque criteria from a prospective trial are lacking, and generalization from studies cited above is complicated due to the limited resolution and variability in the results. The use of MDCT as a screening tool for vulnerable plaque detection is hampered by the absence of such criteria, as well as the use of ionizing radiation. For these reasons, clinical use of coronary MDCT remains mainly angiographic¹⁶.

Coronary magnetic resonance (MR) imaging has greater potential for tissue specificity than MDCT imaging, due to the use of multicontrast MR, generated by T1- and T2-weighted, proton-density-weighted, and time-of-flight imaging¹⁷. These imaging sequences allow for differentiation of plaque components on the basis of biophysical and biochemical parameters such as chemical composition and concentration, water content, physical state, molecular motion, or diffusion. MR provides imaging without ionizing radiation and can therefore be repeated over time and thus used to serially monitor patients with high-risk plaques. It suffers from the same limitations as MDCT though, but to a larger degree: current coronary MR sequences have resolutions in the order of 1 mm¹⁸ and temporal resolutions of 100 ms acquisition time per heartbeat, at best¹⁹. Especially in the case of coronary MR, the low temporal resolution hinders quantitative analysis. Additionally, the long acquisition time render it more susceptible to cardiac and respiratory motion artifacts. These technological limits have precluded coronary plaque imaging studies of a significant size.

Intravascular imaging techniques

The current standard for intravascular assessment of coronary atherosclerotic disease and guidance of interventional procedures is intravascular ultrasound (IVUS). This modality produces images based on the reflected amplitude of ultrasound pulses, providing information on both lumen geometry and the structure of the vascular wall with a resolution of approximately 100 μm and an imaging depth of 7 mm. The typical IVUS longitudinal pullback scanning rate is 0.5 mm/s. IVUS is used in clinical practice and trials to measure lumen dimensions, degree of stenosis, plaque burden, and to

assess calcification and stent deployment. The sensitivity and specificity of IVUS grayscale for plaque composition is limited²⁰ because the contrast between soft tissue types is minimal. Examples of IVUS cross-sectional images of a healthy and diseased section a human LAD are shown in Figures 5b and 5c, respectively

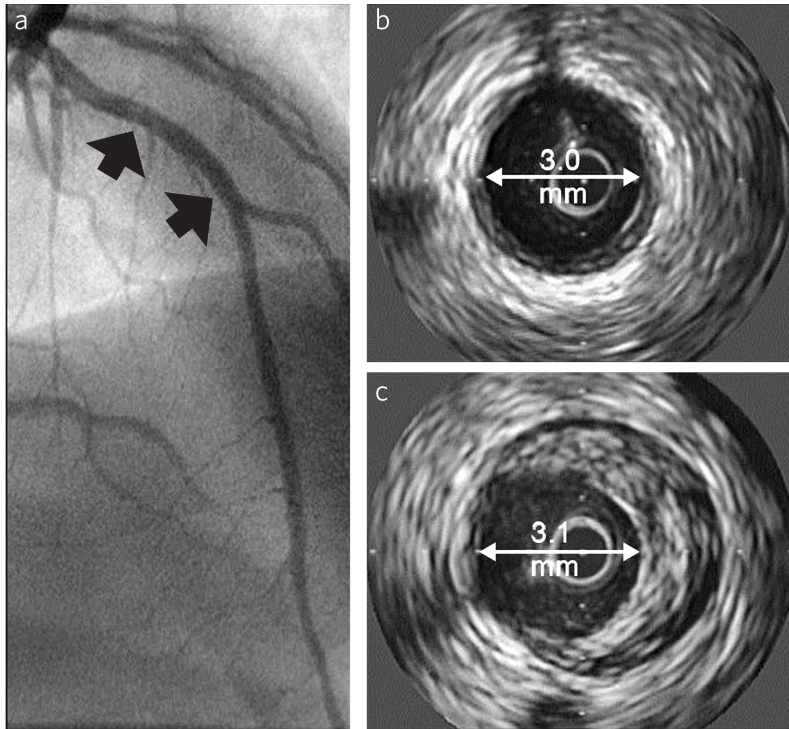


Figure 5. Example of a false-negative angiogram due to outward remodeling. a) Angiogram of left anterior descending artery (LAD) is completely normal. The 2 sites indicated by the arrows have comparable lumen size but while the IVUS image of the more distal site b) shows little disease, the IVUS image of the more proximal site c) reveals a large eccentric lesion.²¹

IVUS radiofrequency data analysis techniques for tissue characterization have been developed as an extension to grayscale imaging²². Today, two commercial IVUS systems offer coronary tissue characterization: VH-IVUS (20 MHz, phased-array transducer, Volcano Therapeutics), and iMap™ (40 MHz, mechanical-type transducer, Boston Scientific). VH-IVUS differentiates four tissue types: necrotic core, fibrous, fibrofatty, and dense calcium²³ but has shown limited accuracy in complex lesions in a porcine model^{24,25}. iMap distinguishes similar tissue types: fibrotic, lipidic, necrotic, and calcified tissue. An in vivo comparison between VH-IVUS and iMap yielded a significant and systematic variability in plaque composition estimates, as illustrated by Figure 6²⁶.

Therefore, further exploration of these tissue characterization techniques in a large population is warranted to establish clinical utility.

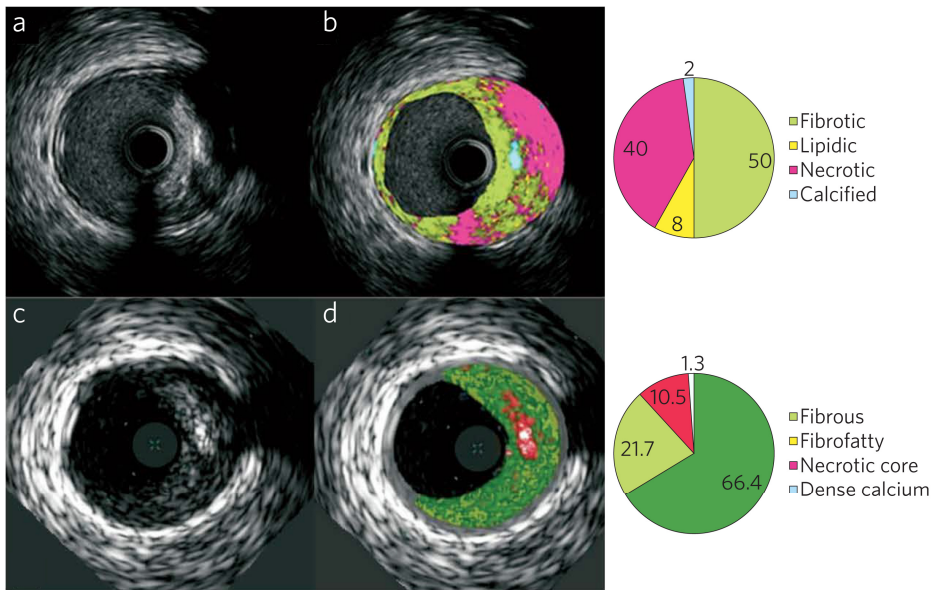


Figure 6. Corresponding iMap (top) and VH-IVUS (bottom) cross-sections of atherosclerotic human coronary artery. a) iMap IVUS only and b) iMap tissue characterization images. c) VH-IVUS IVUS only image and d) VH-IVUS tissue characterization images. iMap interprets the wire artifact and calcium shadow as necrotic tissue, while VH-IVUS reports the same area as fibrous or fibrofatty tissue²⁶.

Intravascular optical coherence tomography (IVOCT) is another modality based on the echo delay of light backscattered from the tissue. IVOCT provides high resolution images (15 μm) but with limited depth penetration (1-2 mm)²⁷. Flushing of the artery under inspection is required due to the strong signal attenuation through blood. Widespread clinical acceptance was achieved after the introduction of high frame rate (> 100 frames per second; fps) and pullback speed (20-40mm/s). Compared to IVUS, OCT offers better assessment of lumen geometry, fibrous cap thickness, stent structure, stent strut coverage and detection of macrophages^{28,29}. On the other hand, tissue characterization by IVOCT is less straightforward and is currently a topic of intense research³⁰. Figure 7 depicts an OCT cross-sectional image of a human coronary artery presenting a TCFA.

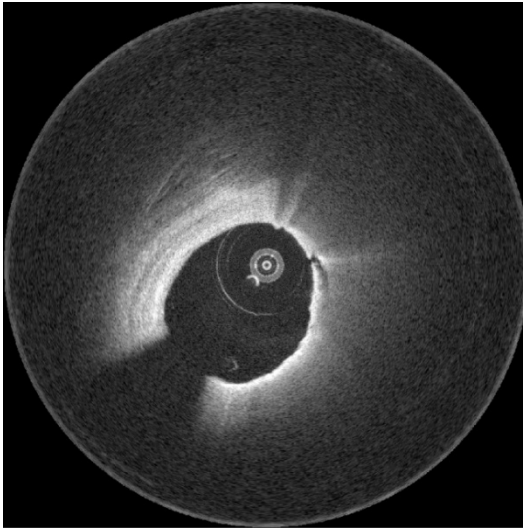


Figure 7. OCT image of an eccentric plaque with an intimal rupture. The signal-poor area from 12 to 7 o'clock indicates presence of a necrotic core, overlaid by a signal-rich fibrous cap. The layered structure from 8 to 12 o'clock shows a mildly thickened fibrous intima covering the darker media.

In the past decade, a number of other optical technologies have aimed to improve intravascular tissue characterization. The most advanced in terms of clinical penetration is near-infrared reflection spectroscopy (NIRS), which is developed and commercialized by Infraredx. It collects a reflection spectrum of the arterial wall, through blood, and identifies the presence of lipid-core plaque in the artery wall. Recently, our laboratory collaborated with Infraredx Inc. to develop a hybrid NIRS/IVUS catheter that combines morphological imaging and lipid detection³¹⁻³³. This is the first multimodality device to enter the clinical arena. Combined interpretation of IVUS and NIRS data may yield an assessment of the lesion morphology, as is illustrated by Figure 8. This also highlights a limitation of NIRS: it is not an imaging modality. Because it lacks depth resolution, NIRS can identify the presence but not the amount or the location, relative to the lumen, of the lipid core. The sensing depth of NIRS is not well quantified.

What is needed?

Since composition is a major determinant of the vulnerability of an atherosclerotic plaque, there is a need for an imaging technique that provides adequate pathological and plaque composition information, preferably in combination with a morphology showing modality. Imaging modalities such as IVUS and OCT provide morphological images with limited plaque composition information. Chemical diagnostic methods such as Raman spectroscopy and near-infrared absorption spectroscopy, on the other hand, supply tissue characterization but provide no depth resolution. A rapid and non-destructive technique to assess the lipid content of atherosclerotic plaques could have a direct

impact on patient management, improve our understanding of the progression or regression of the disease and can be used to investigate drug efficacy.

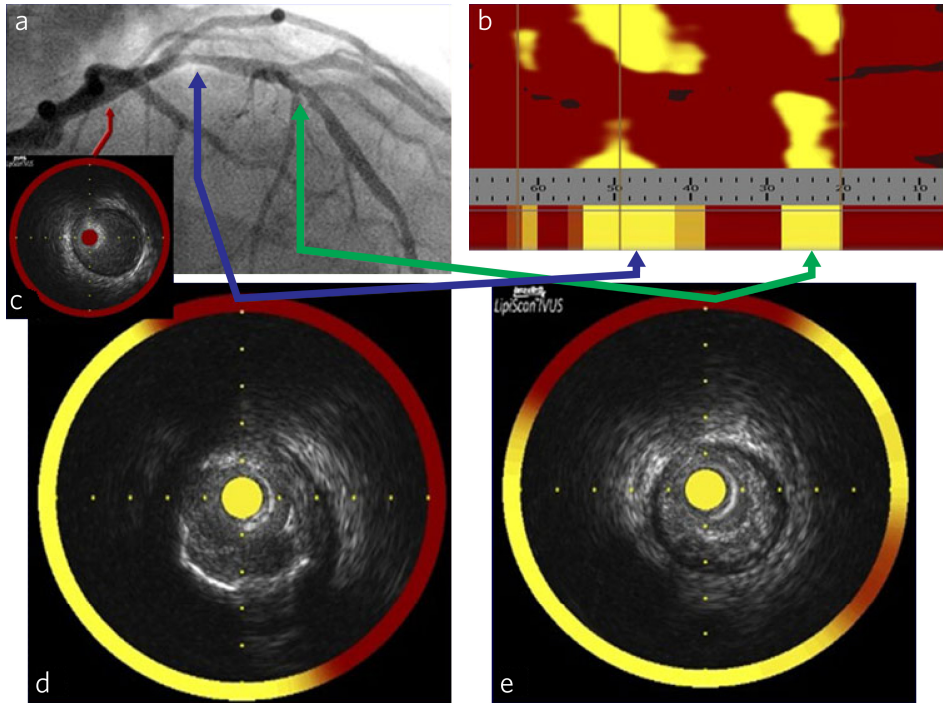


Figure 8. NIRS-IVUS images of a human LAD. a) The angiogram demonstrates a mild stenosis in the proximal LAD (blue arrow), and a more severe stenosis in the mid-LAD (green arrow). b) The NIRS-IVUS chemogram (top) and block chemogram (bottom) show that both lesions contain large lipid core plaques (LCP). Cross-sectional IVUS views c,d,e), with the chemogram data overlaid in a halo around the IVUS image and the block chemogram color value portrayed in the central catheter area. IVUS reveals the proximal LAD lesion d) is an ulcerated LCP and the mid-LAD lesion e) is a bulky LCP with tight stenosis³⁴.

To fulfill this need, we are developing a novel intravascular technique, called intravascular photoacoustic (IVPA) imaging. IVPA is the most recent addition to spectroscopic diagnostic techniques. It has demonstrated the ability to directly image tissue components in the vessel wall, with high chemical specificity for lipid type. There is potential to extend the technology to identify other factors, such as dense macrophage infiltration, associated with plaque vulnerability. The same catheter can be used simultaneously to image the arterial wall architecture by IVUS.

Thesis outline

Chapter 2 introduces IVPA imaging. The photoacoustic principle is explained and an overview of the developments in the field of IVPA to date is given. Lipids and calcification have been the primary targets of IVPA imaging, using endogenous contrast provided by the tissue absorption spectra but considerable work has also been done on visualizing macrophages and matrix metalloproteinase using exogenous absorbers. Additionally, the trade-offs and choices in the design of dedicated IVPA catheters are discussed.

Chapter 3 describes the design and performance of two prototype integrated IVPA/IVUS catheters that were developed and built in-house. The performance of the catheters was tested on several phantoms using an experimental setup.

Chapter 4 demonstrates co-registered IVPA/IVUS imaging of human coronary atherosclerotic plaque. Data was obtained from two fresh coronary arteries *ex vivo*, showing different stages of disease. Spectroscopic IVPA at different wavelengths between 1180 and 1230 nm was performed to visualize the lipid content of an atherosclerotic lesion.

Chapter 5 presents more chemically detailed imaging of the lipid content of human coronary atherosclerotic arteries. The natural history of atherosclerosis is marked by changes in the lipid biochemistry in the diseased arterial wall. As lesions become more vulnerable, different cholesterol species accumulate in the plaque. We demonstrate spectroscopic IVPA imaging of the most important lipid components of human atherosclerotic plaques and visualize connective tissue layers of the adventitia and the fatty acid containing adipose cells in the peri-adventitial tissue.

Chapter 6 reports the development of several methods for the automatic detection and the differentiation of lipids in atherosclerosis development. Such methods make atherosclerotic lipid content information readily available to the clinician, without the need for observer-dependent and time-consuming image interpretation.

Chapter 7 compares the performance of spectroscopic IVPA imaging of human coronary in two spectral bands that signal the presence of lipids: 1.2 μm and 1.7 μm . Tradeoffs in terms of sensitivity, imaging depth, and possibly chemical specificity exist between the two spectral bands are discussed. We measured a lipid containing vessel phantom and an atherosclerotic human coronary artery *ex vivo* in both spectral bands to provide a direct comparison between the two wavelength ranges.

Chapter 8 summarizes the accomplishments and conclusions of the work presented in this thesis, and discusses future directions for the field of IVPA.

Chapter 2

Intravascular photoacoustic imaging: a new tool for vulnerable plaque identification

Based on book chapter by Krista Jansen, Gijs van Soest, and Antonius F.W. van der Steen, **Photoacoustic Imaging of Coronary Arteries: current status and potential clinical application**, in: C. Arampatzis, E.P. McFadden, L.K. Michalis, R. Virmani, P.W. Serruys (Eds.) *Coronary atherosclerosis: current management and treatment*, Informa Healthcare, London, UK, 2012, pp. 166-174.

and the manuscript by Krista Jansen, Gijs van Soest, and Antonius F.W. van der Steen, **Intravascular photoacoustic imaging: a new tool for vulnerable plaque identification**.
submitted

Abstract

The vulnerable atherosclerotic plaque is believed to be at the root of the majority of acute coronary events. Even though the exact origins of plaque vulnerability remain elusive, the thin cap fibroatheroma, characterized by a lipid-rich necrotic core covered by a thin fibrous cap, is considered to be the most prominent type of vulnerable plaque. No clinically available imaging technique can characterize atherosclerotic lesions to the extent needed to determine plaque vulnerability prognostically. Intravascular photoacoustic imaging (IVPA) has the potential to take a significant step in that direction by imaging both plaque structure and composition. IVPA is a natural extension of intravascular ultrasound (IVUS) that adds tissue type specificity to the images. IVPA utilizes the optical contrast provided by the differences in the absorption spectra of plaque components to image composition. Its capability to image lipids in human coronary atherosclerosis has been demonstrated extensively *ex vivo* and has recently been translated to an *in vivo* animal model. Other disease markers that have been successfully targeted are calcium and inflammatory markers, such as macrophages and matrix metalloproteinase (MMP); the latter two through application of exogenous contrast agents. By simultaneously displaying plaque morphology and composition, IVPA can provide a powerful prognostic marker for disease progression, and as such has the potential to transform the current practice in percutaneous coronary intervention.

Principle of photoacoustics

In photoacoustic imaging, the tissue is irradiated by short laser pulses with a length of several nanoseconds. Absorption of laser light transfers the optical energy to the tissue, which causes a transient pressure rise³⁵. This initial pressure rise acts as an acoustic source which generates a broadband wave propagating through the tissue. The acoustic wave can be detected with an ultrasound transducer. In IVPA, the same ultrasound transducer that is used in IVUS can be employed. The principle of IVPA is shown in Figure 1.

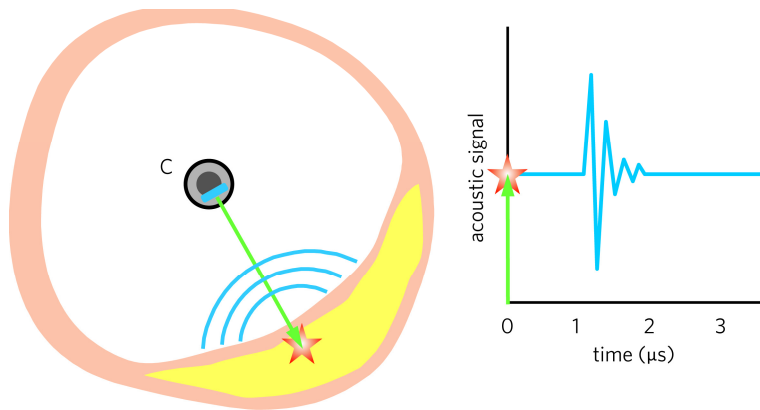


Figure 1. Sketch of the IVPA principle. A laser pulse (green) is sent from the catheter C to the vessel wall containing a plaque (yellow). The light excites an acoustic wave (blue curves) through optical absorption and the associated thermoelastic expansion (red star). The graph on the right shows a time trace of the acoustic signal after the laser fires at time $t = 0$.

The signal strength in photoacoustics is proportional to the local absorption coefficient of the tissue, the light intensity, and the Grüneisen parameter, describing the thermo-acoustic conversion efficiency. The variation of the absorption coefficient with the excitation wavelength is the tissue-specific chemical absorption spectrum, which permits differentiation of tissue type (Figure 2). The photoacoustic excitation wavelengths can be selected to give maximum absorption contrast between the relevant components in the vessel wall and plaque, such as collagen, calcified tissue, and lipids^{36,37}, to image plaque composition using endogenous contrast. Alternatively, exogenous absorbers can be utilized to generate contrast for vulnerable plaque markers that would otherwise remain invisible due to their relatively featureless or low-amplitude absorption spectra. Macrophages are an example of such plaque components.

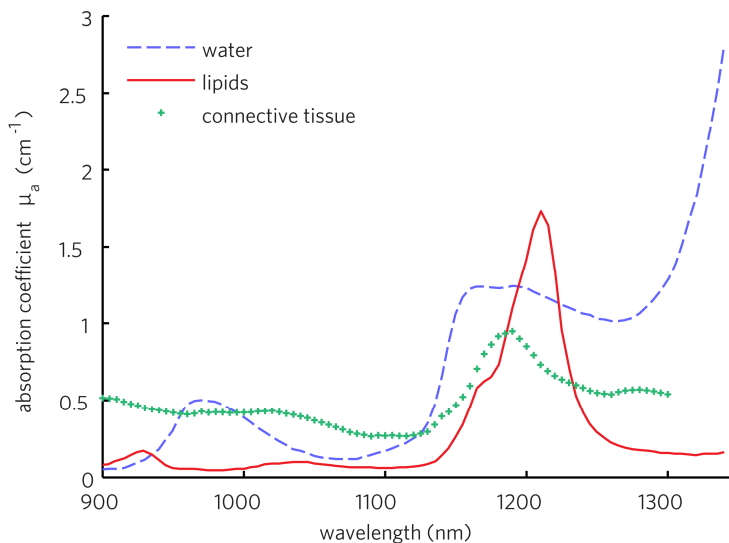


Figure 2. Absorption spectra of various absorbers present in coronary artery vessel wall. Water, fat, and connective tissue (collagen and elastin) are the major contributors to the absorption spectra of human tissues in the NIR spectral region³⁸.

Development of IVPA

Endogenous contrast: imaging of lipids and calcification

The goal of IVPA imaging is the chemical characterization of vessel wall components. Historically, development has been driven by the availability of suitable light sources. For this reason the first spectroscopic measurements focused on the visible wavelength range (410–680 nm)^{39,40}. Through PA imaging of human atherosclerotic aorta specimens, contrast for lipids was found at 461 and 532 nm⁴¹, and contrast for calcium at 308 nm⁴². Discrimination between normal and atheromatous areas of arterial tissue in the visible range has an important drawback: at these wavelengths blood (hemoglobin) absorption is also very high. Introduction of infrared sources prompted investigation of a wider range of excitation wavelengths (680–1800 nm). Blood absorption is especially low in the wavelength range from 680 to 1300 nm. In this wavelength range, the absorption spectrum of lipids exhibits a large peak around 1210 nm, see Figure 2. The group led by Emelianov pioneered spectroscopic IVPA to distinguish between lipid-rich tissue and collagen⁴³. They performed imaging of ex vivo normal and atherosclerotic rabbit aorta samples using a bench-top setup with a commercial IVUS catheter and external illumination. They found different spectral slopes in the IVPA image in regions identified as lipid-rich, collagen type I, and collagen type III. The same group

subsequently exploited the absorption peak around 1210 nm to image lipids in atherosclerotic rabbit aorta⁴⁴.

Allen and Beard were the first to exploit the low blood absorption in the near infrared to discriminate between lipid-rich and normal vascular tissue while imaging through blood^{45,46} (up to a depth of 2.8 mm). Imaging through blood is difficult because of the strong attenuation of the excitation light. They investigated samples of atherosclerotic human aorta and confirmed the presence of lipids by comparing the photoacoustic spectra obtained in a region within the plaque to the spectral signature of a lump of fat.

Investigation of photoacoustic response at longer wavelengths yielded an additional lipid specific absorption feature around 1720 nm⁴⁵. Bo Wang et al.⁴⁷ imaged an atherosclerotic rabbit aorta ex vivo in the presence of luminal blood using excitation light at that wavelength. They demonstrated single wavelength IVPA imaging of lipids through blood using relatively low laser output energy. However, the specificity of this single wavelength method for lipids in human atherosclerotic plaques remains to be investigated.

The first demonstration of in vivo IVPA was performed using the same 1720 nm single wavelength in a hypercholesterolemic rabbit model⁴⁸, see Figure 3. The study was limited by the slow laser system, which necessitated a complex breath gating acquisition. It did show, however, that in vivo imaging without flushing the blood from the artery is possible.

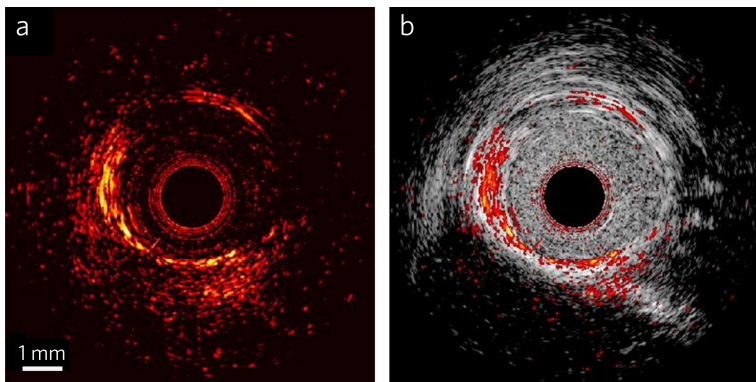


Figure 3. In vivo IVPA/IVUS imaging of lipid in an abdominal rabbit aorta. IVPA image a) and combined IVPA/IVUS image b). The location of lipid deposits in the vessel wall is visualized in the combined IVPA/IVUS image. Adapted from Wang et al.⁴⁸

In most IVPA experiments, lipid rich atherosclerotic plaques were distinguished from normal arterial tissue by simply comparing the tissue spectral signature to the absorption spectra of lipids. A more sophisticated spectroscopy inversion approach

could provide robust identification of a wider range of tissue types, including collagen, elastin and calcifications. Pu Wang et al.⁴⁹ recorded spectroscopic PA data of a phantom consisting of rat-tail tendon and fat between 1650 and 1850 nm. A multivariate curve fit analysis yielded the spatial distribution of collagen and lipids in the phantom.

Recently, single wavelength IVPA imaging at 1720 nm was also demonstrated on human coronary atherosclerosis ex vivo⁴⁸.

Exogenous contrast: imaging of macrophages and matrix metalloproteinase (MMP)

Vulnerable plaque markers that lack sufficient endogenous contrast can be imaged using exogenous absorbers. Macrophages are an example of such plaque components. They do not provide endogenous contrast but can be visualized using gold nanoparticles.

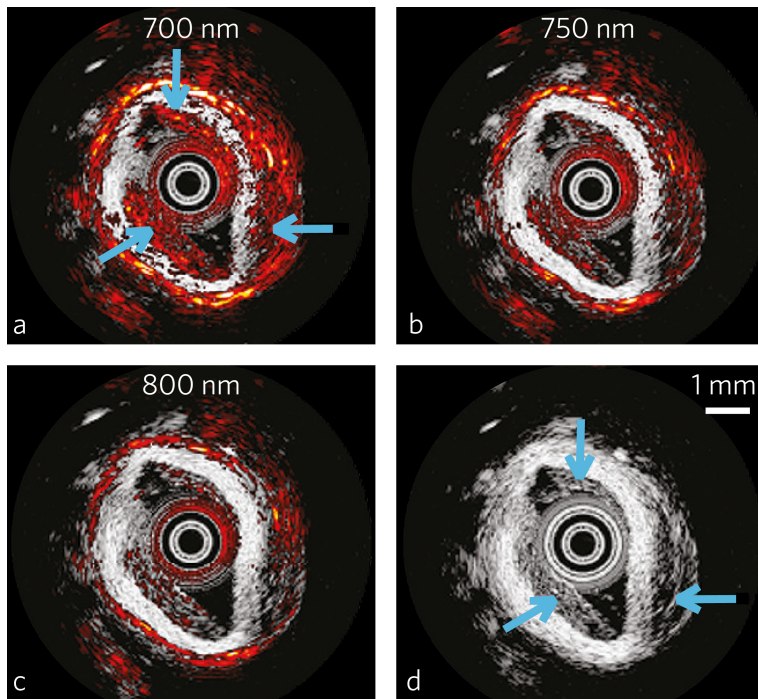


Figure 4. Combined IVPA/IVUS images and IVUS image of a diseased rabbit aorta injected with macrophages loaded with gold nanoparticles (blue arrows). The combined IVPA/IVUS images taken at 700 nm wavelength a) showed high photoacoustic signal at the injected regions denoted by arrows. Adapted from Wang et al.⁵⁰

The gold nanoparticles have a distinct absorption peak in the visible wavelength range. When the nanoparticles are endocytosed by macrophages, they aggregate. These aggregated gold nanoparticles have a shifted peak in the absorption spectrum compared to the (extracellular) non-aggregated gold nanoparticles, providing image contrast. This principle was proven in an atherosclerotic rabbit aorta injected with macrophages loaded with gold nanoparticles in a bench-top experimental setting⁵⁰. The resulting IVPA images, shown in Figure 4, demonstrate that the aggregated gold nanoparticles produce the strongest photoacoustic signal at 700 nm wavelength. The extravasation of nanoparticles in atherosclerotic regions with compromised luminal endothelium and acute inflammation, was demonstrated by systemic injection of gold nanoparticles in a live rabbit model, followed by ex vivo IVPA imaging⁵¹. IVPA/IVUS imaging at 750 nm revealed a high photoacoustic signal from localized gold nanoparticles in regions with atherosclerotic plaques.

Matrix metalloproteinase (MMP) activity, an indicator of plaque instability, can be detected using a MMP-activatable fluorescent imaging agent. MMPsense (MMPsense™ 680; VisEn Medical) is such an imaging agent and is activated by different enzymes, most prominently MMP2/9 and trypsin, and to a lesser extent by other proteases. Once activated, it becomes optically absorbing. More than 80% of the absorbed energy is transferred into photoacoustic signals, due to the low quantum yield of the dye. It has a much lower absorption than gold nanoparticles, however, and thus produces a much lower PA signal intensity.

MMPsense was used for detecting MMP activity in human carotid arteries⁵². Immediately after endarterectomy, the atherosclerotic specimens were incubated in MMPsense. The morphological photoacoustic images, shown in Figures 5a,c,e, were obtained using a small-animal imaging system. The activated probe was distinguished from the background and the inactive probe, by acquiring photoacoustic data at several wavelengths and analyzing spectral contributions on a per-pixel basis. The results matched well with fluorescence microscopy (Figures 5b,d,f).

Photoacoustic generation is temperature dependent, and the dependence is tissue specific, which provides another contrast mechanism. With increasing tissue temperature, the PA amplitude of atherosclerotic plaque lipids decreased while the PA amplitude of peri-adventitial lipids and abdominal fat remained relatively constant between 20–38°C⁵³. Thermal IVPA imaging of atherosclerotic lipids has the advantage over spectroscopic IVPA that only one wavelength is needed. However, creating reliable temperature differences in vivo might prove difficult.

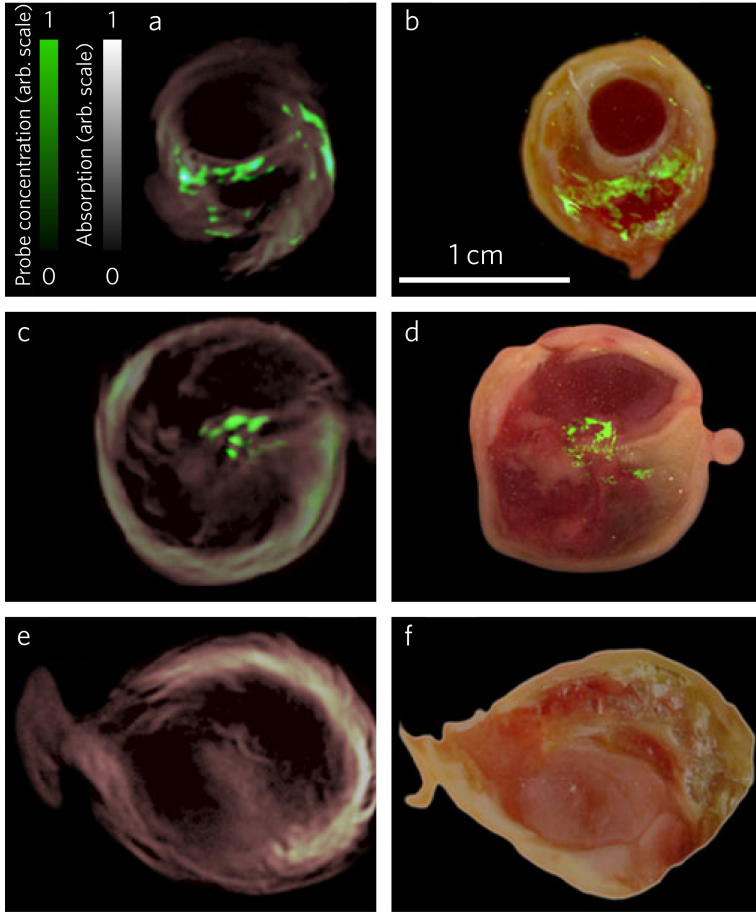


Figure 5. Localization of MMP activity in three carotid specimen. Samples 1 (top row) and 2 (middle row) were incubated in MMPsense 680 while sample 3 (bottom row) was incubated in PBS. a), c) and e) PA imaging results of intact plaques. Cross-sectional spectroscopic reconstruction, revealing location of MMPsense 680 activity in the slice, is shown in green color that is superimposed onto morphological photoacoustic images. b), d) and f) The corresponding epi-fluorescent images from dissected plaque (in green) superimposed onto color images of cryosections from the three carotid plaque specimen. Adapted from Razansky et al.⁵²

IVPA catheter development

Practical in vivo implementation of IVPA requires the development of a dedicated catheter device. Such a device needs to incorporate an optical axis to deliver the light to the vessel wall and an ultrasound detector to detect the photoacoustic signals. Various designs have been proposed.

A miniature, all-optical IVPA probe based on a Fabry-Perot ultrasound sensor was built^{53,54}. It had a diameter of only 250 μm and exhibited good acoustic sensitivity. This all-optical design of an IVPA imaging probe lacks IVUS functionality but has the potential for multi-modal operation, and could be combined with OCT and other optical imaging and sensing methods.

Devices that contain an ultrasound transducer for detection of photoacoustic signals, can be used for combined IVPA/IVUS imaging to provide simultaneous information on composition and morphology of the arterial wall. Two early prototype catheters combined an optical fiber for light delivery with a commercially available IVUS imaging catheter (AtlantisTM SR plus, Boston Scientific, Inc.) for both pulse-echo ultrasound imaging and detection of photoacoustic signals⁵⁵. Light was directed toward the vessel wall using an angle-polished fiber ("side-fire fiber") or a silver coated glass mirror.

A step towards an array catheter for photoacoustic imaging analogous to Volcano's electronic IVUS catheter was made⁵⁶. When using omni-directional optical excitation and ultrasound transmission and detection, no rotation is needed and the required laser pulse repetition rate is reduced. A prototype of a catheter with omni-directional light delivery consisted of a multimode optical fiber coupled to a cone-shaped mirror for illumination and an optical ultrasound detector. The outer diameter of the device was 3 mm.

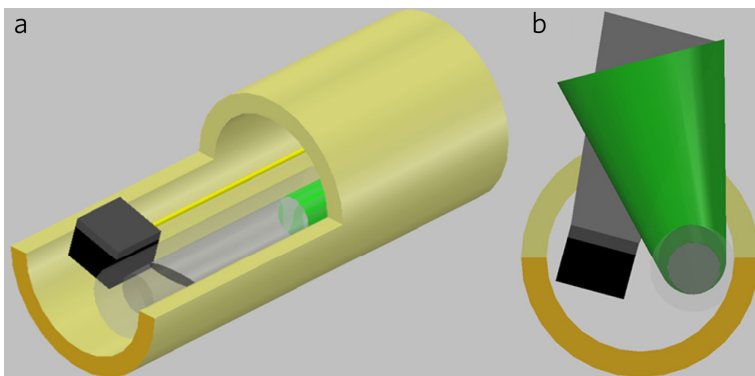


Figure 6. Schematic of the integrated IVUS/IVPA probe: top view a) and front view b); the light beam is in green and the acoustic beam in gray. Adapted from Li et al.⁵⁷

Since the diameters of the catheters used in the above-mentioned studies were too large to allow use in human coronary arteries, they have only been tested on phantoms, rabbit aortas, and on human arteries that were opened up to enable en-face scanning of the luminal surface. Recently, a hybrid IVPA/IVUS catheter with an outer diameter of 1.2 mm was built, see Figure 6. It consisted of a side-firing optical probe and a side-viewing ultrasonic transducer arranged side-by-side⁵⁷. The optical probe comprised a fiber tip connected to a 45-deg polished microprism that was sealed inside a glass capillary tube to preserve an air-glass interface deflecting the beam by total reflection. The fiber ensemble and transducer were packaged in polyimide tubing. The side-by-side arrangement of the fiber and transducer minimizes the offset of the beams which provides good optical-acoustic overlapping, especially close to the probe.

Chapter 3

Development of an integrated photoacoustic and ultrasonic catheter

Based on the publication by Krista Jansen, Geert Springeling, Charles Lancée, Robert Beurskens, Frits Mastik, Antonius F.W. van der Steen, and Gijs van Soest, **An intravascular photoacoustic imaging catheter**. *International Ultrasonics Symposium (IUS)*, 2010 IEEE, San Diego, U.S.A., 2010, pp. 378-381.

Abstract

We developed two prototype intravascular photoacoustics (IVPA) and ultrasound (IVUS) catheters, based on different geometries, to image atherosclerotic plaque structure and composition, important determinants of plaque vulnerability. The first prototype consists of an optical fiber that is mounted in the central hole of a ring shaped ultrasound transducer and a silver mirror that deflects both the light and ultrasound beam sideways (30 MHz coaxial probe). The second prototype comprises an angle-polished optical fiber and a cylindrical transducer (30 MHz dual beam probe). In both cases, a 30 MHz single-element transducer was used. We quantified the imaging performance of the catheters on isolated point targets. Based on the results, we elected the dual beam design for further miniaturization and built a catheter comprising the same angle-polished optical fiber and a 44.5 MHz single crystal transducer. This prototype had an outer diameter of 1 mm only. We tested its imaging performance on isolated point targets and a vessel mimicking phantom.

Introduction

Intravascular photoacoustic (IVPA) imaging has the potential to image atherosclerotic plaques in unprecedented chemical detail. It uses a combination of light and ultrasound to image the vessel wall anatomy (using pulse-echo intravascular ultrasound [IVUS] imaging) and photoacoustic imaging, employing the chemical specificity of the optical absorption spectrum to identify tissue type. It requires a catheter that can perform IVUS, and has an optical port to illuminate the artery wall. IVUS imaging requires a high-frequency (> 30 MHz center frequency) transducer. In order to access a coronary vessel, the outer diameter of the probe must eventually be less than 1 mm.

Optical access is realized by the use of an optical fiber which runs along the length of the catheter. The illuminated area must lie within the field of view of the ultrasound element. We explore two geometries here to assess their performance for IVPA.

An elegant solution to fulfill the geometrical requirements is the use of coaxial beams. In this realization, the optical fiber illuminates the tissue through a central hole in the transducer, and a mirror directs both beams towards the vessel wall. Advantages of this design are exact optical/ultrasound coregistration and longer acoustic path lengths, allowing to remove transmit artifacts. A downside is the loss of transducer area and the need for fluid filling the space in front of the transducer. Alternatively, the beams may be longitudinally or transversely offset, and positioned at an angle. This configuration allows the use of stock transducers. It also leads to a more complex relation between the IVUS and IVPA imaging planes, depending on the amount of optical scattering. We explore both geometries in this chapter.

Methods

30 MHz coaxial probe

The first prototype catheter (Figure 1) consists of a multimode optical fiber (Thorlabs, 400 μm core diameter, low OH) to deliver the light pulses that is mounted in the central hole of a ring shaped lead-zirconium-titanate (PZT) ultrasound transducer (custom built by TU Delft; design by DuMED) for ultrasound transmission and reception. The ultrasound transducer has a center frequency of 30 MHz and a -6 dB bandwidth of 60%. A silver mirror is placed distal from the fiber tip and transducer at an angle of 45° to deflect both the light and ultrasound beam sideways towards the vessel wall. The diameter of the silver mirror is 5 mm, generating a catheter outer diameter of approximately the same size. This design ensures exact co-registration of the IVPA and IVUS images, due to the coaxial configuration of the light and ultrasound beam.

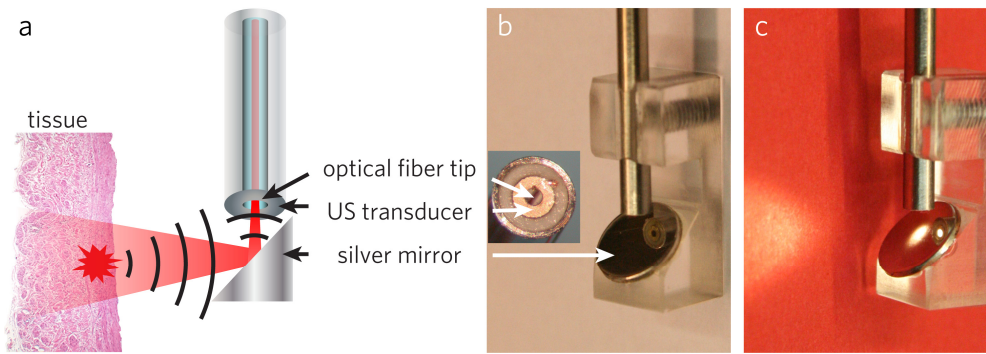


Figure 1. Schematic a) and pictures b) and c) of the 30 MHz coaxial probe. a) The schematic depicts the light path (red) and generated ultrasound signal (black arcs). Both the light pulses and the ultrasonic waves are reflected by the silver mirror and remain completely coaxial along their path. b) Photograph of catheter tip. The reflection of the optical fiber tip and the ring shaped transducer surrounding it are visible in the silver mirror. c) The light can be seen exiting the optical fiber and being deflected by the mirror under 45° angle.

30 MHz dual beam probe

In the second design (Figure 2), the light is deflected towards the vessel wall by an angle-polished optical fiber (Pioneer Optics, 400 μm core diameter, low OH).

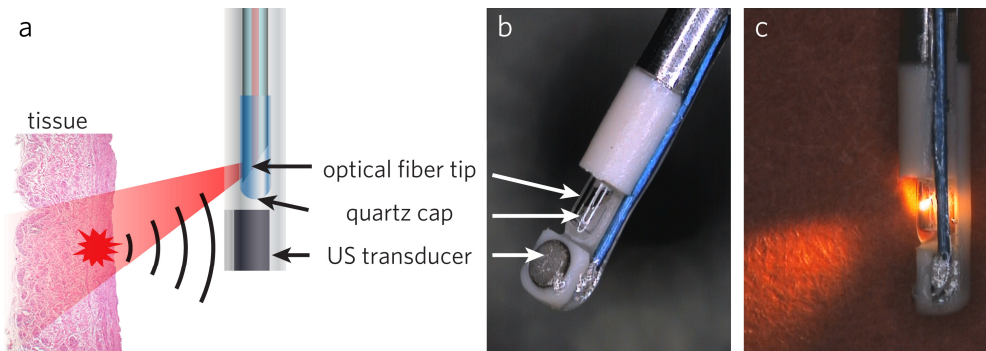


Figure 2. Schematic a) and pictures b) and c) of the 30 MHz dual beam probe. a) The schematic depicts the light path (red) and generated ultrasound signal (black arcs) b) Photograph of catheter tip, showing the angle polished optical fiber tip enclosed by the air filled quartz cap and the ultrasound transducer distal to quartz cap. c) Side view with light leaving the optical fiber tip under a 68° angle.

The fiber tip is polished under a 34° angle and covered with a glued-on quartz cap to preserve an air-glass interface deflecting the beam by total reflection. A lead-zirconium-titanate (PZT) circular ultrasound transducer with a diameter of 1.0 mm (custom built by TU Delft; design by DuMED) for PA signal reception is placed distal from the quartz tube. We optically isolated the transducer with silver leaf of $4\text{ }\mu\text{m}$ thickness to eliminate artifacts in the PA images. The transducer is also used for generating and receiving an ultrasound wave for pulse-echo imaging. The optical and acoustic beams intersect at 4.5 mm from the catheter at an angle of 22° . Figure 2b shows the light path exiting the probe under an angle (68°). The fiber and transducer were placed in a custom machined polyether ether ketone (PEEK, bio-compatible) assembly with an outer diameter of 1.25 mm. The transducer has again a center frequency of 30 MHz and a -6 dB bandwidth of 60%.

45 MHz dual beam probe

We designed and built a second dual beam hybrid IVPA/IVUS catheter (45 MHz dual beam probe), utilizing the same angle-polished optical fiber but with a different ultrasound transducer. Photographs of the catheter are shown in Figure 3.

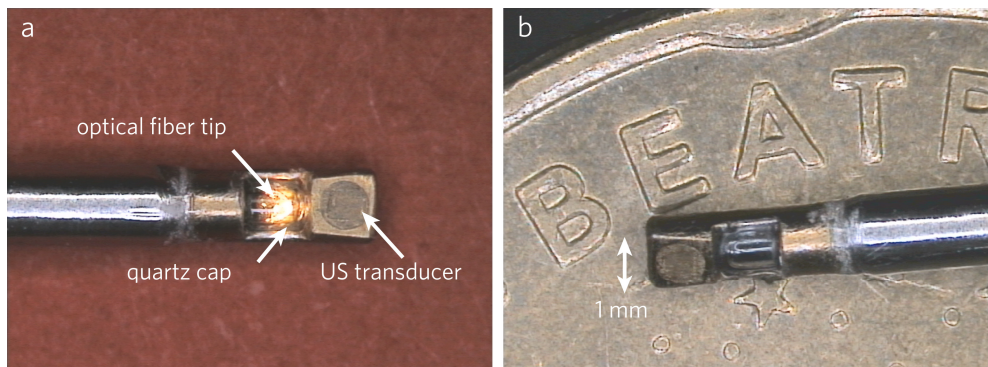


Figure 3. 45 MHz dual beam probe. a) Front view photograph of probe with light exciting the optical fiber tip. The 0.4×0.4 mm PMN-PT single crystal transducer⁵⁸ has a center frequency of 44.5 MHz and a -6 dB bandwidth of 45%. b) Photograph of the catheter tip on the edge of a 10 eurocent coin. The outer diameter of the tip is 1 mm.

The 0.4×0.4 mm lead magnesium niobate-lead titanate (PMN-PT) single crystal ultrasound transducer was custom built by the Department of Biomedical Engineering of the University of Southern California⁵⁸ and had a center frequency of 44.5 MHz and a -6 dB fractional bandwidth of 45%. Fiber and transducer were mounted in a custom machined stainless steel assembly with an outer diameter of 1 mm. The front of the

transducer was bonded to a conductive gold particle matching layer, after which an outer matching layer of parylene was formed by vapor deposition. The fiber tip and transducer center were separated by approximately 1.1 mm. The angle between the optical and acoustical beams was 22° ; the beams overlapped between 0.5 and 4.5 mm from the transducer.

Combined IVPA/IVUS imaging system

We built an experimental imaging system to test the IVPA and IVUS imaging performance of the prototype catheters. The system is illustrated in Figure 4.

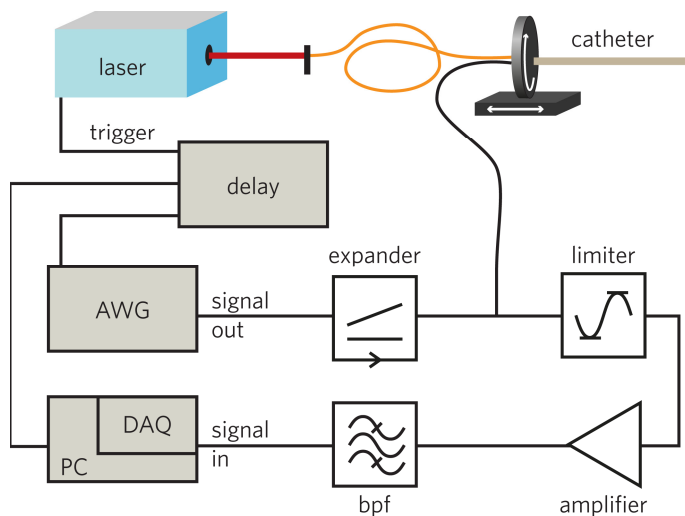


Figure 4. Diagram of the combined IVPA/IVUS imaging system; AWG: arbitrary wave generator, DAQ: data acquisition, delay: pulse/delay generator; bpf: band pass filter.

The light energy for photoacoustic imaging is delivered by a tunable laser (Opotek Vibrant B/355-II). It produces 5 ns high energy (> 10 mJ) light pulses in the wavelength range of 420 to 1800 nm with a spectral linewidth of $\sim 4 - 7$ cm^{-1} ($\sim 0.3 - 0.4$ nm @ 800 nm; $\sim 0.6 - 1$ nm @ 1200 nm; $\sim 1 - 2$ nm @ 1700 nm) and a repetition rate of 10 Hz. A tapered multimode fiber (Oxford Electronics, Four Marks, UK; input diameter 1mm; output diameter 360 μm) couples the laser light to the catheter. An arbitrary waveform generator (Tabor Electronics WW2571A) transmits Gaussian-modulated cosine waves for pulse echo imaging. The ultrasound waves are transmitted to the probe through a custom-built expander and limiter. The received US and PA signals are amplified by a 43 dB amplifier (Miteq AU1263), band pass filtered (13–60 MHz 5th order Butterworth, custom built) and digitized at a sample frequency of 350 MS s^{-1} by a 12-bit data

acquisition card (Acqiris DP310). A pulse/delay generator (BNC model 575) adapted and distributed the trigger provided by the Q-switch of the laser to the arbitrary waveform generator and data acquisition card. The catheter is translated and rotated by a motorized translational and rotary stage (Steinmeyer GmbH & Co. KG), respectively.

Experiments

We have tested the PA and US imaging performance of the three integrated IVPA/IVUS probe prototypes. For pulse-echo imaging, a $16 V_{pp}$ Gaussian modulated cosine wave with a center frequency of 30 MHz and a -6 dB bandwidth of 75 % was applied to the transducer of the first two prototype catheters; for the 45MHz dual beam probe, we applied a similar wave with a center frequency of 45 MHz and a -6 dB bandwidth of 50 %. To create images with spatially matched PA and US information, every light pulse was followed by 10 acoustic pulses. The received echo signals of these pulses were averaged to construct the US image; no averaging was applied for PA imaging.

We performed measurements on isolated point targets in water at room temperature to determine the point spread function (PSF) widths and signal to noise ratios (SNRs) of the two first prototype IVPA/IVUS catheters (30MHz coaxial and 30 MHz dual beam probe). The point targets were formed by six evenly spaced metallic (wolfram) wires of 50 μm diameter located at approximately 2 to 7 mm from the transducer. We acquired co-registered PA (800 nm) and US images of the point targets by translation of the catheter in steps of 50 μm and acquire a PA and US image line at every position.

Next, using the 30 MHz dual beam probe, we imaged a cylindrical vessel phantom, which is shown in Figure 7c. The phantom is made of poly-vinyl-alcohol (PVA) with enamel as acoustic scatterers and has a 3 mm diameter lumen. Six metallic wires of 100 μm diameter located at 1.5 to 4 mm distance from the lumen function as optical absorbers. We placed the phantom in water and acquired a cross-sectional scan by rotation of the catheter in 1 step and recording a PA and US image line at every position.

We repeated the measurement on the isolated point targets with the 45 MHz dual beam probe. We then added 1 vol. % intralipid (Intralipid® 20 %, Fresenius Kabi Nederland BV) to the water bath and acquired another scan of the point targets.

Data processing

The digitized PA data were band pass filtered between 10 and 40 MHz for the 30 MHz probes and 10 and 70 MHz for the 45 MHz dual beam probe, using a 100th order zero-phase forward and reverse finite impulse response (FIR) filter. Despite the application of silver leaf to the transducer of the 30 MHz dual beam probe, the vessel phantom data were affected by an artifact caused by the absorption of laser pulses in the ultrasound transducer. It showed up in the IVPA images as bright rings, concealing the

photoacoustic signals produced by the vessel phantom close to the catheter. An adaptive filter was designed and applied to the IVPA data to remove this artifact. A similar circular artifact in the IVUS data of the vessel phantom, caused by the ‘ringing’ of the transducer as a result of the transmission of ultrasound pulses, was removed by subtracting the mean in the angular direction of the affected part of the data. All PA and US data were subsequently Tukey windowed and envelope filtered. The vessel phantom data were scan-converted to Cartesian coordinates, after which all data were log compressed for display. The ‘hot’ and ‘gray’ colormaps in Matlab (R2007b) were used for the PA and US images, respectively. To create combined PA/US images, we overlaid the PA data on the US images using a nonlinear red-yellow-white color scale and a linear transparency scale. All data processing was done using Matlab (R2007b).

Results

30 MHz coaxial probe

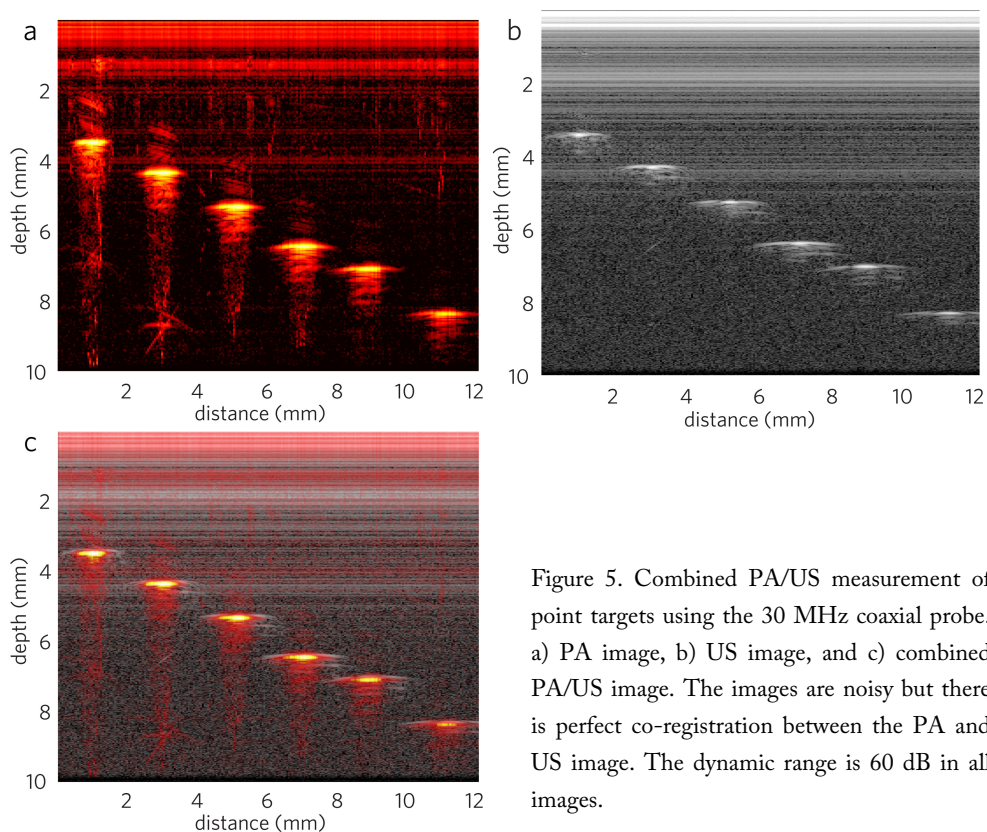


Figure 5. Combined PA/US measurement of point targets using the 30 MHz coaxial probe. a) PA image, b) US image, and c) combined PA/US image. The images are noisy but there is perfect co-registration between the PA and US image. The dynamic range is 60 dB in all images.

The results of the measurements on the isolated point targets with the 30 MHz coaxial probe are presented in Figure 5. The PA image, shown in Figure 5a, contains many artifacts. The bright horizontal lines, visible up to approximately 4 mm depth, are the result of ultrasound pulses that are reflected back by the mirror, hitting the transducer. A fraction of the light may be reflected back towards the transducer as well, which would add to the effect. The horizontal lines are also visible in the US image, shown in Figure 5b, up to approximately 4.5 mm depth. In the US image, this artifact is superimposed on the artifact caused by the 'ringing' of the transducer as a result of the transmission of ultrasound pulses. Reverberation or 'comet-tail' artifacts behind the wire signals are present in the PA image^{59,60}. In the combined PA/US image, presented in Figure 5c, the perfect co-registration of the PA and US signals in the longitudinal direction (along the axis of the catheter) can be seen.

30 MHz dual beam probe

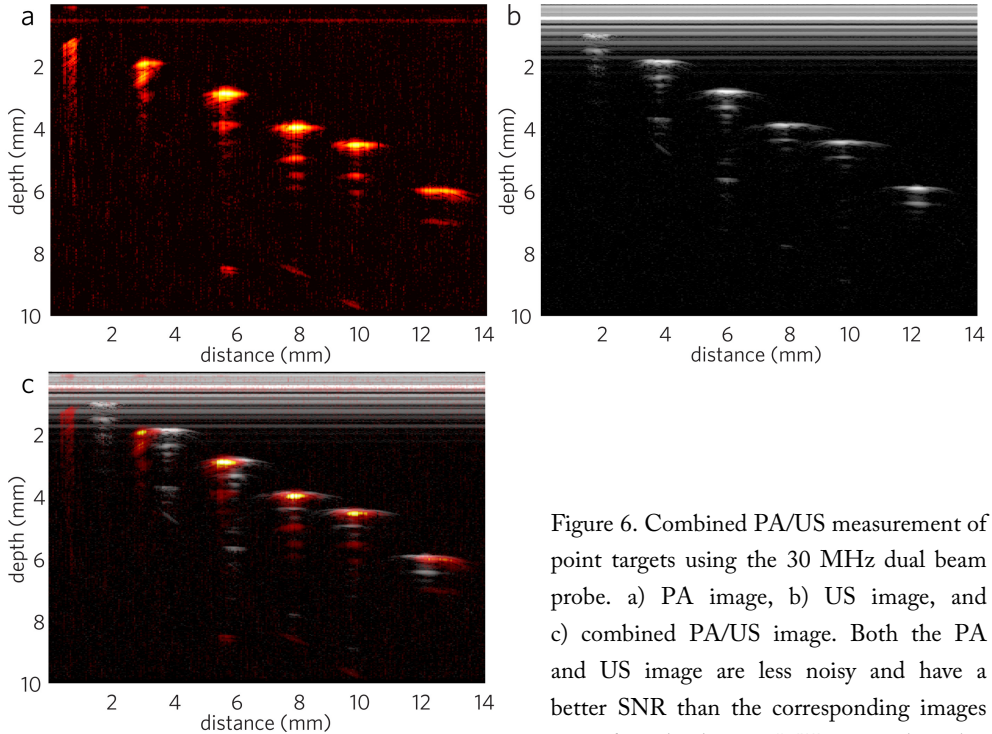


Figure 6. Combined PA/US measurement of point targets using the 30 MHz dual beam probe. a) PA image, b) US image, and c) combined PA/US image. Both the PA and US image are less noisy and have a better SNR than the corresponding images created with the 30 MHz coaxial probe.

A spatial mismatch can be seen between the PA and US signals from the wires closest and furthest away from the transducer. The dynamic range is 60 dB in all images.

Figure 6 shows the results of the measurements on the isolated point targets with the 30 MHz dual beam probe. The PA image has less clutter than the PA image acquired with the 30 MHz coaxial probe. The bright lines that were seen in the coaxial probe PA and US images are virtually absent because the light and ultrasound are not reflected back to the transducer. In the US image, however, the artifact caused by the ‘ringing’ of the transducer as a result of the transmission of ultrasound pulses is still visible, up to approximately 1.6 mm depth. In both the PA and US image, a double signal from each point target is visible, which is caused by an incomplete damping of the ultrasound by the backing of the transducer. Behind the PA signal of the point targets closed to the transducer, comet tail artifacts are again visible. As can be seen in Figure 6c, the co-registration of the PA and US image in the axis of the catheter is excellent between 4 and 6 mm from the transducer, while closer to transducer the mismatch is almost 1 mm. The SNR is clearly higher for the PA as well as the US image when compared to the corresponding images obtained with the 30 MHz coaxial probe. Table 1 lists the PSFs and SNRs of all point target measurements.

Table 1. Point spread function (PSF) widths and signal to noise ratios (SNRs) of all PA and US measurements on the isolated point targets in water and 1 vol. % intralipid (numbers in brackets). The axial PSF widths of the PA and US images of all three probes are in the same order of magnitude; the lateral PSF widths are comparable as well. All SNRs are above 50 dB, with the exception of the 30 MHz coaxial probe US measurement. PSF width: -6 dB point spread function width; SNR: signal to noise ratio. The axial PSF is averaged over the 6 wires; the lateral PSF and SNR are measured on the wire closest to the natural focus (at 5 mm and 2.1 mm for the 30 MHz probes and 45 MHz dual beam probe, respectively).

Probe	Imaging Modality	PSF width (μm)		SNR (dB)
		axial	lateral	Water
30 MHz Coaxial	PA	90	450	59
	US (10x)	56	275	39
30 MHz dual beam	PA	100	300	58
	US (10x)	61	400	52
45 MHz dual beam	PA	77 (50)	525 (350)	57 (57)
	US (10x)	87 (45)	225 (200)	60 (62)

The IVPA and IVUS image of the vessel phantom created with the 30 MHz dual beam probe are presented in Figures 7a and 7b, respectively. All 6 wires are clearly visible in both images. The circular artifacts, mentioned in the Methods section, are effectively suppressed, revealing the data close to the transducer. Comet tail artifacts

can be seen behind the two point targets closest to the transducer. The combined IVPA/IVUS image (Figure 7d) shows the perfect overlap of the PA and US wire signals in the transverse direction (perpendicular to the axis of the probe).

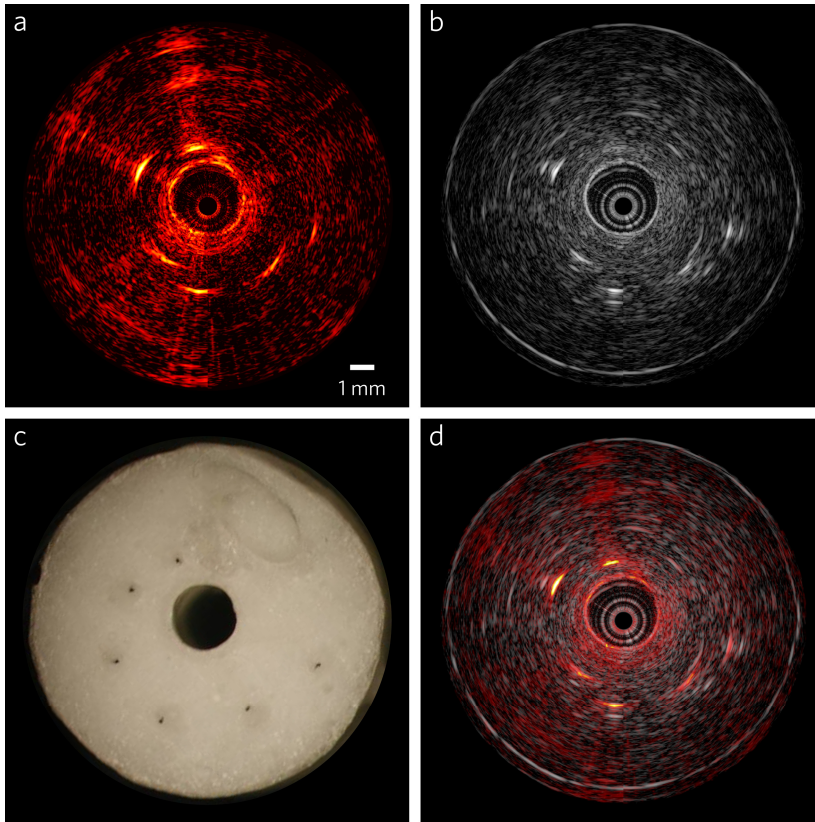


Figure 7. Cylindrical vessel phantom, imaged with the 30 MHz dual beam probe. a) IVPA image (dynamic range 45 dB), and b) IVUS image (dynamic range 50 dB) of the phantom. c) Photograph of the phantom, taken from the top. d) Combined IVPA/IVUS image.

45 MHz dual beam probe

The results of the 45 MHz dual beam probe measurements of the isolated point targets are presented in Figure 8. The horizontal lines in the PA image are caused by photoacoustic signals generated in the catheter tip. In the US image, the 'ringing' of the transducer is again visible. In the PA image, the comet tail artifacts can be clearly discerned behind the first four point targets. The combined PA and US image of the point target measurement in water is shown in Figure 8c. The PA and US signals overlap between 2 and 4 mm from the transducer (wire 2 and 3), while closer to and further

away from transducer the signals are misaligned. Introduction of light scattering by adding 1 % vol. intralipid to the water bath, yields perfect co-registration of all PA and US wire signals (Figure 8d), without lowering the SNR significantly (Table 1). While a comparable SNR at the natural focus distance is found for all catheters, the SNR of the 45 MHz dual beam probe falls sharper with depth, due to the higher ultrasound attenuation at higher frequencies.

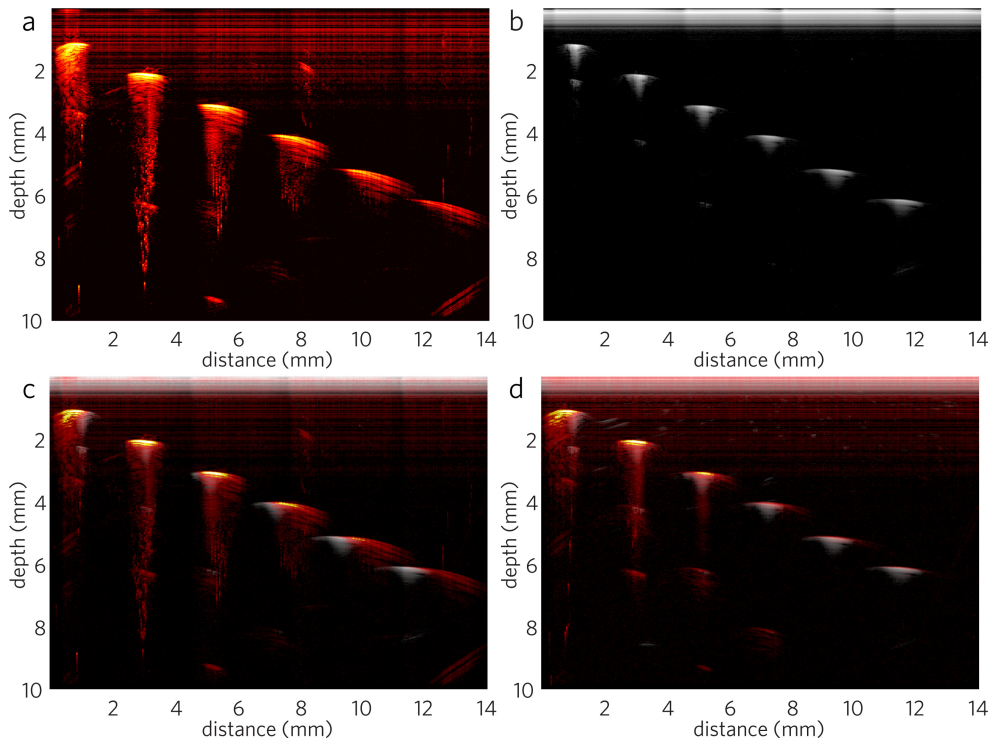


Figure 8. Combined PA/US measurement of point targets using the 45 MHz dual beam probe. a) PA image, b) US image, and c) combined PA/US image of measurement in water. A spatial mismatch can be seen between the PA and US signals from the wires closest and furthest away from the transducer. d) PAUS 1% vol. intralipid. The dynamic range is 60 dB in all images.

Discussion

We presented three prototype integrated optical/acoustic catheters for combined IVPA/IVUS imaging: one 30 MHz coaxial probe and 30 and 45 MHz dual beam probes. We characterized their imaging performance using a point target phantom. We found PA and US axial PSF widths equal to or less than 100 μm and lateral PSF widths at the natural focus distance between 200 and 550 μm . The SNRs at the natural focus distance

ranged from 52 to 62 dB, with the exception of the US SNR of the coaxial probe, which was only 39 dB. The coaxial design suffered from artifacts in the PA and US images due to the reflection of the ultrasonic waves and possibly the absorption of light energy at the mirror surface. We demonstrated good imaging performance of the 30 MHz dual beam probe on a cylindrical vessel phantom containing metal wires as optical absorbers.

For the coaxial probe design it is imperative that the mirror is placed as close as possible to the optical fiber tip to minimize the length of light path through water and thus the water absorption. This is especially important at longer wavelengths in the near-infrared, where the high water absorption limits the penetration depth. Furthermore, to avoid damage to the mirror in the PA image, the material of the mirror needs to have a high damage threshold and thus a low absorption coefficient in the wavelength range of interest.

Based on the results presented here and, we elected the dual beam design for future prototype catheters. The design will be further improved to fully eliminate the PA artifacts due to incompletely optical isolation of the ultrasound transducer. We will fabricate the catheter tip of future prototype catheters out of PEEK to minimize the generation of photoacoustic waves in the catheter tip. The small size of the USC ultrasound transducer allows for further reduction of the catheter diameter to the desired dimension of 0.7 mm. However, the optical fiber diameter will have to be reduced as well to attain this objective. This will require an adjustment of the light coupling to the catheter and ultimately a different light source.

Chapter 4

Intravascular photoacoustic imaging of human coronary atherosclerosis

Based on the publication by Krista Jansen, Antonius FW van der Steen, Heleen MM van Beusekom, J Wolter Oosterhuis, and Gijs van Soest, **Intravascular photoacoustic imaging of human coronary atherosclerosis**, *Optics Letters*, 36 (2011) 597-599.

Abstract

We demonstrate intravascular photoacoustic imaging of human coronary atherosclerotic plaque. The data was obtained from two fresh human coronary arteries *ex vivo*, showing different stages of disease. A 1.25 mm diameter intravascular imaging catheter was built, comprising an angle-polished optical fiber adjacent to a 30 MHz ultrasound transducer. Specific photoacoustic imaging of lipid content, a key factor in vulnerable plaques that may lead to myocardial infarction, is achieved by spectroscopic imaging at different wavelengths between 1180 and 1230 nm. Simultaneous imaging with intravascular ultrasound was performed.

The majority of acute coronary events are precipitated by the rupture of a vulnerable atherosclerotic plaque in the coronary system, and subsequent thrombogenesis^{4,61}. Among the parameters that influence plaque vulnerability are the presence of a lipid-rich necrotic core, the thickness of the fibrous cap overlying that core, inflammation, and intraplaque hemorrhage³. The key to plaque vulnerability is still elusive, even though recent advances in intravascular imaging technology have enabled the collection of a wealth of data on unstable atherosclerosis in all its stages of development⁶², both in clinical and in *ex vivo* settings. Plaque type and morphology are relevant for intervention planning, and significantly affect long term treatment outcome⁶³.

The present standard for intravascular diagnostic imaging is intravascular ultrasound (IVUS)⁶⁴. It images the lumen geometry and the structure of the vascular wall with a resolution of approximately 100 μm . IVUS clearly shows the presence of calcified tissue, but has a limited specificity for different soft tissue types⁶⁵. Recently, a device combining IVUS with near-infrared reflection spectroscopy (NIRS) was demonstrated³¹. This technology marks the lipid-containing sectors of the IVUS image with the aim to detect lipid-core plaques. It has no depth sensitivity, however: NIRS can identify the presence but not the amount or the position of the lipid concentration relative to the lumen.

Intravascular photoacoustics (IVPA) is a tool for plaque composition imaging. Like NIRS, it capitalizes on the differences in the chemical absorption spectra of various tissue types: by selecting the excitation wavelength, a photoacoustic signal can be excited from specific tissue types in the artery wall. Wang et al. applied this principle to imaging lipid in atherosclerotic rabbit aorta, using a bench-top setup with external illumination near 1200 nm⁴⁴. Allen and Beard studied human aorta samples, outlining the spectral difference between lipid-rich and normal vascular tissue⁴⁵. Several designs for IVPA/IVUS probes have been proposed^{55,56,60}, but these have not been applied to actual atherosclerotic tissue.

In this paper we demonstrate imaging of human atherosclerotic arteries *ex vivo* with a custom-built IVPA/IVUS catheter. The imaging capability of the device is demonstrated, unveiling prominent disease features in a human coronary lesion that shows hallmarks of a vulnerable plaque.

A hybrid IVPA/IVUS catheter was built (Figure 1a), consisting of a 400 μm diameter core optical fiber (Pioneer Optics, Bloomfield, CT) and a lead-zirconium-titanate (PZT) ultrasound transducer with a diameter of 1.0 mm (custom built by TUDelft; design by DuMED, Rotterdam). The tip of the fiber was polished at an angle of 34° and covered with a glued-on quartz cap to preserve an air-glass interface deflecting the beam by total reflection. The transducer had a center frequency of 30 MHz and a 6-dB fractional bandwidth of 65%. Fiber and transducer were mounted in an assembly with an outer diameter of 1.25 mm; see Figure 1b.

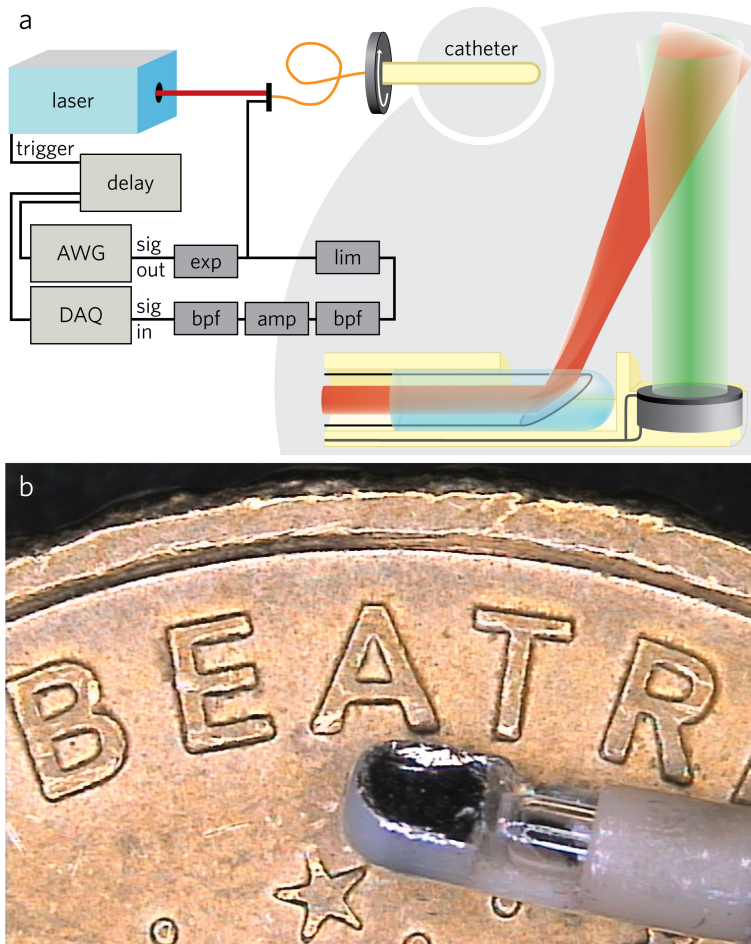


Figure 3: a) Diagram of the experimental setup, including a detailed schematic of the catheter tip, showing the beam layout; AWG: arbitrary wave generator, DAQ: data acquisition, exp: expander, lim: limiter, bpf: band pass filter, amp: amplifier. b) Photograph of the catheter tip on the edge of a 10 eurocent coin.

The fiber tip and transducer center were separated by approximately 1 mm. The angle between the optical and acoustical beams is 22° ; the beams overlap between 0.5 and 4.5 mm from the transducer. Our catheter is comparable in design to the one discussed in⁵⁵ but is about half the size in diameter.

Coronary arteries were obtained from the Dept. of Pathology of the Erasmus MC at autopsy and imaged within 24 h post mortem. Consent was obtained from the relatives and the protocol was sanctioned by the Medical Ethics Committee of the Erasmus MC.

The specimens were mounted on two cannulas in a tank containing saline solution. Large side branches were closed and arteries were pressurized to 100 mmHg to maintain

an open lumen. The arteries were screened by an IVUS pullback (Boston Scientific iLab, Atlantis SR Pro catheters) and sites of interest were marked with suture needles. Markers were located with IVPA for further data acquisition.

After imaging the artery specimens were cut at the image plane. The segments proximal from the image plane were fixed in 4% buffered formaldehyde, paraffin embedded, and serially sectioned at the imaging plane for histology; segments distal from the imaging plane were frozen in isopentane and sections prepared for lipid staining (Oil Red O).

Cross-sectional scans at sites of interest were made by rotation of the catheter in 1° steps using a motorized rotary stage (Steinmeyer GmbH & Co KG). At every position IVPA and IVUS image lines were acquired, ensuring image co-registration. Pulse echo imaging was performed using an arbitrary waveform generator (Tabor Electronics WW2571A) transmitting a Gaussian-modulated cosine wave (30 MHz; 10 Vpp; 100% bandwidth). A tunable laser (OPOTEK Vibrant B/355-II) provided the excitation light (pulse width 5 ns, repetition rate 10 Hz, pulse energy 1.2 mJ at catheter tip) for photoacoustic imaging. Images were acquired at several excitation wavelengths between 715 and 1800 nm. We concentrated on the spectral range near 1200 nm where a prominent harmonic of the C—H stretch vibrational mode signals the presence of lipids^{38,66}. In addition, full spectral scans were made at particular angular locations, which were selected based on IVUS morphology. All received IVUS and IVPA signals were band-pass filtered, amplified (Miteq AU1263), and digitized (Acqiris DP310). No averaging was applied for IVPA imaging; IVUS traces were averaged 10-fold. Acquisition of one IVPA/IVUS image took 36 s. The dynamic range of all IVUS and IVPA images shown in this paper is 40 dB.

IVPA/IVUS was performed in an advanced lesion (left anterior descending artery, male aged 56). The results are shown in Figure 2. The histology shows circumferential intimal thickening with a large eccentric lipid-rich lesion, as well as a calcified area and regions of peri-adventitial fat. The IVUS data confirms this morphology. The IVPA image at 1210 nm exhibits a bright signal along the intimal border, and also from deeper tissue layers in the eccentric plaque and the peri-adventitial fat in the bottom right corner. At 1230 nm the signal is markedly lower, in accordance with the absorption spectrum of lipids in this wavelength range. Collocated with the enhanced 1210 nm IVPA signal a positive Oil Red O stain is observed, particularly in the plaque, indicating the presence of lipids. Variation in the laser pulse energy and tissue scattering properties is negligible over the wavelength range 1210 to 1230 nm.

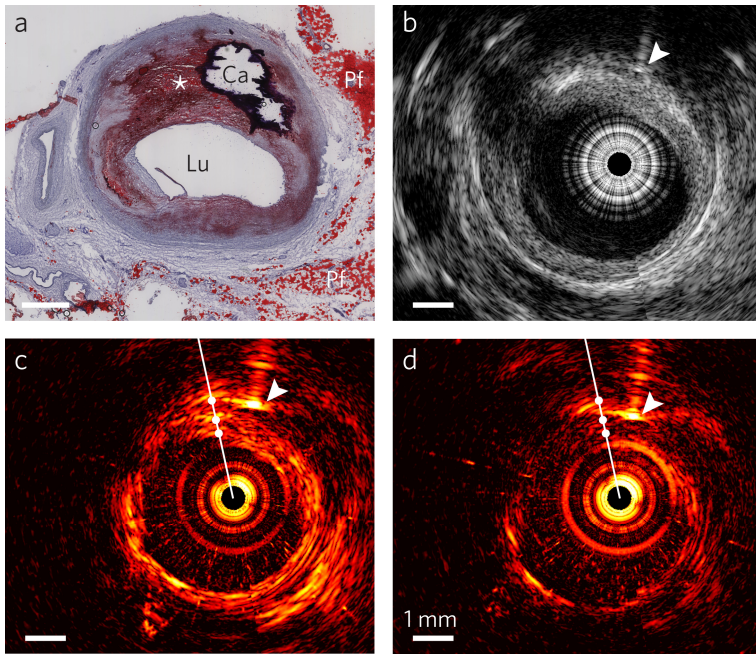


Figure 2. IVPA/IVUS imaging of an advanced human atherosclerotic plaque. a) Histology: Oil Red O stain shows the presence of a lipid rich plaque (*) as well as a calcified area (Ca); Lu: lumen, Pf: peri-adventitial fat. b) IVUS image, IVPA images at c) 1210 nm (high lipid absorption) and d) 1230 nm (low lipid absorption). Arrowheads indicate the needle used for marking. Full spectral scans were made along the white line in c) and d). The spectra at the locations marked by the white dots are shown in Figure 3.

Photoacoustic spectra were acquired along image lines sampling the plaque tissue. The resulting data sets are two-dimensional matrices of wavelength vs. depth. In Figure 3, spectra are shown at three locations, two inside the lipid-rich plaque region and one just outside. Absorption spectra of lipids and connective tissue³⁸ are included for reference. The two spectra located in the plaque clearly match the lipid reference, while the third clearly lacks the pronounced peak.

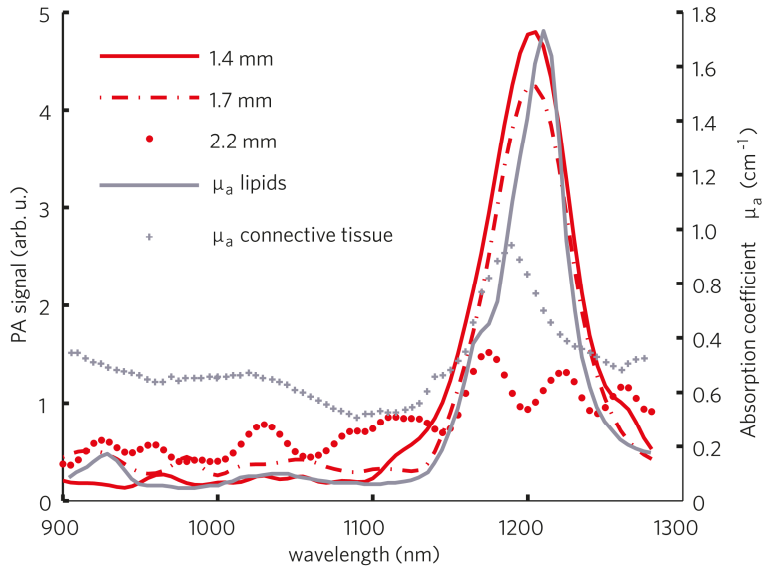


Figure 3. Photoacoustic spectra at 3 locations on the white line shown in Figure 2d. The sites at 1.4 mm and 1.7 mm distance from the catheter are located within the lipid rich plaque. The corresponding PA spectra show strong resemblance to the lipid absorption reference. The site at 2.2 mm is located just outside the plaque area.

Spectroscopic imaging is demonstrated on a second specimen (left main stem, female aged 43). The results are shown in Figure 4. The IVUS image of this cross section shows mild fibrous intimal thickening. Comparison of the combined IVPA/IVUS images at 1210 and 1230 nm shows the presence of lipids outside the vessel wall; this peri-adventitial fat is part of the normal anatomy. The average IVPA signal strength in this region, acquired from IVPA images at various wavelengths between 1180 and 1230 nm, closely tracks the lipid absorption peak shape.

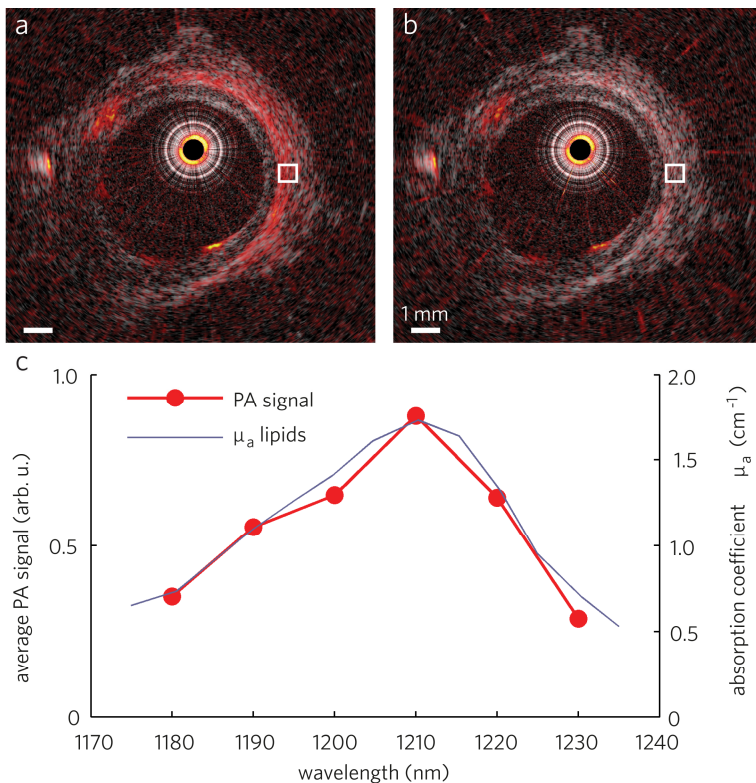
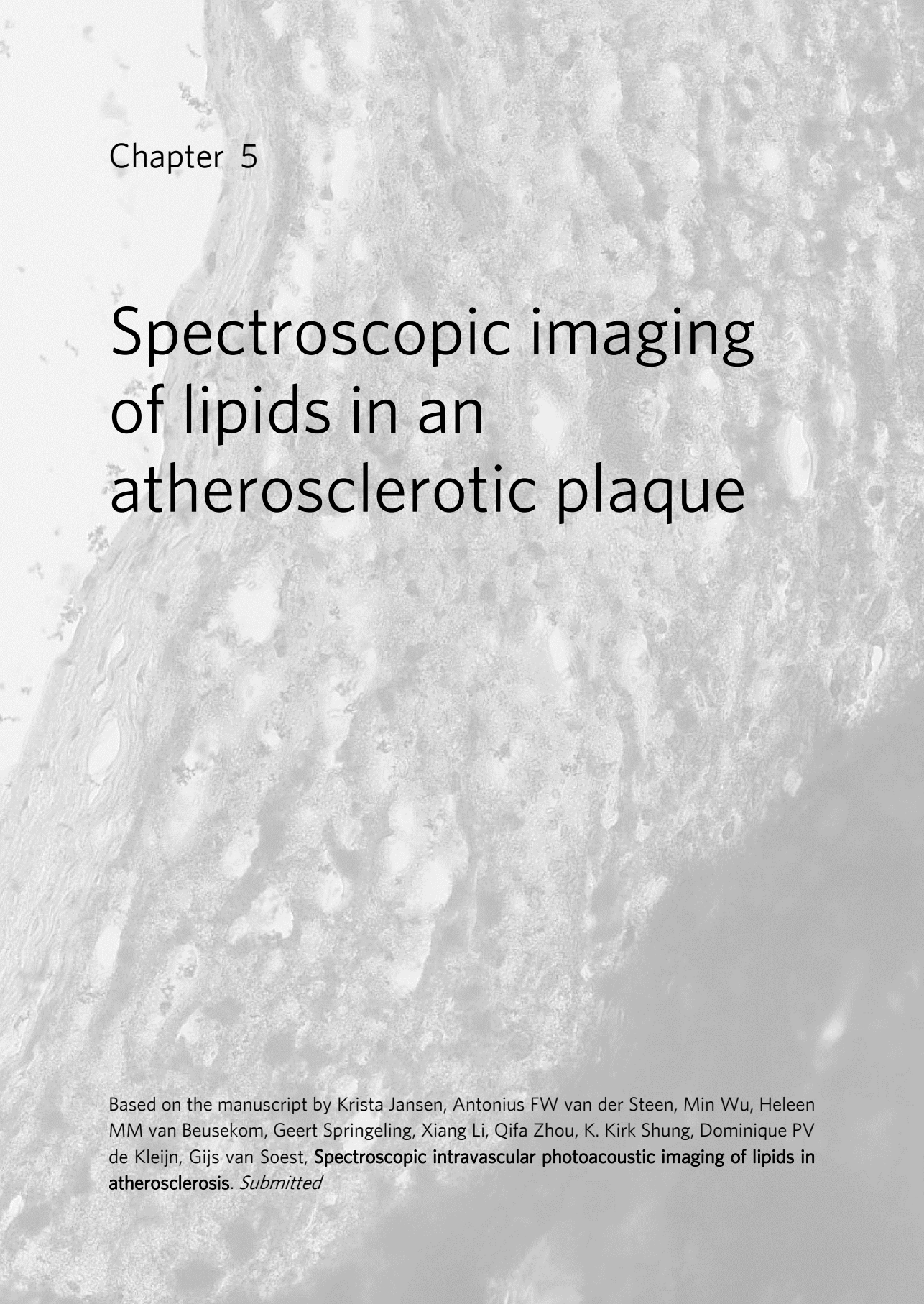


Figure 4. Combined IVPA/IVUS image at a) 1210 nm and b) 1230 nm of a healthy human coronary artery. c) Average IVPA signal strength in the area indicated in a and b, obtained from images at wavelengths between 1180 nm and 1230 nm, closely tracks the peak in the reference lipid absorption spectrum.

The design of a small diameter IVPA probe and the successful imaging of the lipid content of a human atherosclerotic plaque *ex vivo* demonstrated in this paper are important steps toward the realization of *in vivo* IVPA imaging. Two factors that prevent immediate translation to *in vivo* imaging are the diameter of our probe and the repetition rate of the laser. While our catheter is the smallest IVPA probe to date, it needs to be reduced to < 1 mm for clinical imaging. *In vivo* imaging at a frame rate of 20 images per second requires a significantly faster excitation source.

We have demonstrated specific imaging of lipids in *ex vivo* human coronary plaques. By combining data at different wavelengths in the lipid absorption spectrum, this key component of vulnerable plaques can be identified. By its hybrid optical/acoustic nature, IVPA is a natural addition to IVUS and extends its imaging capability with tissue type sensitivity.

A grayscale microscopic image of an atherosclerotic plaque, showing a complex, textured surface with various shades of gray and white, indicating different tissue components like lipids and fibrous structures.

Chapter 5

Spectroscopic imaging of lipids in an atherosclerotic plaque

Based on the manuscript by Krista Jansen, Antonius FW van der Steen, Min Wu, Heleen MM van Beusekom, Geert Springeling, Xiang Li, Qifa Zhou, K. Kirk Shung, Dominique PV de Kleijn, Gijs van Soest, **Spectroscopic intravascular photoacoustic imaging of lipids in atherosclerosis. *Submitted***

Abstract

The natural history of atherosclerosis is marked by changes in the lipid biochemistry in the diseased arterial wall. As lesions become more vulnerable, different cholesterol species accumulate in the plaque. Understanding unstable atherosclerosis as a pharmacological and interventional therapeutic target requires chemically specific imaging of disease foci. In this study, we aim to image atherosclerotic plaque lipids and other vessel wall constituents with spectroscopic intravascular photoacoustics (sIVPA). sIVPA imaging can identify lipids in human coronary atherosclerotic plaque by relying on contrast in the near-infrared absorption spectra of the arterial wall components. Using reference spectra acquired on pure compounds, we analyzed sIVPA data from human coronary plaques *ex vivo*, to image plaque composition in terms of cholesterol and cholesterol ester content. In addition, we visualized the deeper lying connective tissue layers of the adventitia, as well as the fatty acid containing adipose cells in the peri-adventitial tissue. We performed simultaneous co-registered IVUS imaging to obtain complementary morphological information. Results were corroborated by histopathology. sIVPA imaging is capable of distinguishing the most important lipid components of human atherosclerotic plaques: cholesterol and the two most prominent cholesterol esters, cholesterol oleate and cholesterol linoleate. It can also visualize the connective tissue layers of the adventitia and the fatty acid containing adipose cells in the peri-adventitial tissue.

Atherosclerosis is a chronic cardiovascular disease characterized by inflammation and lipid accumulation in the vessel wall. Myocardial infarctions are a leading cause of death worldwide¹. In the majority of cases, myocardial infarctions and strokes are caused by the rupture of an atherosclerotic plaque and the subsequent release of its thrombogenic content into the bloodstream². The term “vulnerable plaque” has been coined to indicate a plaque at high risk of rupture that could lead to thrombosis³. The susceptibility of a plaque to rupture – its vulnerability – is known to be related to plaque composition, mechanical stress distribution, inflammatory state^{3,4} and presence of positive remodeling⁶⁷. A prominent type of vulnerable plaque is the thin-cap fibroatheroma (TCFA). These lesions are characterized by a lipid-rich necrotic core covered by a thin fibrous cap that is weakened by macrophage infiltration and decreased smooth muscle cell content⁷.

The chemical composition of the lipid core is related to the age and stability of a lesion. Starting as a foam cell rich lesion (fatty streak) that contains cholesterol esters, supersaturation leads to cholesterol crystallization and cell death resulting in a more complex atherosclerotic plaque containing a necrotic core⁶⁸. The necrotic core contains cholesterol crystals and extracellular droplets of cholesterol esters. At the periphery of the lesion, cholesterol esters in foam cells dominate⁶⁹. The esterified lipid concentrations at the edge of advanced plaques often coincide with an increased macrophage activity and decreased cap thickness, leading to a predisposition to rupture⁶⁹. A concurring degradation of the supporting structure in the necrotic core enables its thrombogenic content to freely flow into the bloodstream upon rupture of the cap⁶⁸.

During plaque regression, for instance due to cholesterol lowering drugs or lifestyle changes, cholesterol ester content and numbers of foam cells and macrophages decrease. The lipid content of the cells is deposited in cholesterol crystals and the relative proportion of free cholesterol increases. Prolonged regression returns the lipid content of the artery wall towards normal, slowly dissipating the cholesterol crystals, and results in a lipid-poor but scarred intima⁷⁰. Interestingly, the cholesterol ester spectrum differs between developing and regressing lesions⁶⁸.

Temporal lipid content and composition changes of atheromatous plaques are a hallmark of atherosclerotic disease stage. Established techniques are unable to positively identify and quantify lipid content, or to distinguish between lipid types present in atherosclerotic plaques. Catheter-based near-infrared reflection spectroscopy (NIRS) uses optical absorption to signal the presence of lipid-core plaque in the coronary wall. It is, however, a sensing technology which cannot locate the position of the lipid-core relative to the lumen boundary³². By combining NIRS with intravascular ultrasound (IVUS), the most commonly used intravascular imaging technology in clinics worldwide, morphological information is added but lipid mapping still lacks depth resolution³¹. Other imaging modalities, like IVUS, optical coherence tomography (OCT), or X-ray computed tomography (CT), rely on backscatter and signal attenuation to interpret images in terms

of tissue type⁷¹⁻⁷³. In IVUS, percent atheroma volume (PAV) is the most commonly applied imaging markers for plaque regression^{74,75}. A modality that can assess plaque composition and morphology addresses multiple needs in cardiovascular medicine. It provides a chemical imaging biomarker that may acquire a role in clinical trials of drug or device therapies, to grade and monitor plaque regression. By the same merits, such a technique is a likely candidate to attain a prospective definition of vulnerable plaque, a diagnostic criterion that has been elusive since the concept was proposed^{7,76,77}.

Photoacoustic (PA) signals are generated in tissue when the absorption of short laser pulses causes the tissue to thermo-elastically expand. Since PA signals are acoustic waves, they can be recorded in the same manner as the pulse-echo ultrasound waves⁷⁸. Intravascular photoacoustic (IVPA) imaging is a catheter-borne version of PA imaging. It uses the intrinsic contrast in optical absorption between tissue types to visualize different constituents of atherosclerotic plaques. IVPA has been demonstrated to distinguish calcified plaque⁴², atheroma^{40,41}, and more specifically lipids^{44,46,79} from healthy vessel wall, as well as the presence of macrophages through the use of exogenous contrast agents⁵⁰.

We demonstrate that spectroscopic intravascular photoacoustic (sIVPA) imaging is capable of distinguishing the most important lipid components of atherosclerotic plaques: cholesterol and the two most prominent cholesterol esters, cholesterol oleate and cholesterol linoleate. In addition, we visualize the deeper lying connective tissue layers of the adventitia, as well as the fatty acid containing adipose cells in the peri-adventitial tissue. We performed simultaneous co-registered IVUS imaging to obtain complementary morphological information. We first determined the PA spectra of cholesterol, cholesterol oleate (CE18:1) and linoleate (CE18:2) to use as reference absorption spectra of lipids present in atherosclerotic lesions. These are primarily enhanced as atherosclerosis progresses and detailed absorption spectra are currently not available for these substances.

We then conducted spectroscopic photoacoustic imaging of human coronary arteries ex-vivo and show detailed local spectra of the different tissue constituents of the atherosclerotic vessel wall, demonstrating the ability of spectroscopic photoacoustic imaging to differentiate lipid types as well as connective tissue. For this purpose, we built an integrated photoacoustic and ultrasound imaging system capable of simultaneous, co-registered imaging of human coronary arteries ex-vivo. Histopathology of the imaged artery cross sections was performed to corroborate our findings.

Methods

Integrated catheter and system for intravascular imaging

We designed and built a hybrid IVPA/IVUS catheter, see Figure 1. The design is similar to devices we used in earlier work^{79,80}. It comprised a 400 μm diameter core optical fiber (Pioneer Optics, Bloomfield, CT) to deliver light pulses to the vessel wall and a lead magnesium niobate-lead titanate (PMN-PT) single crystal ultrasound transducer (custom built⁵⁸) to send and receive ultrasound waves. The tip of the fiber was polished at an angle of 34° and covered with a glued-on quartz cap to preserve an air-glass interface deflecting the beam by total reflection. The transducer had a center frequency of 44.5 MHz and a -6 dB fractional bandwidth of 45%. Fiber and transducer were mounted in an assembly with an outer diameter of 1 mm. The fiber tip and transducer center were separated by approximately 1.1 mm. The angle between the optical and acoustical beams was 22° ; the beams overlapped between 0.5 and 4.5 mm from the transducer. The imaging performance of the catheter is shown in Figure 2. We used this catheter to perform the PA spectroscopy measurements of cholesterol and cholesterol derivatives. Imaging of arteries was performed with the device described in Jansen et al.⁷⁹

The catheter was connected to a spectroscopy/imaging system⁷⁹. A tunable laser (Vibrant B/355-II, OPOTEK, Santa Clara, CA, USA) provided the excitation light (pulse width 5 ns, repetition rate 10 Hz, pulse energy 1.2 mJ at catheter tip) for photoacoustic imaging. An arbitrary waveform generator (WW2571A, Tabor Electronics Tel Hanan, Israel) transmitted a Gaussian-modulated cosine wave for pulse echo imaging, which was transmitted to the probe through a custom-built expander and limiter. The received US and PA signals were band pass filtered (13–60 MHz 5th order Butterworth, custom built), amplified by a 43 dB amplifier (AU1263, Miteq, Hauppauge, NY, USA) and digitized at a sample frequency of 350 MS s⁻¹ by a 12-bit data acquisition card (Acqiris DP310, Agilent, Santa Clara, CA, USA). A schematic of the experiment and photos of the catheter are shown in Figures 1a–1c.

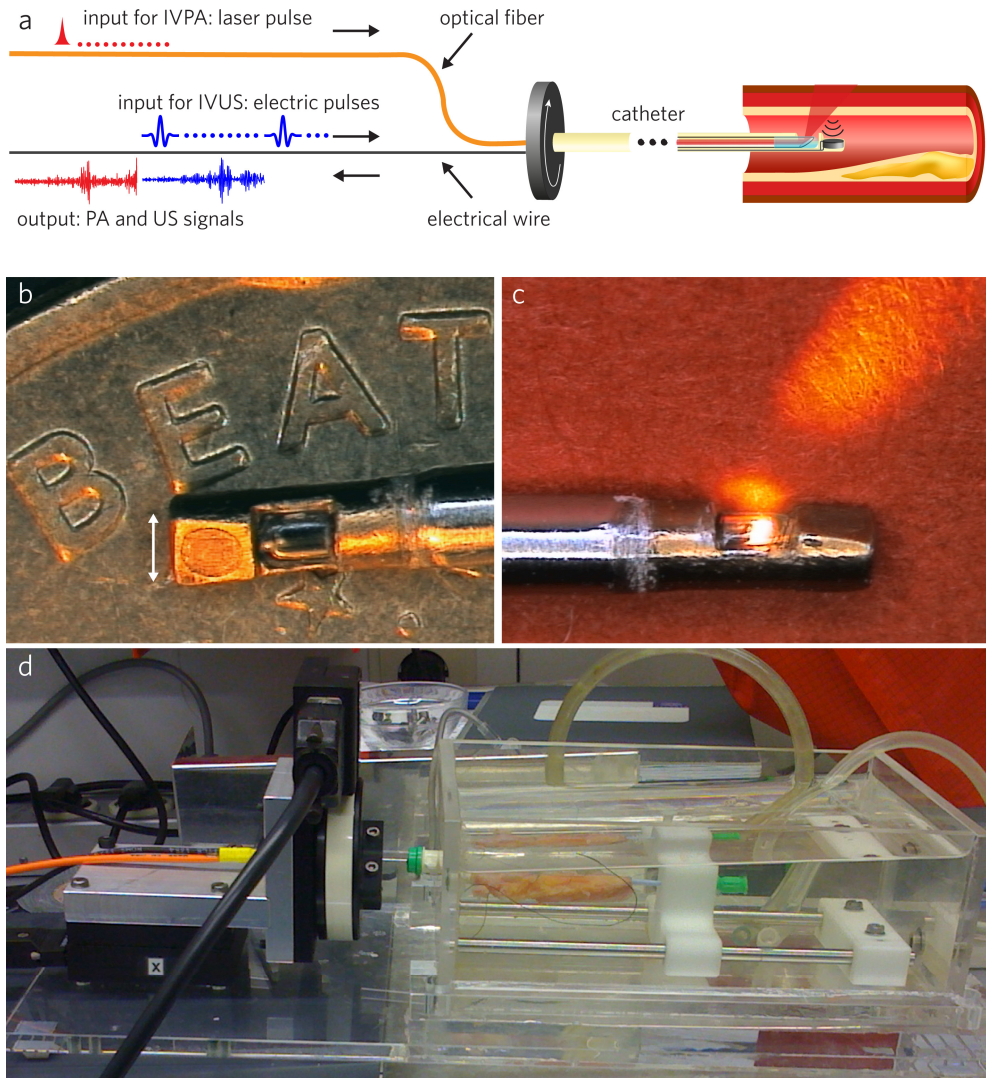


Figure 1. Combined IVPA and IVUS imaging. a) The intravascular IVPA/IVUS catheter is inserted in an ex vivo human coronary artery and rotated in 1° steps. Laser pulses for IVPA imaging and electric pulses for pulse echo (IVUS) imaging are delivered to the vessel wall interleaved at every angular position. b) Photograph of the catheter tip on the edge of a 10 eurocent coin. White arrow indicates 1 mm. c) Photograph of the catheter tip, showing the light beam exiting the catheter. d) Photograph of artery in setup, side view. On the left, the translation (x) and rotary stage are visible.

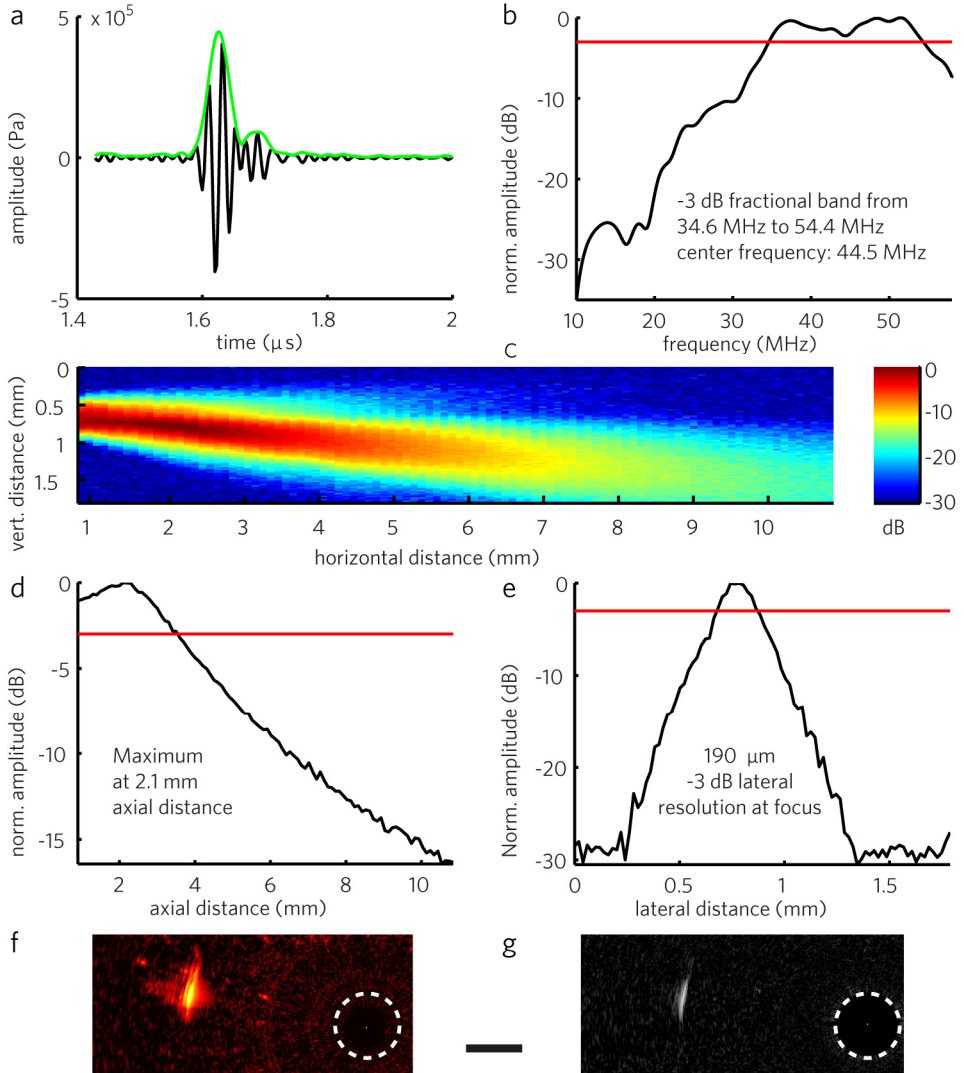


Figure 2. Imaging performance of the combined intravascular photoacoustic and ultrasound probe. a) Impulse response and b) its frequency spectrum measured with a needle hydrophone (75 μm tip, calibrated from 2 to 60 MHz, Precision Acoustics, LTD) in the far field, at 2.3 mm (excitation pulse: monocycle negative impulse, -5 V peak negative, 43 dB amplification). c) Beam profile, d) maximum intensity vs. axial distance, and e) lateral beam profile at the natural focus, measured with the same needle hydrophone (excitation pulse: Gaussian modulated sine, center frequency 44.5 MHz, 44.5% -6dB bandwidth, 10 V_{pp}, 43 dB amplification). f) 1205 nm IVPA, and g) IVUS image (excitation pulse: Gaussian modulated sine, center frequency 44.5 MHz, 50% -6 dB bandwidth, 10 V_{pp}, 43 dB amplification) of a 15 μm diameter metallic wire at 3 mm from the transducer.

Cadaver coronary artery acquisition and handling

We obtained coronary arteries from the Department of Pathology of the Erasmus MC at autopsy and imaged them within 24 h post mortem. Consent was obtained from the relatives and the protocol was sanctioned by the Medical Ethics Committee of the Erasmus MC (MEC-2007-081).

The specimens were mounted on two cannulas in a tank containing saline solution. Large side branches were closed and arteries were pressurized to 100 mmHg to maintain an open lumen. A photograph of an artery mounted in the setup is shown in Figure 1d.

Combined photoacoustic and ultrasound imaging of human coronary arteries

The cadaveric coronary arteries were imaged at room temperature within 24 h *post mortem*. We performed an IVUS pullback of the arteries (iLab system with Atlantis SR Pro catheters; Boston Scientific, Fremont, CA, USA) to find sites of interest, and marked them using suture needles. The combined IVPA/IVUS catheter was mounted in a rotation/translation stage (Steinmeyer, Albstadt, Germany; see Figure 1d. The suture needles were located and at these sites co-registered IVPA and IVUS cross-sectional scans were made.

Optical and ultrasound transmissions alternate for exactly coregistered data acquisition, as illustrated in Figure 1a. This procedure results in IVPA and IVUS images of the arterial cross section, as shown in Figures 2a and 2b, respectively. The image shown here was acquired at 1210 nm. The IVUS and IVPA data sets may be overlaid to create a compound display (Figure 3c). Spectral scans were made at selected angles. One scan results in a two-dimensional data matrix, shown in Figure 3d, containing the PA spectra at the different distances from the catheter. Local absorption spectra can be extracted, as shown in Figure 3e. Histology (Oil Red O stain; Figure 3f) confirms the presence of lipids in the areas with a high photoacoustic signal at 1210 nm.

The ultrasound images were created in conventional pulse-echo mode. We transmitted a 10 V peak to peak Gaussian-modulated cosine wave with a center frequency of 30 MHz and a 100% -6 dB bandwidth. Two-dimensional images were obtained by rotating the catheter in 1° steps and repeating the ultrasound pulse-echo measurement in every direction.

IVPA images were acquired at several excitation wavelengths around 1200 nm. No averaging was applied for IVPA imaging; IVUS traces were averaged 10-fold. Digitized IVPA and IVUS data were band pass filtered (10–40 MHz 300th order zero-phase forward and reverse finite impulse response [FIR] filter), Tukey windowed, enveloped and log compressed. The data were then converted to Cartesian coordinates and displayed using the 'hot' and 'gray' colormaps in Matlab (The Mathworks, Natick, MA, USA) for the IVPA and IVUS images, respectively. Combined IVPA/ IVUS images were

created by overlaying the IVPA data on IVUS image using a nonlinear red-yellow-white color scale and a linear transparency scale. All data processing was done using Matlab R2007b.

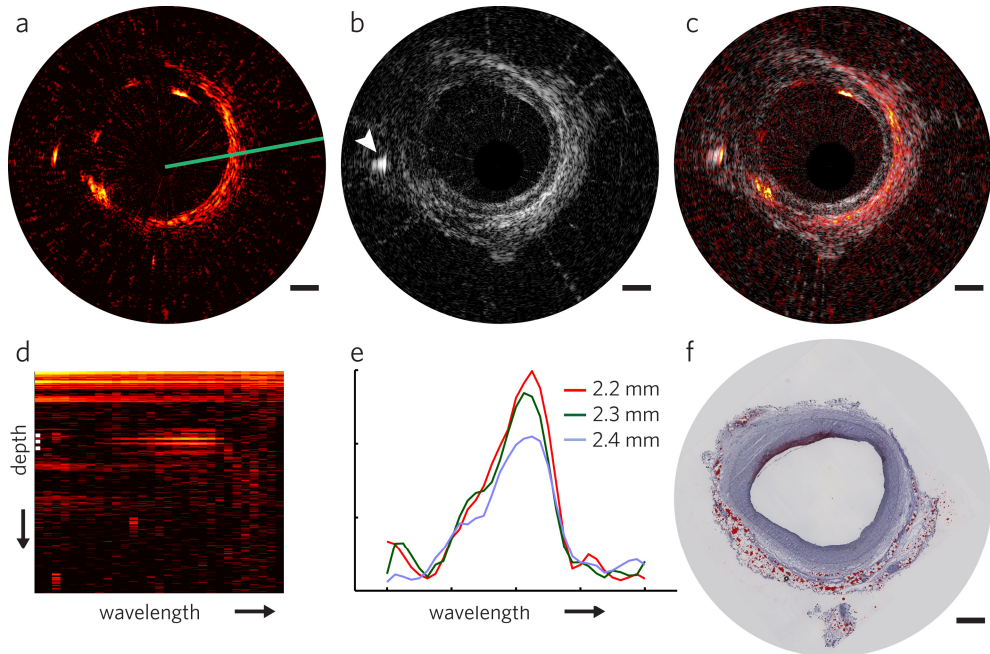


Figure 3. Spectroscopic IVPA imaging. Co-registered IVPA and IVUS data are processed to create IVPA a), IVUS b) and combined IVPA/IVUS c) images. At selected angular positions, indicated by the green line, 2D spectral IVPA d) data are recorded by changing the wavelength of the light while keeping the catheter at rest. e) Spectra at several locations in the vessel wall are extracted f) IVPA and IVUS images are matched to histology stains for tissue characterization. Scale bars indicate 1 mm. Dynamic range of IVPA and IVUS images is 28 dB.

PA spectroscopy of cholesterol and cholesterol derivatives

A small volume of lipid material (cholesterol, cholesterol oleate and cholesterol linoleate; all from Sigma Aldrich Chemie BV, Zwijndrecht, The Netherlands) was positioned directly in front of the catheter tip. They were contained in a holder, made of TPX and designed to minimize acoustic reflections. We recorded spectral PA data by recording the signal trace generated by the lipids at wavelengths between 1125 nm and 1275 nm, spaced by 2 nm. This procedure resulted in a two-dimensional data set as in Figure 3d. The differences in molecular structure between the three cholesterol species are illustrated in Figure 4.

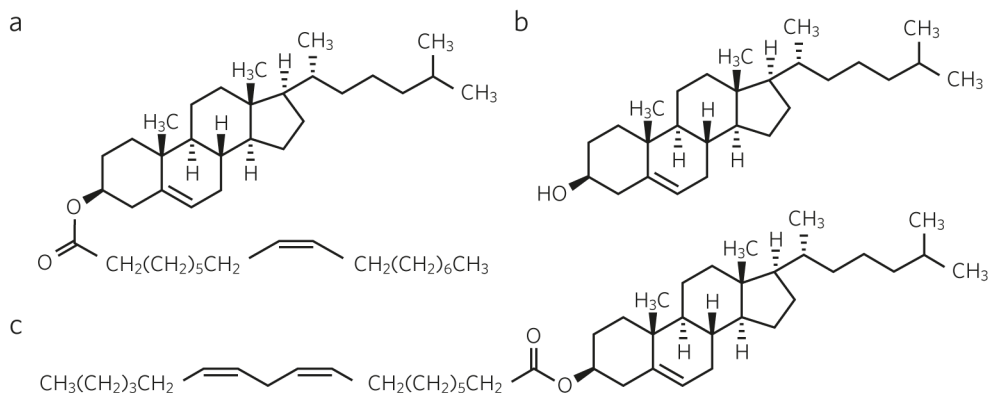


Figure 4. The molecular structure of the main lipid species in atherosclerotic lesions. Molecular structures of a) cholesterol oleate ($C_{45}H_{78}O_2$), b) cholesterol ($C_{27}H_{46}O$) and c) cholesterol linoleate ($C_{45}H_{76}O_2$).

The magnitude of the locally generated PA signal is dependent on the local fluence, the absorption coefficient and the Grüneisen parameter of the tissue. The Grüneisen parameter, representing the thermo-acoustic efficiency, is dependent on the sound speed, the thermal expansion coefficient and the specific heat at constant pressure. It therefore varies between different tissue types. Since the differences in local fluence are negligible within a small wavelength range, local variations in the PA signal amplitude with wavelength can be interpreted as changes in the absorption coefficient. We concentrated on the spectral range near 1200 nm where a prominent harmonic of the C—H stretch vibrational mode signals the presence of lipids⁶⁶. Moreover, we take advantage of the fact that the absorption spectrum of connective tissue is markedly different from that of lipids in this wavelength range, while the absorption of water is relatively low. We analyzed the data and determined the 32 times averaged normalized PA spectra for the three lipids.

Robustness of the spectra was investigated by studying the individual variations in single-shot spectra, and monitoring the spectral shape for different depths in a sample. The stability of the spectrum was evaluated by repeating the measurement several times over 75 minutes.

PA spectroscopy of human coronary arteries

At each imaging location, in addition to the IVPA/IVUS images acquired at several excitation wavelengths, full spectral scans were made at particular angular locations, which were selected based on IVUS morphology. Spectral PA data were recorded from 715 to 1800 nm with 5 nm steps. The data were then processed, as illustrated in Figure 5. After the bandpass filtering operation described above, we selected regions containing

the tissue and reference signals. The reference data contain non-saturated signal close to the catheter that is due to light absorption in the catheter, which generates an artifacts. The amplitude of this signal was used to correct for variations in light intensity. Subsequently, the data were upsampled, jitter corrected, and downsampled to the original sample frequency. The data in the signal region was then Tukey windowed and corrected for variations in the light intensity using the jitter corrected reference data. We extracted the envelope of the tissue signal. Next, locations of high signal intensity were chosen automatically by selection of all peaks above a certain threshold in the 1195 nm enveloped signal trace. Spectra at those locations were noise filtered using a fourth order digital smoothing polynomial (Savitzky-Golay; SG) filter.

Histopathology of the atherosclerotic human arteries

After imaging, the arterial specimens were cut at the imaging plane and serially sectioned for histology staining. The segment proximal from the image plane was fixed in 4% buffered formaldehyde and embedded in paraffin. The tissue block was serially sectioned (5 μm thickness) at the imaging plane and stained by Hematoxylin-Eosin (H&E) and Resorcin-Fuchsin (RF). The segment distal from the imaging plane was embedded in optimal cutting temperature (OCT) compound (Tissue-Tek®, Sakura Finetek Europe B.V.), frozen in isopentane vapor at 77K, and stored at $-80\text{ }^{\circ}\text{C}$ until serial sectioning (20 μm thickness) for Oil Red O (ORO) and H&E. Tissue sections were viewed and digitized using a whole-slide scanner (Nanozoomer, Hamamatsu Photonics, K.K.). The ORO staining identifies lipids (stained red). The H&E stained sections were used to assess tissue morphology.

Results

PA spectroscopy of cholesterol and cholesterol derivatives

Measurement of the photoacoustic signal of cholesterol, cholesterol oleate and cholesterol linoleate in the 1200 nm range yielded three distinct photoacoustic spectra (Figure 6). The absorption features in this wavelength range are caused by the second overtones of the vibrational modes of the C-H bonds in the molecules^{38,66}. Wavelength shifts and intensity changes between the spectra of cholesterol, cholesterol oleate and cholesterol linoleate originate from the differences in their molecular structures: the cholesterol esters have a fatty acid tail that consists mainly of CH₂ groups (Figure 4).

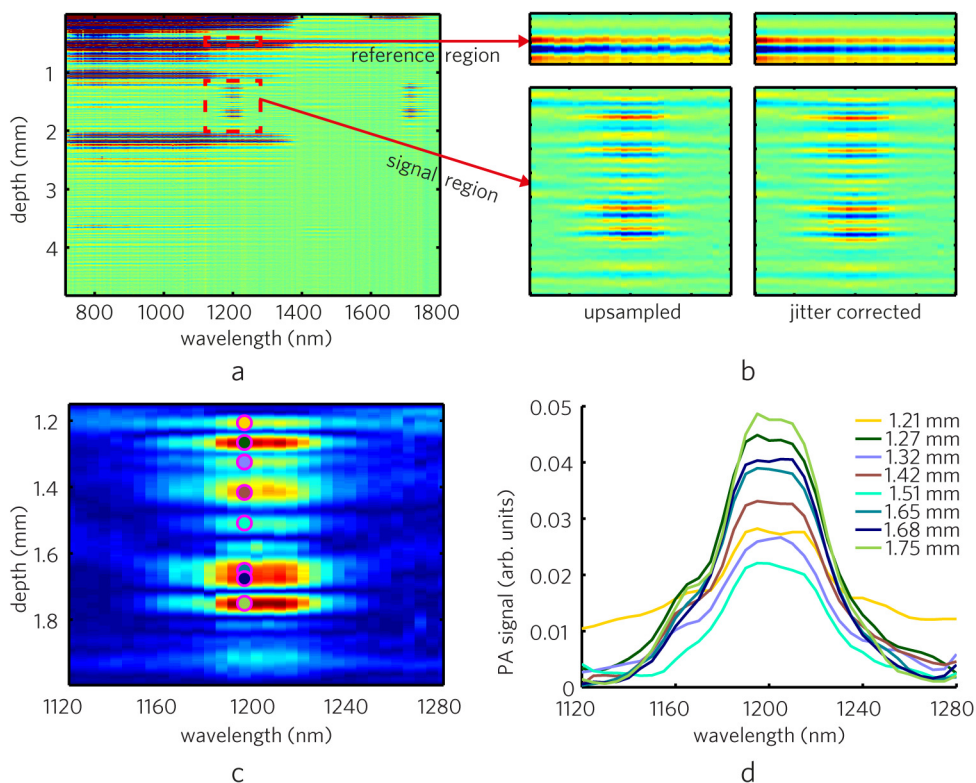


Figure 5. sIVPA data processing to obtain depth-resolved IVPA spectra. a) Band pass filtered PA traces at different wavelengths. Regions containing the tissue (bottom rectangle) and reference (top rectangle) signals, are indicated. b) Upsampling and jitter correction. c) Light intensity corrected data in the tissue signal region with colored circles marking peaks above a certain threshold in the signal envelope of the PA trace at 1195 nm. d) Resulting spectra at those sites after noise filtering.

The two highest peaks at approximately 1196 nm (1192 nm for cholesterol) and 1210 nm are associated with the asymmetrical stretching modes of the methyl (CH₃) and methylene (CH₂) group vibrations, respectively, while the symmetrical stretching modes of the same groups are visible only as a shoulder or inflection points around 1151 nm and 1167 nm, respectively⁸¹.

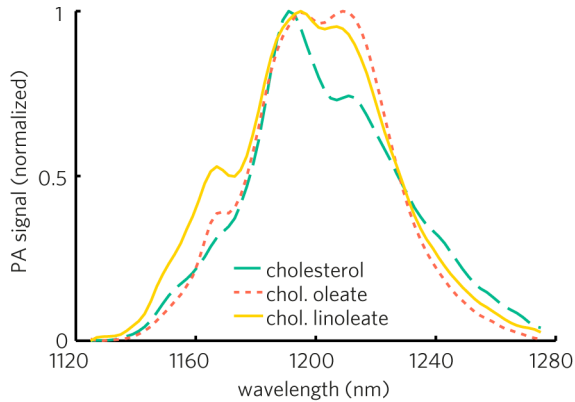


Figure 4. Absorption spectra of cholesterol, cholesterol oleate and cholesterol linoleate in the 1200 nm wavelength region as recorded by photoacoustic spectroscopy exhibit clear differences.

The robustness of the recorded spectra was evaluated by studying the reproducibility of spectra without averaging and by comparing averaged sets at different depths. Figure 5 summarizes the results of these experiments for one of the pure lipid compounds investigated. In Figure 7a the difference between unaveraged spectra is shown to be very small, in the order of a few percent of the total signal. We attribute the remaining variation to measurement noise that is not adequately smoothed by the SG filter. Likewise, the spectra acquired at different depths are very similar (Figure 7b).

The stability of the absorption spectrum over time is demonstrated by the data in Figures 5c and 5d: we see a moderate increase in signal strength, but no change in spectral shape. The change in signal amplitude may be attributed to variations in packing density and water content in the lipid sample. Over time, the (unsaturated) lipid in the container is likely to be oxidized. We see that the spectrum appears to be robust against such variations.

IVPA spectroscopy of human coronary arteries

We performed dual-modality imaging of a human coronary atherosclerotic artery (left anterior descending artery, male aged 56) *ex vivo*. Co-registered IVPA and IVUS data was obtained at multiple cross-sections. The data were processed to obtain combined IVPA/IVUS images (Figure 8a). The artery was then cut at the imaging plane and serially sectioned for histology staining (Figure 8b).

Histology exhibited a large eccentric lipid-rich lesion containing a calcification, and a circumferentially thickened, lipid-laden intima. The artery was embedded in peri-adventitial fat. While the IVUS image confirmed the morphology of the artery as shown in Figure 8a, the 1210 nm IVPA image overlaid on it displayed regions of high PA signal intensities that correspond to the lipid rich regions.

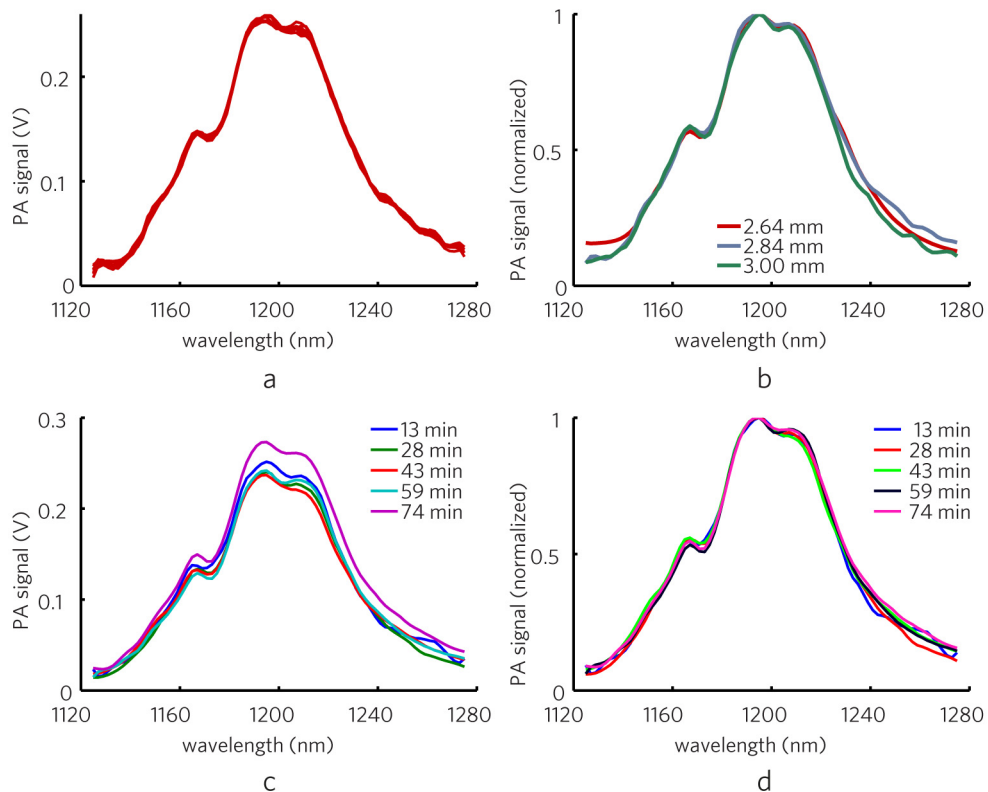


Figure 7. Robustness of lipid PA spectroscopy, showing data from cholesterol linoleate as an example. a) Comparison of “single-shot” spectra. b) Spectra obtained at different depths. c) Evolution of the spectral amplitude over time. d) Data from panel c after normalization.

Positive confirmation of the presence and identification of lipids requires wavelength-dependent measurement. In the two directions indicated by the white lines, labeled # and *, in the IVPA/IVUS image, we acquired spectroscopic IVPA data. Spectra in tissue were composed from one single IVPA acquisition per wavelength, creating a data set as in Figure 3d, and then plotting the signal strength as a function of wavelength at a single pixel in depth. We show the IVPA spectra of different tissues in Figure 8.

The first direction (#) contained atherosclerotic plaque (Figure 8c), while the second line-of-sight (*) intersected with the lipid-rich diseased intima (Figure 8d), the adventitia (Figure 8g) – the outermost layer of the vessel wall consisting of connective tissue – and a region of peri-adventitial tissue (Figure 6h) composed mainly of adipocytes (fat cells) containing fatty acids³⁸.

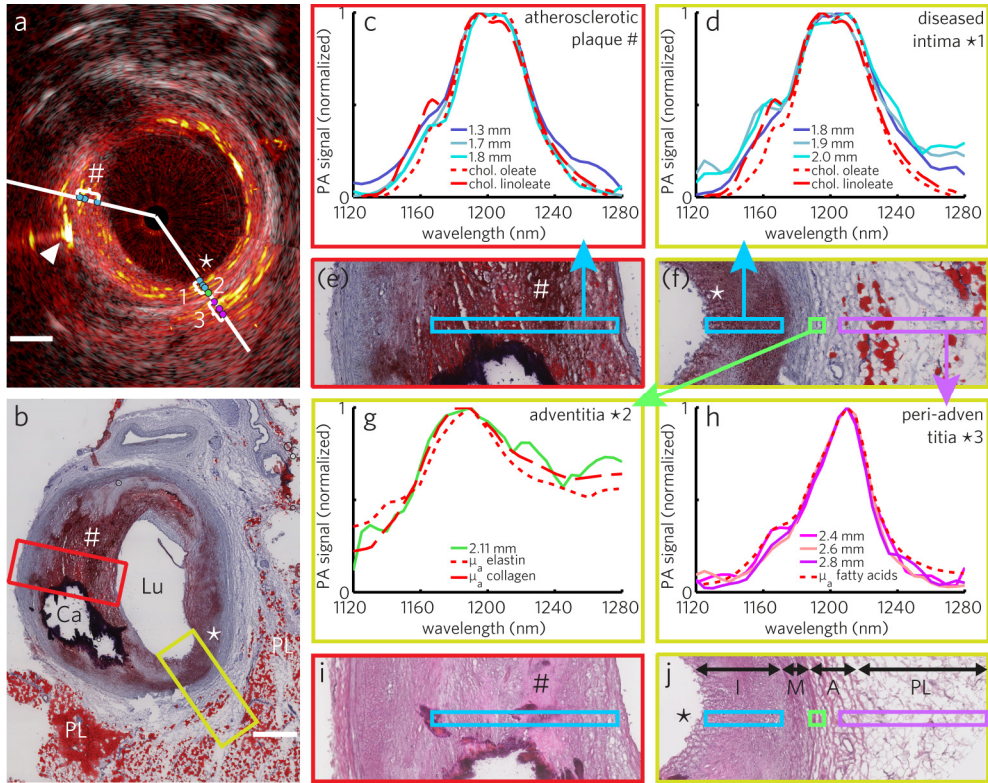


Figure 8. IVPA spectra of a human atherosclerotic coronary artery, ex vivo. a), Dual-modality IVPA/IVUS image, arrowhead indicates suture needle. Along the white lines (# and *), spectral IVPA data were obtained. Normalized IVPA spectra at the locations of the dots are shown in c), d) g), and h), compared to absorption spectra obtained in Figure 6 and reference spectra for collagen, elastin and fatty acids from literature³⁸. b) Histology section of the site imaged in a, showing near circumferential intimal lipid accumulation (red) and presence of a calcification (Ca). The lipid rich core (#) and pathological intimal thickening (PIT; *) are magnified (3x) in e) and f) showing the locations where the IVPA spectral data are recorded. Oil Red O stain, Lu = lumen, PL = peri-adventitial lipid, Ca = Calcium, bar = 1 mm. i) Hematoxylin-Eosin (H&E) histologic stain of the area #, showing reduced cellularity in the plaque. j) H&E stain of the area *, showing PIT and an intact media. Scale bars indicate 1 mm. Dynamic range of IVPA and IVUS image is 40 dB.

We found that the lipid laden atherosclerotic plaque and diseased intima (Figures 6c and 6d, respectively) both had IVPA spectra that closely resemble the reference PA spectra of cholesterol oleate and cholesterol linoleate obtained on the pure compounds. This finding was in agreement with the assessment of the corresponding areas in the histological sections (Figures 6e,i and 6f,j, respectively), that showed lipid rich foam cells

and extracellular lipid droplets, but no cholesterol crystals. The H&E stain (Figures 6i,j) shows differences in cell density and orientation of cells in the intima (cell nuclei are colored blue/purple). The lower cell density of the more central plaque areas (Figure 8i) indicates a more advanced state of atherosclerosis with extracellular lipids (larger red spots in central region of ORO stain (Figure 8e). H&E (Figure 8j) also illustrates the much larger adipocytes in the peri-adventitial region

The IVPA spectrum found in the adventitia, shown in Figure 8g, was very similar to both the absorption spectra of elastin and collagen, while the IVPA spectra of the lipid-rich peri-adventitial tissue (Figure 8h) resembled the absorption spectrum of the reference fatty acid mixture³⁸.

Discussion

Photoacoustic imaging adds highly detailed chemical information to existing diagnostic techniques for coronary atherosclerosis. We show its ability to outline fat deposits and to distinguish between plaque lipids and peri-adventitial lipids. The composition of lipid-rich plaques can be differentiated in cholesterol and a range of cholesterol esters by photoacoustic spectroscopy, opening up a new dimension for in vivo plaque characterization. Characteristic spectral signatures of collagen and elastin identify the adventitia; a contrast that may be of use in plaque imaging as well. No other clinically feasible imaging technique images the vessel wall and atherosclerotic plaque composition with such chemical specificity.

IVPA is unique in its ability to distinguish the lipids present in atherosclerotic plaque at a high depth resolution of approximately 100 μm . Its visualization of different constituents of atherosclerotic plaques and deeper layers of the vessel wall is based on the intrinsic contrast in optical absorption between tissue types. The optical absorption spectrum is a much more specific tissue identification criterion than parameters like the attenuation and backscatter coefficients, that other techniques rely on for plaque composition. The background for this difference is that both optical scattering (which dominates optical attenuation) and acoustic absorption (which dominates acoustic attenuation) are slowly varying with frequency, so distinctive features like those seen in Figure 2 are not available for detailed composition imaging. NIRS, like IVPA, uses absorption spectra to determine lipid content, but does not have depth sensitivity. As a consequence, it can identify the presence but not the amount or the position of the lipid accumulation. NIRS has been combined with IVUS to add structural information but exact localization of the lipid core cannot be realized³¹.

With the composition information provided by IVPA, tissue maps can be created, showing the location of different kinds of lipids (free cholesterol, cholesterol esters in foam cells or extracellular lipid droplets) as well as other tissue types (collagen, elastin) on top of the morphological picture provided by IVUS. Cholesterol oleate and cholesterol

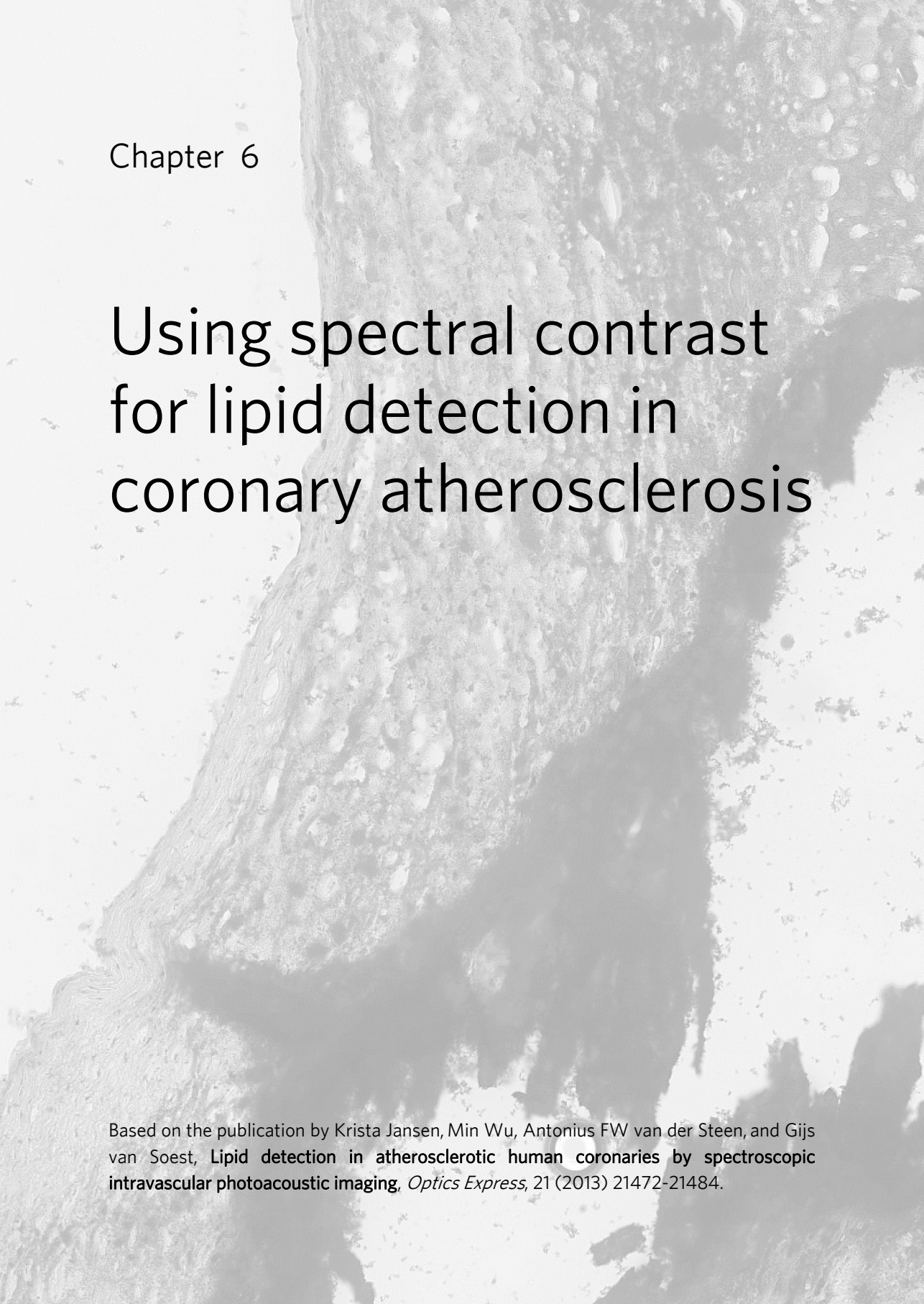
linoleate together account for more than 67% of cholesterol esters present in lipid-rich lesions, while cholesterol esters and cholesterol together make up 79% of total lipids⁸². In the present study, we investigated the contribution of the three most significant components in the plaque lipid spectrum. Future studies need to establish the level of detail to which IVPA can unravel the lipid composition of plaques; this is both a fundamental question of the chemical specificity of the different absorption spectra as well as a technical question: how accurately can we measure the spectra to exploit that specificity, at a practical number of wavelengths? It is unknown at present how much composition detail is needed to establish whether a lesion is progressing towards rupture, quiescent or regressing towards stability. Beyond lipid composition, IVPA may be able to distinguish other tissue types or plaque characteristics that play a role in coronary artery disease, such as calcium, macrophages and intraplaque hemorrhage by choosing a different wavelength range or using exogenous contrast.

Two issues that come into play when imaging *ex vivo* and need addressing, are lipid oxidation and temperature. Unsaturated lipids, such as cholesterol oleate and cholesterol linoleate, become oxidized when imaged *ex vivo*. But lipids in atherosclerotic lesions are partially oxidized as well: in freshly obtained carotid and femoral atherosclerotic plaque approximately 30% of plaque cholesterol linoleate was found to be oxidized, with CE18:2-OH and CE18:2=O (two oxidized forms of cholesterol linoleate) being the predominant forms⁸³. However, since the number of C-H bonds does not change with oxidation, no change in the relative peak strengths in the absorption spectrum is expected; this supposition is strengthened by the results of the separate lipid PA measurements, where an increase in the level of oxidation of the lipids with time was anticipated, and the spectra remained structurally unchanged over time, as demonstrated in Figure 7. Similarly, a change in temperature from body temperature to room temperature is not expected to influence the position of peaks or relative peak height within the IVPA spectra, since these are dependent on the molecular structure, which does not change with temperature. NIRS was validated under the same assumptions³² and spectra were shown to be similar *ex vivo* and *in vivo*⁸⁴.

For translation to *in vivo* imaging, several changes to the system need to be realized. The catheter needs to be further miniaturized and fitted with a compatible outer sheath. It needs to be coupled to a real-time imaging system through an interface unit containing a motorized fiber optical and pullback system, to make continuous rotation and simultaneous translation possible. Furthermore, the minimum number of wavelengths required to determine tissue type needs to be established, reducing acquisition time. A sufficient level of tissue composition information may be obtained by using three wavelengths only, if chosen wisely. Lasers to generate such wavelengths at fast enough pulse rates to achieve clinically feasible frame rates are currently under development.

We demonstrated the ability of IVPA to distinguish lipid types as well as other kinds of tissues in coronary atherosclerosis. This functionality can aid in gaining further

understanding of the disease: it adds a new dimension to in vivo studies of progression and regression processes of plaque. This new functionality has a direct application in more complete visualization of coronary wall pathology for clinical decision making. Impacts in the medium to longer term include the introduction of highly detailed chemical imaging biomarkers as an endpoint in studies evaluating pharmacological therapies, and to measure the response of the arterial system to lifestyle changes in clinical trials. Imaging lipid composition in atherosclerotic plaque in vivo, and relating that information to its stage of advancement will contribute to further understanding of the development of the natural history of atherosclerosis. Finally, detailed imaging of plaque biochemistry and lipidomics may provide a jump-off point for personalized medicine in interventional cardiology, if we can predict the vascular response to an intervention of a specific site in a specific artery in a specific patient.

A grayscale microscopic image of atherosclerotic tissue, showing a large, irregular, and textured plaque area with various shades of gray, indicating different tissue compositions and structures. The plaque is set against a lighter, more uniform background.

Chapter 6

Using spectral contrast for lipid detection in coronary atherosclerosis

Based on the publication by Krista Jansen, Min Wu, Antonius FW van der Steen, and Gijs van Soest, **Lipid detection in atherosclerotic human coronaries by spectroscopic intravascular photoacoustic imaging**, *Optics Express*, 21 (2013) 21472-21484.

Abstract

The presence of lipids in atherosclerotic coronary lesions is an important determinant of their potential to trigger acute coronary events. Spectroscopic intravascular photoacoustic imaging (sIVPA) has the potential to automatically detect lipids in atherosclerotic lesions. For real-time in vivo imaging, limiting the number of excitation wavelengths is crucial. We explored methods for plaque lipid detection using sIVPA, with the aim to minimize the number of laser pulses per image line. A combined intravascular ultrasound (IVUS) and photoacoustic imaging system was used to image a vessel phantom and human coronary arteries ex vivo. We acquired co-registered cross-sectional images at several wavelengths near 1200 nm, a lipid-specific absorption band. Correlating the photoacoustic spectra at 6 or 3 wavelengths from 1185 to 1235 nm with the absorption spectrum of cholesterol and peri-adventitial tissue, we could detect and differentiate the lipids in the atherosclerotic plaque and peri-adventitial lipids, respectively. With two wavelengths, both plaque and peri-adventitial lipids were detected but could not be distinguished.

Introduction

Coronary atherosclerosis is the largest cause of death in Western countries¹. Most myocardial infarctions are triggered by the rupture of a so called vulnerable plaque². The susceptibility of a plaque to rupture, its vulnerability, is determined by the morphology and composition of the plaque. The pathological phenotype associated with vulnerable plaques is the thin-cap fibroatheroma (TCFA), characterized by a macrophage infiltrated thin fibrous cap, covering a lipid rich necrotic core³⁻⁵. The necrotic core contains cholesterol crystals and extracellular droplets of cholesterol esters⁶⁹. When the thin cap ruptures, due to high mechanical stresses, the lipid rich thrombogenic content of the TCFA can flow freely into the bloodstream and potentially causes an occlusion at the rupture location or downstream from that site. The presence and location of atherosclerotic lipids are therefore important markers of plaque vulnerability.

No established technique can positively quantify and locate the lipid content of atherosclerotic plaques. Intravascular ultrasound (IVUS) produces cross-sectional images of the arterial wall based on the reflected amplitude of ultrasound pulses. Due to minimal contrast between soft tissue constituents, the sensitivity and specificity of IVUS grayscale for plaque composition is limited⁸⁵. IVUS radiofrequency data analysis techniques for tissue characterization, namely VH-IVUS (20 MHz, phased-array transducer, Volcano Therapeutics), and iMapTM (40 MHz, mechanical-type transducer, Boston Scientific), have been developed as an extension to grayscale imaging²². However, the accuracy of VH-IVUS in complex lesions in a porcine model was limited^{24,25}. Significant and systematic variability in plaque composition estimates was found in a study comparing VH-IVUS and iMap *in vivo*²⁶. Intravascular optical coherence tomography (IVOCT) utilizes the delay in backscattered light to form an image of the illuminated tissue. Tissue characterization by IVOCT is currently under development³⁰. OCT mainly relies on scattering contrast, which suggests that the chemical specificity is likely to be limited. Near infrared reflection spectroscopy (NIRS) is an intravascular catheter-based technique that utilizes optical absorption to detect lipid-core lesions. It lacks depth resolution, however, and cannot locate the position of the lipid-core relative to the lumen boundary⁸⁶. By combining NIRS with IVUS, morphological imaging is added to lipid detection, but the amount and the location of the lipid relative to the lumen remains unknown³¹.

Intravascular photoacoustics is an emerging technique that has the ability to image lipids in atherosclerotic lesions. It utilizes differences in the optical absorption spectra to identify tissue types. A specific tissue type in the arterial wall can be visualized by selecting an excitation wavelength that is strongly absorbed by that particular tissue. The chemical absorption spectrum then represents the molecular composition of the tissue. Well-known applications of spectroscopic PA imaging are detection of exogenous chromophores⁸⁷ and quantification of blood oxygenation⁸⁸. The capability of

spectroscopic IVPA (sIVPA) to image lipids in human coronary atherosclerotic arteries has been demonstrated *ex vivo*⁷⁹. More recently, *in vivo* IVPA imaging of lipids inside the vessel wall of an abdominal rabbit aorta has been shown⁴⁸. Spectral differences between lipid-rich and normal vascular tissue have been outlined by photoacoustic measurements of human aorta samples⁴⁶ and pig carotid arteries⁸⁹. In sIVPA, lipid content can be deduced from the photoacoustic spectra or comparison of co-registered IVPA images at different wavelengths.

To be useful in the clinic, as a research tool or to guide percutaneous coronary interventions, however, atherosclerotic lipid content information needs to be readily available without the need for observer-dependent and time-consuming image interpretation. Ideally, only the lipids present within atherosclerotic plaques in the vessel wall are displayed, while the peri-adventitial lipids, which are a component of the normal vessel wall anatomy, remain hidden. That way, in an artery pullback, the cross-sections that contain plaque lipids will be obvious and can be distinguished easily, without clutter by false-positives from normal adipose tissue. For translation to *in vivo* imaging, where motion artifacts and thus imaging speed play an important role, the number of wavelengths needs to be as small as possible.

In this study, we present a number of methods that provide sIVPA lipid detection in a semi-automated manner. We obtained sIVPA images of a lipid containing vessel phantom using a combined IVPA/IVUS imaging system and catheter. The collected sIVPA data were used to develop the different lipid detection methods. The methods were then fine-tuned and tested on sIVPA data of *ex-vivo* human coronary arteries, obtained using the same dual modality imaging system.

Methods

Combined intravascular ultrasound and photoacoustic imaging system

The dual modality imaging system for co-registered IVPA/IVUS imaging has been previously developed and described⁷⁹. A tunable laser (OPOTEK Vibrant B/355-II) supplied the excitation light (pulse width 5 ns, repetition rate 10 Hz, pulse energy 1.2 mJ at catheter tip) for photoacoustic imaging. A tapered multimode fiber (Oxford Electronics, Four Marks, UK; input diameter 1 mm; output diameter 360 μm) collected the free space laser light output and delivered it to an in-house designed and built catheter. Two hybrid IVPA/IVUS catheter prototypes were used for this study. They both comprised a 400 μm diameter core optical fiber (Pioneer Optics, Bloomfield, CT) to deliver the light pulses to the vessel wall and an ultrasound transducer to transmit and receive ultrasound waves. The fiber tip was polished under a 34° angle covered by a quartz cap to maintain an air-glass interface deflecting the beam by total reflection. The first prototype, described in detail in earlier work⁷⁹, contained a circular lead-zirconium-

titanate (PZT) ultrasound transducer with a diameter of 1.0 mm (custom built by TUDelft; design by DuMED⁸⁰). The transducer had a center frequency of 30 MHz, a -6 dB fractional bandwidth of 65% and was mounted distal from the fiber in an assembly with an outer diameter of 1.25 mm. The second prototype held a 0.4 by 0.4 mm lead magnesium niobate-lead titanate (PMN-PT) single crystal ultrasound transducer (designed and custom built by the University of Southern California, Department of Biomedical Engineering⁵⁸) with a center frequency of 44.5 MHz and a -6 dB fractional bandwidth of 45%. Fiber and transducer were mounted in an assembly with an outer diameter of 1 mm. In both prototypes, the fiber tip and transducer center were separated by approximately 1 mm and the optical and acoustical beam overlapped between 0.5 and 4.5 mm from the transducer, with an angle of 22°.

An arbitrary waveform generator (Tabor Electronics WW2571A) transmitted a Gaussian-modulated cosine wave for pulse echo imaging, which was transmitted to the probe through a custom-built expander and limiter. The catheter was rotated using a motorized rotary stage (Steinmeyer GmbH & Co. KG). The received US and PA signals were band pass filtered (13–60 MHz 5th order Butterworth, custom built), amplified by a 43 dB amplifier (Miteq AU1263) and digitized at a sample frequency of 350 MS s⁻¹ by a 12-bit data acquisition card (Acqiris DP310).

Phantom design

We designed and constructed a vessel mimicking poly-vinyl-alcohol (PVA, 10% wt. PVA crystals in demineralized water, 2 freeze/thaw cycles) phantom with a 3 mm diameter lumen and four 1.5 mm round by 5 mm deep cylindrical cavities at 500 μ m from the lumen. One cavity was filled with peri-adventitial tissue that we obtained from one of the human coronary artery specimens, see description below. In peri-adventitial tissue, lipids are stored as a mixture of fatty acids³⁸. The other three cavities were filled with cholesterol, cholesterol oleate and cholesterol linoleate (Sigma Aldrich Co., C8667, C9253 and C0289, resp.). These three compounds are the most abundant lipids in atherosclerotic lesions^{90,91}, and are assumed to be representative of plaque lipids.

Reference absorption spectra of pure cholesterol, cholesterol linoleate, cholesterol oleate, and of peri-adventitial tissue, were acquired by recording the wavelength-dependent PA signal. The respective lipids were held in a container made of TPX (TPX® Polymethylpentene) in a water bath in such a way that there was a clear optical and acoustic path between the probe and the target. The data were averaged and processed to obtain spectra that were reproducible in time and depth, see Figure 1a.

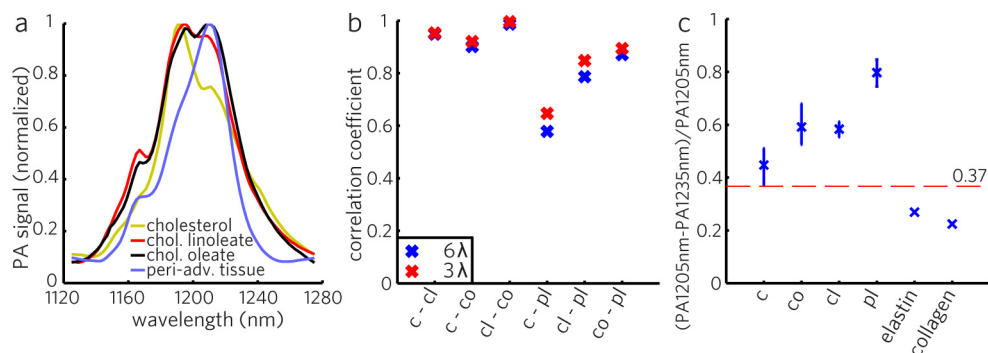


Figure 1. a) Normalized reference PA spectra of cholesterol, cholesterol linoleate, cholesterol oleate, and peri-adventitial tissue, measured on the pure compounds. b) Correlation coefficients between the 6 and 3-wavelength PA spectra of the different lipid types. c) 5th to 95th percentile of the relative difference of 1205 nm and 1235 nm PA signal strength of cholesterol, cholesterol oleate, cholesterol linoleate and peri-adventitial lipids (672, 864, 512 and 372 spectra, respectively). The values for elastin and collagen are taken from literature³⁸. c = cholesterol; cl = cholesterol linoleate; co = cholesterol oleate; pl = peri-adventitial lipids.

Coronary artery acquisition and handling

We collected human coronary arteries at autopsy from the Department of Pathology of the Erasmus Medical Center (MC). We obtained consent from the relatives and our research protocol was approved by the Medical Ethics Committee of the Erasmus MC (MEC-2007-081). The coronary arteries were measured freshly within 24h post mortem or frozen within 4h at -80° to be thawed and measured at a later date.

Combined photoacoustic and ultrasound imaging

We acquired combined photoacoustic and ultrasound images of the lipid containing vessel phantom and the human coronary arteries ex vivo. The vessel phantom was placed in a water bath, after which we inserted our combined IVPA/IVUS catheter in the lumen and recorded co-registered IVPA/IVUS cross-sectional data. The coronary arteries were placed in a holder and mounted on two cannulas in a water tank containing saline solution at room temperature. The holder was made of TPX with thin (200 μm) metal wires glued at every 1.5 mm perpendicular to the longitudinal axis to mark imaging locations. We then performed an IVUS pullback of the arteries using a commercial IVUS system (Boston Scientific iLab, Atlantis SR Pro catheters) to find sites of interest. Using our combined IVPA/IVUS catheter, the selected wires were found and at these locations co-registered IVPA and IVUS cross-sectional scans were made.

To create the ultrasound images, we transmitted a 10 V peak to peak Gaussian-modulated cosine wave with a center frequency of 30 MHz and a 100% bandwidth for

the first prototype catheter and a center frequency of 44.5 MHz and a 50% bandwidth for the second prototype catheter. Transmission bandwidths are specified at a -6dB level relative to the peak. With the exception of the phantom and first artery, the results of which are shown in Figure 2 and Figure 3, respectively, all arteries were measured using the second prototype catheter (44.5 MHz center frequency).

We acquired IVPA images at several excitation wavelengths around 1200 nm. In this wavelength range, the second overtone of C-H bond vibrations within the different structural groups of the lipid molecules produce several overlapping peaks in the lipid absorption spectra. By staying within a relatively narrow wavelength range, we ensured that variations in the laser pulse energy and tissue scattering properties are negligible.

Two-dimensional spatially co-registered spectroscopic IVPA and IVUS images were obtained by rotating the catheter in 1° steps and repeating the photoacoustic and ultrasound acquisitions at every step. IVUS images were obtained by averaging the echoes from 10 transmissions per line; IVPA was not averaged (one laser pulse per image line). At every angle, the laser was tuned through the spectral range of interest to ensure co-registration of the IVPA data at all wavelengths. Digitized IVPA and IVUS data were band pass filtered between 10 and 40 MHz and 10 and 70 MHz for the first and second catheter prototype, respectively (100th order zero-phase forward and reverse finite impulse response [FIR] filter). Filtered data were upsampled, corrected for jitter and downsampled to the original sampling frequency. Data that was affected by (environmental) noise benefited from additional median filtering in the angular direction, this concerned arteries 2 and 4 (kernel width 3° and 5°, respectively).

IVPA data can be affected by an artifact caused by the absorption of laser pulses in the ultrasound transducer and catheter tip. It shows up in the images as bright rings, concealing the photoacoustic signals produced by the arterial tissue close to the probe. An adaptive filter was designed and applied to the IVPA data to remove this artifact. The IVUS data contained a similar circular artifact, caused by the ‘ringing’ of the transducer as a result of the transmission of ultrasound pulses, that we removed by subtracting the mean in the angular direction of the affected part of the data. Both the IVPA and IVUS data were then Tukey windowed and envelope filtered. The spectroscopic IVPA data was corrected for variations in the light energy between individual pulses and between the different wavelengths, using the amplitude in the ring artifact mentioned above. The data were subsequently scan-converted to Cartesian coordinates and log compressed. We used the ‘hot’ and ‘gray’ colormaps in Matlab (R2007b) to display the IVPA and IVUS images, respectively. Combined IVPA/IVUS images were created by overlaying the IVPA data on the IVUS images using a nonlinear red-yellow-white color scale and a linear transparency scale. All data processing was done using Matlab (R2007b).

After imaging, the arteries were cut at the two wires adjacent to the imaging planes to obtain 3 mm thick artery segments with the imaged cross-section in the middle. The segments were embedded in optimal cutting temperature (OCT) compound (Tissue-

Tek®, Sakura Finetek Europe B.V.), frozen in liquid nitrogen cooled isopentane vapor, and stored at -80 °C until serial sectioning for staining. Oil Red O (ORO) staining was performed to identify lipids (stained red). A Hematoxylin-Eosin (H&E) stain was used as an overview stain. To demonstrate the morphology and fibrous structure of the vessel cross-sections, a Resorcin-Fuchsin (RF) stain was used.

Lipid detection methods

Per imaging location, the spatially co-registered sIVPA data were used to obtain the lipid distribution within the vessel wall. We imaged a cross-section of the vessel phantom and the first artery at six equally spaced wavelengths between 1185 and 1235 nm. Acquisition of a full image at six wavelengths is a time-consuming procedure, mainly because the laser takes time to tune. To limit tissue degradation, we performed 6-wavelength imaging on one vessel only. The data were first processed as described above, up to scan-conversion. Then, for each pixel in the resulting data set, the correlation coefficient $R_{n=6}$ (n is the number of wavelengths) of the 6-wavelength PA spectrum with two different reference spectra was computed. We used the PA spectra of cholesterol and peri-adventitial tissue as reference spectra for plaque and peri-adventitial lipids, respectively. The correlation coefficients between the various spectra (Figure 1b) show that the cholesterol spectrum has the lowest correlation with the peri-adventitial spectrum and therefore is the most suitable to distinguish plaque from other lipids.

The 6-wavelength correlation coefficients $R_{x,6}$ (x is lipid type; “c” for cholesterol or “pl” for peri-adventitial lipids) were median filtered over 4° in the angular direction and 8 samples in the radial direction. The threshold values $R_{th,x,6}$ for the correlation coefficients were chosen empirically as the lowest values for which plaque lipids could be separated from peri-adventitial lipids. This exercise was performed in the phantom and in the artery specimens, discriminating lipid type based on location inside or outside the vessel wall. The lipid matching regions – those with a correlation coefficient equal to or higher than the threshold $R_{th,x,6}$ – were colored red and overlaid on the corresponding IVUS image to create a lipid map.

We investigated the potential for identification and differentiation of the lipids using three and two wavelengths only. Several combinations of three wavelengths within the 1185–1235 nm range were tested on the 6-wavelength data sets of the phantom and first artery. A three wavelength correlation will necessarily suffer more from accidental high correlation of the noise with the reference spectrum than a six wavelength correlation and therefore can be improved by applying a mask that cuts off the data at the noise level. We determined the noise level at 1205 nm by sampling the PA signal inside the lumen (identified in the IVUS image). All PA signal below that level was masked out. In these masked data, lipids were then detected in a manner similar to the 6-wavelength

data sets, and a new pair of correlation coefficients $R_{th,x,\lambda}$ was chosen for both the phantom and artery measurement.

Two-wavelength lipid detection was implemented using sIVPA data obtained at 1205 and 1235 nm. At 1205 nm, lipid absorption is high, while at 1235 nm, the lipid absorption is reduced by 40 to 85%. Lipid maps were computed using the following algorithm: we determine the noise level at 1205 nm by sampling the PA signal inside the lumen (which can be identified in the IVUS image). All PA signal below that level is masked out. We compute the relative difference $\delta = [I_{1205} - I_{1235}] / I_{1205}$, where I_{λ} is the PA signal amplitude at wavelength λ . δ is median filtered (4° angular by 8 samples radial). Lipids are identified by $\delta > \delta_{th} = 0.37$, where δ_{th} is a threshold value determined from the analysis of the absorption spectra of pure lipids, see Figure 1c. We applied this method to the sIVPA data at 1205 and 1235 nm of the phantom and at several cross-sections of the human coronary arteries.

Results

Phantom

We performed IVPA/IVUS on a lipid-containing vessel phantom at 6 evenly spaced wavelengths from 1185 to 1235 nm. The co-registered combined IVPA/IVUS images at 1205 and 1235 nm are shown in Figures 2a and 2b, respectively. All four lipid containing cavities exhibit an increased PA signal at 1205 nm compared to the PA signal at 1235 nm. The lipid map resulting from the 6-wavelength correlation with the cholesterol reference spectrum, Figure 2d, detects the cholesterol and cholesterol esters, representative of plaque lipids, while the peri-adventitial tissue remains concealed. The correlation with the peri-adventitial reference spectrum, Figure 2e, results in detection of the peri-adventitial tissue, while suppressing the other lipids. Figure 2f illustrates the resemblance of the average IVPA spectra in the lesion area indicated by the green sector in Figure 2d, and the peri-adventitial area (blue sector in Figure 2e), with their respective reference spectra. The atherosclerotic plaque and peri-adventitial lipid maps created using the 3 wavelength correlation with the associated reference spectra, overlaid on the IVUS image, are shown in Figures 2g and 2h, respectively. The results shown here are obtained using 1185, 1205 and 1235 nm, which was the combination of wavelengths that resulted in the most specific separation between plaque and peri-adventitial lipids.

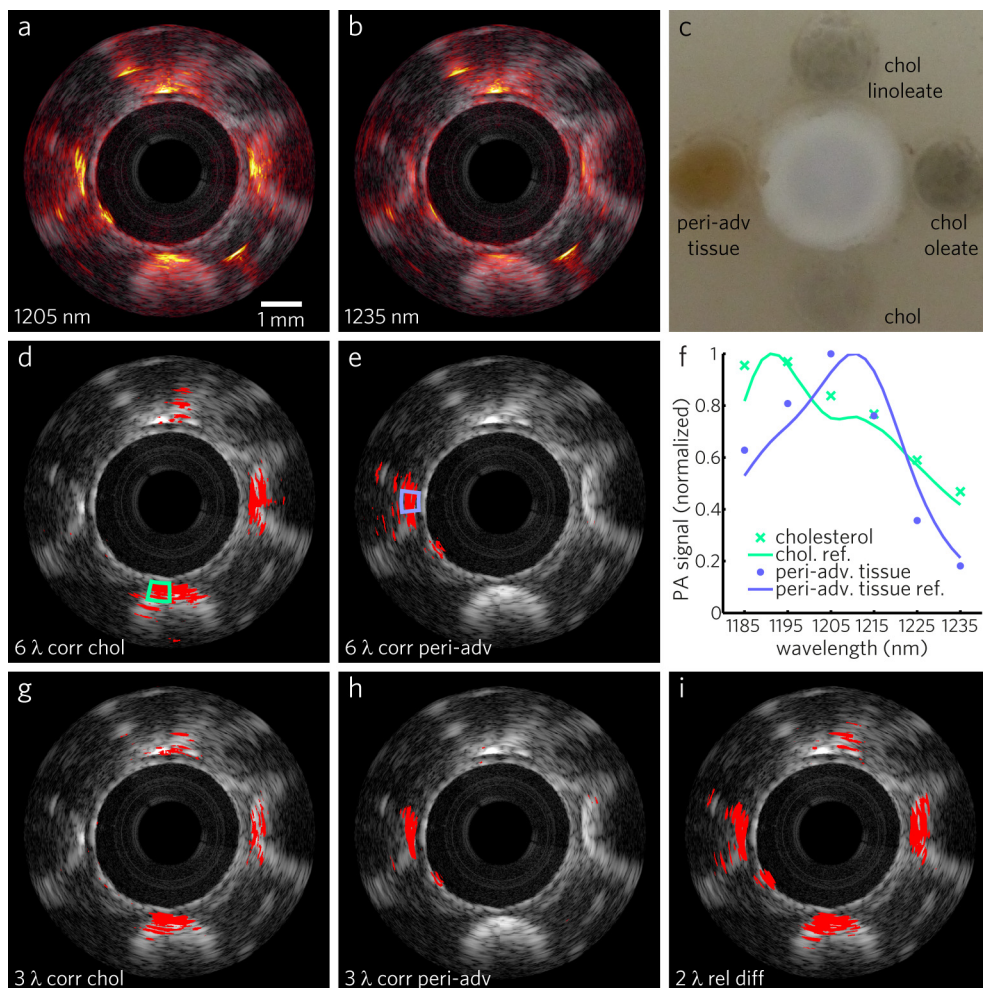


Figure 2. Lipid-detection in a lipid-containing vessel phantom. a) 1205 nm and b) 1235 nm combined IVPA/IVUS images (IVPA 50 dB, IVUS 65 dB) of PVA phantom filled with cholesterol (bottom), cholesterol oleate (right), cholesterol linoleate (top) and peri-adventitial tissue (left). c) Photograph of the phantom (top-view). Lipid map based on 6-wavelength correlation with the cholesterol d) and peri-adventitial reference spectrum e). f) Average IVPA signal spectra in the cholesterol and peri-adventitial tissue areas indicated in d and e, respectively, are highly correlated with their respective reference spectra. Lipid map based on 3-wavelength correlation with the cholesterol g) and peri-adventitial reference spectrum h). i) Lipid map based on 2-wavelength relative difference. All lipid maps are shown overlaid on the corresponding IVUS image.

The result of the 2-wavelength relative difference method using 1205 and 1235 nm is shown in Figure 2i. The method succeeds to display all the lipid regions well, but does not distinguish between atherosclerotic and peri-adventitial lipids.

Table 1 lists the threshold correlation values $R_{th,x,6}$ and $R_{th,x,3}$ for 6 and 3 wavelengths respectively, which were used to create the lipid maps in Figures 2d-2e and 2g-2h. The 3-wavelength correlation method distinguishes equally well between the two lipid types as the 6-wavelength correlation. A slight decrease in the amount of lipids detected can be seen, however, which is caused by the addition of the noise masking step.

Table 1. Threshold values $R_{th,x,n}$ and δ_{th}

Method	Threshold variable	Phantom	Artery
6 λ	$R_{th,c,6}$	0.88	0.93
	$R_{th,p,6}$	0.85	0.85
3 λ	$R_{th,c,3}$	0.96	0.98
	$R_{th,p,3}$	0.96	0.95
2 λ	δ_{th}	0.37	

Arteries

IVPA/IVUS was performed on a human coronary artery specimen exhibiting early stage atherosclerosis (left anterior descending artery, female aged 41, imaged < 24 h post mortem). Figures 3a and 3b show the co-registered combined IVPA/IVUS images at 1205 nm (high lipid absorption) and 1235 nm (low lipid absorption), respectively. In the IVUS image, the luminal border and the external elastic lamina are clearly visible. The images show two thickened intimal regions that exhibit a brighter signal in the 1205 nm IVPA image than in the 1235 nm IVPA image. A brighter signal is also observed in the 1205 nm IVPA image in the peri-adventitial regions all around the vessel. The corresponding lipid stain, shown in Figure 3c, confirms the presence of lipids in the regions with enhanced 1205 nm IVPA signal. The three different lipid detection methods were applied to the co-registered IVPA data. The obtained optimal threshold values $R_{th,x,n}$ listed in Table 1, differ slightly from those found with the phantom data but show a similar trend. The findings are comparable to the lipid detection results in the phantom: Figure 3d clearly depicts the lipids in the fatty streak at the bottom right while suppressing successfully the peri-adventitial lipids. However, it fails to distinctly show the lipids present in the smaller fatty streak at the top of the vessel. In contrast, Figure 3e depicts the peri-adventitial lipids while suppressing the lipids present within the thickened intima. The plaque and peri-adventitial lipid maps created using the

3 wavelength (1185, 1205 and 1235 nm) correlation with the associated reference spectra, overlaid on the IVUS image, are shown in Figures 3g and 3h, respectively.

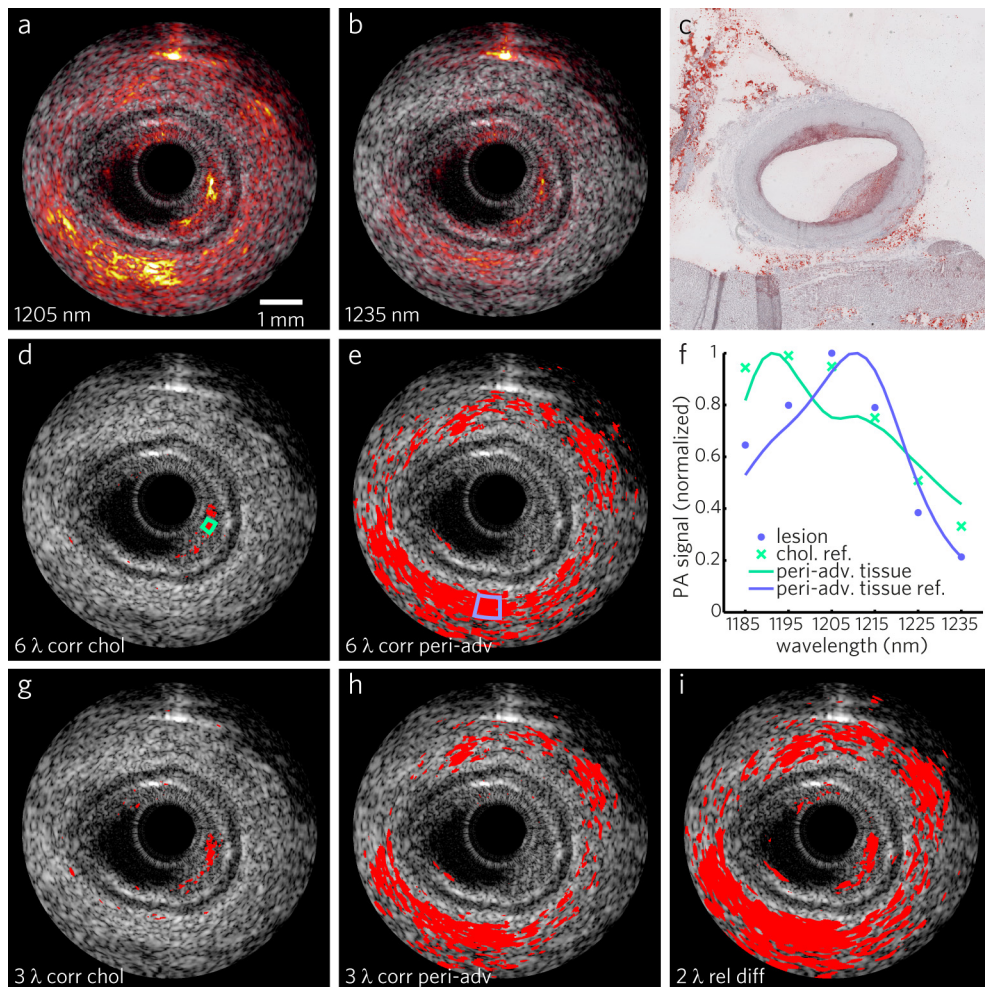


Figure 3. Lipid detection in an early stage atherosclerotic human coronary artery. a) 1205 nm and b) 1235 nm combined IVPA/IVUS images (IVPA 35 dB, IVUS 40 dB). c) Lipid histology stain (ORO); lipids are stained red. Lipid map based on 6-wavelength correlation with the cholesterol d) and peri-adventitial reference spectrum e). f) Average IVPA signal strength in the lesion and peri-adventitial areas indicated in d and e, respectively, shows high correlation with the respective reference spectra. Lipid map based on 3-wavelength correlation with the cholesterol g) and peri-adventitial reference spectrum h). i) Lipid map based on 2-wavelength relative difference. All lipid maps are shown overlaid on the corresponding IVUS image.

The 3-wavelength correlation with cholesterol seems to be working equally well as the 6-wavelength correlation, whereas the 3-wavelength peri-adventitial lipid correlation degrades slightly. The result of the 2-wavelength relative difference method using 1205 and 1235 nm is shown in Figure 2i. As in the phantom case, the method succeeds to display all the lipid regions well, but does not distinguish between atherosclerotic and peri-adventitial lipids. Note that all lipid detection methods effectively suppress the strong PA signal from the wire that can be seen at the top of the IVPA images in Figure 2a and 2b.

Subsequently, we acquired co-registered IVPA/IVUS images at 1205 and 1235 nm of several human coronary arteries exhibiting varying degrees of atherosclerosis. The lipid maps resulting from the 2-wavelength lipid detection method, overlaid on the IVUS images, are shown in Figure 4 through Figure 6 with collocated histology, always showing the ORO stain. Figure 4 demonstrates the lipid detection method on a healthy coronary artery (left anterior descending artery, male aged 65, imaged after frozen storage). Lipids are found in the peri-adventitial tissue only; this is confirmed by the lipid histology stain. The peri-adventitial fat is a very fragile structure, and as a result some of it has fallen off in tissue handling after imaging.

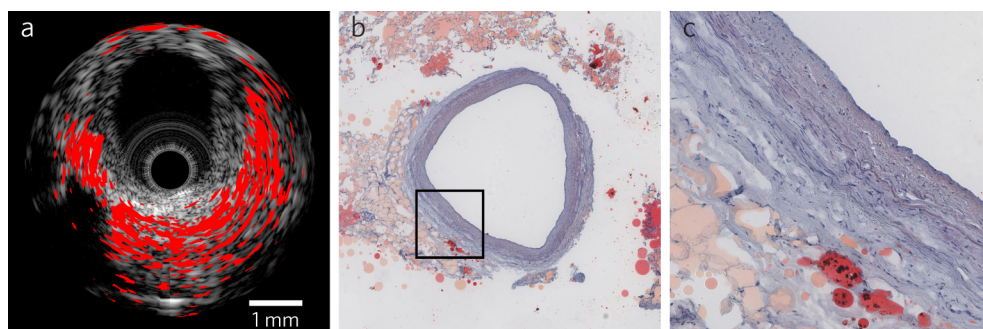


Figure 4. Lipid detection in a healthy human coronary artery. a) Lipid map based on relative difference between PA signal at 1205 and 1235 nm, overlaid on IVUS image (40 dB). b) Lipid histology stain (ORO). c) 5 x magnification of a part of the healthy vessel wall and peri-adventitial lipids (area outlined in black in b). Both in the lipid map and the lipid stain, lipids are found in the peri-adventitial region only.

Two sites in an atherosclerotic human coronary specimen (left anterior descending artery, male aged 80, imaged after frozen storage) are shown in Figure 5. The IVUS image in Figure 5a shows a narrowed lumen with two plaques at the top right and the bottom of the vessel wall. The shadowing deeper in the plaque area at the bottom of the image indicates the presence of a calcification.

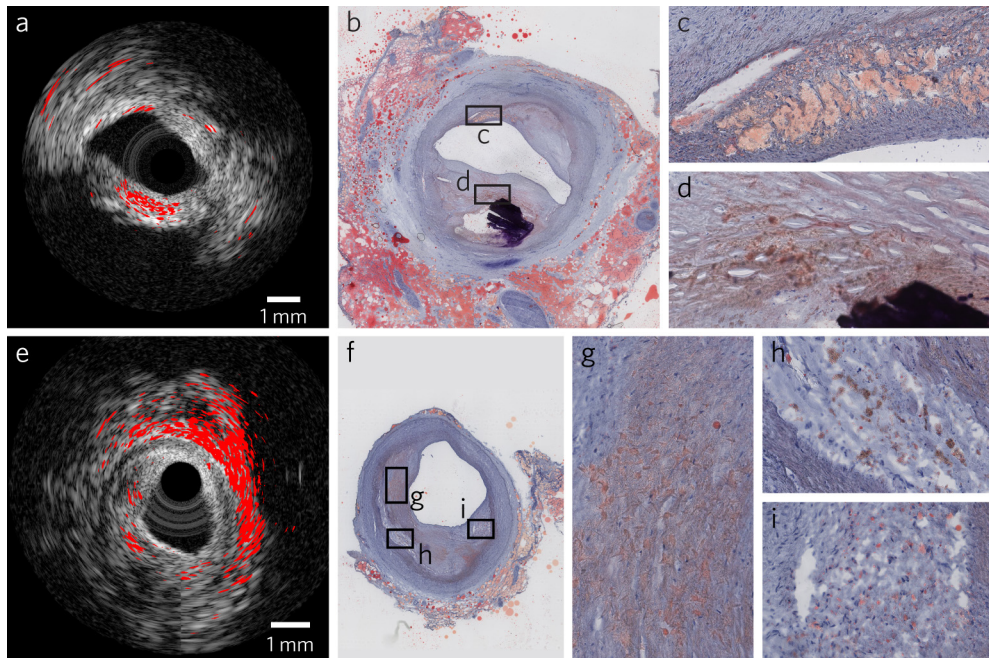


Figure 5. Lipid detection in a diseased coronary artery. a) Lipid map at first imaging location, based on relative difference between PA signal at 1205 and 1235 nm after masking the noise, overlaid on IVUS image (45 dB). b) Corresponding lipid histology stain (ORO). Lipids are found in the top and bottom plaque areas, as well as in the peri-adventitial region, in correspondence with the lipid stain. 10x magnifications of area c and d are shown in c) and d), respectively. e) Lipid map, created using the same 2-wavelength method, overlaid on 45 dB IVUS image, and f) lipid histology stain at second imaging location. The lipid map displays all locations with extracellular lipid droplets and cholesterol (areas g, h and i, shown 10x magnified in subfigures g, h and i, respectively) accurately. Peri-adventitial lipids that are located beyond the lesion are obscured.

These findings are confirmed by the ORO lipid stain, which is depicted in Figure 5b. The lipid map, overlaid on the IVUS image, shows lipids in both the bottom and top plaque regions, accurately collocated with the atherosclerotic lipids visible in the lipid histology stain. The peri-adventitial lipids are only visible in the lipid map on the top left and bottom right, where the light and ultrasound waves penetrate deep enough to reach the tissue surrounding the vessel. At the next imaging location, excellent agreement between the lipid map overlaid on the IVUS image and the lipid histology stain is observed. The lipid stain reveals an eccentric plaque, with lipids located at specific locations in the lesion, see Figures 5e-5i. The lipid map assesses these lipid rich locations

accurately. The peri-adventitial lipids appear in all directions except behind the plaque, where the vessel wall is thickened considerably.

Figure 6 shows the results of the combined IVPA/IVUS measurement of an eccentric plaque with diffuse intracellular lipid according to histology (left anterior descending artery, female aged 51, imaged fresh). The lipid-rich eccentric plaque, as imaged by IVPA, has a mottled appearance due to the lipids that are scattered throughout most of the lesion. The lipid map closely mimics the appearance of the plaque by showing small lipid specks distributed throughout the plaque region. Small lipid deposits in the vessel wall opposite the lesion and the larger lipid deposits of the peri-adventitial tissue show up as well.

Discussion and conclusions

This study demonstrates that spectroscopic intravascular photoacoustic imaging can automatically detect atherosclerotic and peri-adventitial lipids, as well as distinguish between them, with a small number of excitation wavelengths. We have developed and tested a number of, progressively simpler, methods using the co-registered sIVPA/IVUS data we acquired in a lipid containing vessel phantom and several human coronary arteries *ex vivo*. Correlation with a cholesterol PA spectrum, as reference for atherosclerotic lipids, and with a peri-adventitial reference spectrum, using 6 equally spaced wavelengths from 1185 to 1235 nm, distinguishes very well between atherosclerotic lipids and peri-adventitial lipids. Correlation using just 3 well-chosen wavelengths within this wavelength range, namely 1185, 1205 and 1235 nm, still achieves a satisfactory distinction between these two lipid types. Utilizing the relative difference between the PA signal at 1205 and 1235 nm, we successfully detected both the atherosclerotic and peri-adventitial lipids in several human coronary arteries. Separate depiction of the two lipid types was not achieved, even though PA data of the pure compounds (Figure 1c) suggest this as a possibility. In actual tissue, however, variability in optical properties and a lower signal-to-noise level preclude separation of lipid types.

Evaluation of two-wavelength sIVPA in human coronary arteries *ex vivo* shows the appearance of different manifestations of disease, compared to histology: Figure 4 shows a healthy artery, which by IVPA is characterized by an absence of lipid signal in the intima and media. Figures 5 and 6 compare large lipid deposits (Figures 5c and 5d) with small (Figures 5g–5i) and larger (Figure 6) extracellular lipid droplets. The lipid distribution by IVPA closely follows the histological appearance.

Other methods have been reported for separating lipids from other tissue types⁴⁹, relying on the acquisition of more wavelengths. This richer spectral sampling may increase robustness against measurement noise, permits automated spectral unmixing⁹², and possibly enhances chemical detail. A drawback is, however, that additional wavelengths lower the imaging speed proportionally, lengthening the acquisition time

and increasing the susceptibility to motion artifacts. For *in vivo* imaging, the number of wavelengths should be kept as small as possible. The difference in our approach compared to other techniques in the literature does complicate a direct performance comparison.

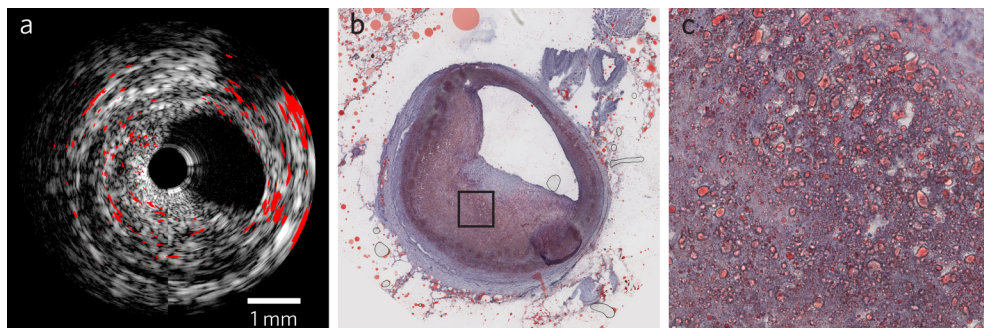


Figure 6. Lipid detection in a coronary artery with an eccentric atherosclerotic lesion with lipids distributed throughout the plaque. a) Lipid map based on relative difference between PA signal at 1205 and 1235 nm after masking the noise, overlaid on IVUS image (30 dB). b) Lipid histology stain (ORO). c) 10 x magnification of part of the plaque (area outlined in black in b). The distributed plaque lipids are displayed in the lipid map as small red marks throughout the lipid containing area.

Catheter-based coronary imaging is usually performed by pulling back the catheter inside the artery under investigation, as it rotates. In this way, a large, volumetric data set is accumulated, which is reviewed during or after acquisition. A technology that automatically identifies lipid-rich plaques in the vessel greatly simplifies the review and interpretation process, and development of this functionality is one of the main drivers of this study. In principle, segmentation of the peri-adventitia based on the IVUS image is possible. In practice, however, automated IVUS image analysis has proven to be a very difficult problem, which is why we propose to exploit the chemical differences that exist between plaque lipids and others to generate image contrast.

Incomplete depiction of the topmost fatty streak in the correlation lipid maps of the human coronary artery specimen imaged using six wavelengths (Figures 3d and 3g), was caused by filtering the data for artifact reduction, as discussed in section 2.4. The filter is nonlinear and this affects the spectral correlation that we compute. The 2-wavelength analysis (Figure 2i) appears to be more robust, retaining the feature partially. The catheter design will be adapted to considerably reduce this artifact in future experiments. In the peri-adventitial (Figures 3e and 3h), as well as the 2-wavelength lipid map (Figure 3i), of the same cross-section, a thin lipid-positive layer can be seen at the bottom left of the luminal border that is unmatched by histology. A piece of adipose

tissue may have been moved into the lumen in preparation for the experiment, and subsequently dislodged by tissue handling.

This qualitative study demonstrates the viability of detecting arterial lipid with a limited number of wavelengths. It will be compounded in the future with a larger quantitative study to establish the optimal experimental and analysis procedures. Such a study should also include a statistical analysis to quantify the sensitivity and specificity of IVPA for lipid-rich plaque detection. Our findings seem to indicate a high sensitivity for extracellular lipid droplets, as illustrated in Figure 6, while intracellular lipids remain mostly undetected. The selection of wavelengths may be further optimized to improve sensitivity. Alternatively, sensitivity might be increased by imaging in the 1700 nm wavelength range, where lipid absorption is much higher^{48,49}. Tradeoffs exist in the form of a high water absorption, which may present a challenge in this wavelength range, and the chemical specificity of the absorption spectra of the different lipids, which remains to be explored. Further automation of the analysis could be achieved by automatic contour detection in IVUS to determine the luminal noise level. The dynamic range in the images was adjusted to accommodate the dynamic range of the acquired data.

In summary, we presented an analysis of sIVPA data to detect atherosclerotic lesion lipid content in a semi-automated fashion and with high resolution. The methods were demonstrated on human coronary arteries ex vivo and have the potential to be used in an in vivo setting. Automatic depth-resolved lipid detection of human coronary atherosclerosis may find an important role in the clinical detection and treatment, as well as the expansion of our understanding, of coronary artery disease.

A grayscale microscopic image of a human coronary artery cross-section. The image shows a large, irregularly shaped lumen on the left, surrounded by a thick, textured wall. The wall is composed of various layers, including a dark, fibrous outer layer and a lighter, more granular inner layer. There are several small, dark, circular spots scattered throughout the wall, which are likely atherosclerotic plaques. The overall texture is rough and uneven, characteristic of biological tissue.

Chapter 7

Photoacoustic imaging of human coronary atherosclerosis in two spectral bands

Based on the manuscript by Krista Jansen, Min Wu, Antonius F. W. van der Steen, and Gijs van Soest, **Comparison of spectroscopic photoacoustic imaging of human coronary atherosclerosis in two spectral bands**. *Photoacoustics*, accepted for publication.

Abstract

Spectroscopic intravascular photoacoustic imaging (sIVPA) has shown promise to detect and distinguish lipids in atherosclerotic plaques. sIVPA generally utilizes one of the two high absorption bands in the lipid absorption spectrum at 1.2 μm and 1.7 μm . Specific absorption signatures of various lipid compounds within the bands in either wavelength range can potentially be used to differentiate between plaque lipids and peri-adventitial lipids. With the aim to quantify any differences between the two bands, we performed combined sIVPA imaging in both absorption bands on a vessel phantom and an atherosclerotic human coronary artery *ex vivo*. Lipid detection in a human atherosclerotic lesion with sIVPA required lower pulse energy at 1.7 μm than at 1.2 μm (0.4 mJ versus 1.2 mJ). The imaging depth was 5 mm at 1.7 μm versus 10 mm at 1.2 μm . Adequate differentiation between plaque and peri-adventitial lipids was achieved at 1.2 μm only.

Introduction

Myocardial infarction is a leading cause of death worldwide¹. In the majority of cases, they are caused by the rupture of an atherosclerotic plaque and the subsequent release of its thrombogenic content into the bloodstream². The presence of a lipid rich necrotic core is one of the determinants of the susceptibility of a plaque to rupture^{3,4}. For that reason, the identification of necrotic core is a highly coveted imaging target. Intravascular ultrasound (IVUS) radiofrequency data analysis techniques for tissue characterization (VH-IVUS, iMap) have been developed, but their accuracy and mutual consistency are still under investigation²⁴⁻²⁶. Near infrared spectroscopy (NIRS) in combination with IVUS, can identify the presence but not the amount or location, relative to the lumen, of the lipid core³¹⁻³³.

Intravascular photoacoustic (IVPA) imaging has demonstrated the ability to directly image tissue components in the vessel wall, with high chemical specificity for lipid type. It utilizes differences in the absorption spectra of the vessel wall constituents to identify tissue types. Efforts have primarily concentrated on lipid detection, and started in the visible wavelength range. With the introduction of suitable light sources, focus shifted to the near-infrared wavelength range, where hemoglobin absorption is much lower, allowing for better light penetration. In this wavelength range, the absorption spectra of lipids are characterized by two prominent features around 1.2 and 1.7 μm . These absorption bands are the result of the second and first overtones of the C-H bond vibrations within the lipid molecules, respectively. The 1.2 μm absorption band has been exploited extensively to distinguish lipids from healthy vessel wall, in rabbit^{43,44} as well as human^{45,46,79} atherosclerotic arteries. In recent years, lipid detection using excitation wavelengths around 1.7 μm has seen increased interest^{45,47-49}. In this wavelength range, the higher lipid absorption possibly leads to increased sensitivity using lower light intensity. However, water absorption is higher too, which could potentially offset the increased sensitivity for lipids by limiting the penetration depth (Figure 1).

Both absorption bands each consist of several overlapping peaks as a result of C-H bond vibrations within the different structural groups ($-\text{CH}_3$, $>\text{CH}_2$, $\equiv\text{CH}$ and $>\text{CH}$ [aromatic]) of the lipid molecules^{66,81,93}. The position and relative height of the peaks vary with the number and location of these different structural groups within the molecules and therefore provide chemical specificity. The possibility for differentiating between plaque lipids and peri-adventitial lipids, based on the specific absorption signature of the various lipid compounds, remains to be explored.

These considerations outline tradeoffs in terms of sensitivity, imaging depth, and possibly chemical specificity connected to the choice of IVPA wavelength. In this paper, we present spectroscopic IVPA (sIVPA) imaging of a lipid containing vessel phantom and an atherosclerotic human coronary artery ex vivo at 1.2 μm and 1.7 μm , providing a direct comparison between the wavelength ranges. In the phantom, we acquired high-

resolution spectra of cholesterol, cholesterol oleate and cholesterol linoleate, representative of plaque lipids, and peri-adventitial tissue. The resulting spectra were used to determine a limited number of wavelengths that maximize the difference between plaque and peri-adventitial lipids. At these wavelengths, we obtained co-registered sIVPA/IVUS images of the vessel phantom that we used to detect the plaque and peri-adventitial lipids alternatively. With two wavelengths per spectral range only, the lipid detection capability in each range was examined using both the phantom data and the ex vivo data of a diseased human coronary artery specimen.

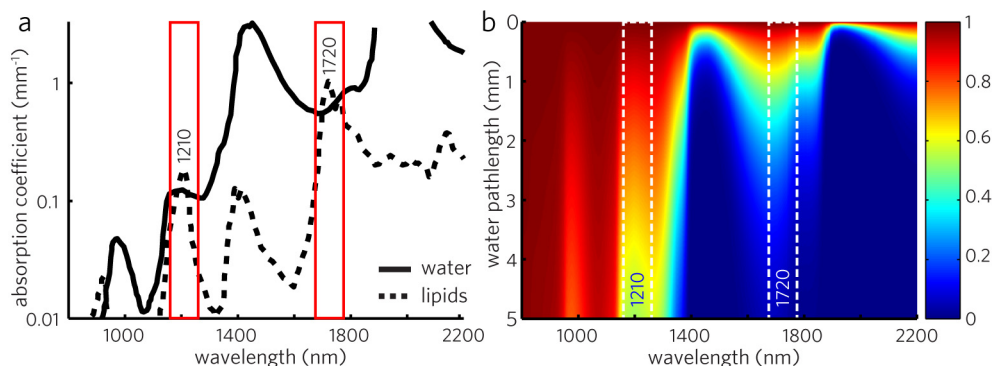


Figure 1. a) Lipid and water absorption in the near-infrared wavelength region, showing the two high peaks in the lipid absorption spectrum around 1210 and 1720 nm. In these two optical windows, lipid absorption exceeds water absorption. Lipid absorption at 1720 nm is 5.5 times higher than at 1210 nm; water absorption is 5 times higher. Adapted from⁹⁴. b) Transmission of light through water; computed based on data from <http://omlc.ogi.edu/spectra/water/abs>.

Methods

Phantom design

To determine the capacity for lipid detection and differentiation at 1.2 and 1.7 μm , we made a cylindrical vessel mimicking phantom (Figure 1a). The phantom consisted of 10% (by weight) poly-vinyl-alcohol (PVA) crystals in demineralized water, that formed an acoustically transparent gel after 2 freeze/thaw cycles. It had a central lumen with a diameter of 3 mm and four 5 mm deep cylindrical cavities with a diameter of 1.5 mm, located at 500 μm from the lumen. We filled three cavities with cholesterol, cholesterol oleate and cholesterol linoleate (Sigma Aldrich Co., C8667, C9253 and C0289, resp.). These are the three most abundantly present lipids in atherosclerotic lesions^{90,91}, and are assumed to be representative of plaque lipids. The fourth cavity was filled with peri-adventitial tissue that was obtained from a human coronary artery specimen, see

description below. In peri-adventitial tissue, lipids are deposited as a mixture of fatty acids³⁸.

Human artery acquisition and handling

A human coronary artery was collected at autopsy from the Department of Pathology of the Erasmus Medical Center (MC), after obtaining consent from the relatives and approval of the research protocol by the Medical Ethics Committee of the Erasmus MC (MEC-2007-081). The coronary artery was frozen within 4h at -80°C and stored. It was thawed and measured three months later.

Combined intravascular photoacoustic and ultrasound imaging system

All co-registered sIVPA/IVUS images were acquired using a combined IVPA/IVUS imaging system described previously⁷⁹. The excitation light for photoacoustic imaging was supplied by a tunable laser (OPOTEK Vibrant B/355-II) with a pulse duration of 5 ns and a repetition rate of 10 Hz. The laser was coupled to the custom-built catheter by a tapered multimode fiber (Oxford Electronics, Four Marks, UK; input diameter 1 mm; output diameter 360 μm).

The hybrid IVPA/IVUS catheter prototype we used is similar to those used earlier⁷⁹, but with a different transducer. It comprised a 400 μm diameter core optical fiber (Pioneer Optics, Bloomfield, CT) to deliver the light pulses to the vessel wall. The fiber tip was polished under a 34° angle covered by a quartz cap to maintain an air-glass interface deflecting the beam by total reflection. An ultrasound transducer was placed distal from the fiber tip to transmit and receive ultrasound waves. The 0.4 by 0.4 mm lead magnesium niobate-lead titanate (PMN-PT) single crystal ultrasound transducer was designed and custom built by the Department of Biomedical Engineering of the University of Southern California⁵⁸ and had a center frequency of 44.5 MHz and a -6 dB fractional bandwidth of 45%. The separation between fiber tip and transducer center was approximately 1 mm; the optical and acoustical beam overlapped between 0.5 and 4.5 mm from the transducer, with an angle of 22°. The catheter tip assembly had an outer diameter of 1 mm.

The catheter was rotated using a motorized rotary stage (Steinmeyer GmbH & Co. KG). For pulse echo imaging, an arbitrary waveform generator (Tabor Electronics WW2571A) transmitted a Gaussian-modulated cosine wave which was transmitted to the probe through a custom-built expander and limiter. Received US and PA signals were band pass filtered (13–60 MHz 5th order Butterworth, custom built), amplified by a 43 dB amplifier (Miteq AU1263) and digitized at a sample frequency of 350 MS s⁻¹ by a 12-bit data acquisition card (Acqiris DP310).

Phantom measurements

Using the dual modality imaging system described above, we imaged the lipid containing vessel phantom in a water bath, with the combined IVPA/IVUS catheter positioned in the lumen. We first acquired a cross sectional IVUS image to locate the lipid inclusions. In the direction of each inclusion, we acquired sIVPA data from 1125 to 1275 nm and from 1620 to 1780 nm in steps of 2 nm, to determine the PA spectra of each lipid compound. At every wavelength, 32 image lines were recorded. The average pulse energy at the catheter tip was 1.2 mJ in the 1.2 μm and 0.4 mJ in the 1.7 μm spectral range. By staying within a relatively narrow spectral window, the average laser pulse energy and tissue scattering properties could be assumed constant within each wavelength range. The resulting spectra were normalized to the peak value and analyzed to determine the wavelengths most suitable to distinguish plaque from other lipids: per wavelength range, 4 wavelengths for which the cholesterol spectrum differed most from the spectrum of peri-adventitial lipids were selected, after which 2 wavelengths were added to create a fairly distributed spacing.

Next, we obtained two-dimensional spatially co-registered spectroscopic IVPA and IVUS images of the phantom at these 12 wavelengths (6 per wavelength range) by rotating the catheter in 1° steps and acquiring photoacoustic and ultrasound image lines at every step. At every angle, the laser was tuned through the spectral range of interest (1.2 and 1.7 μm) to ensure co-registration of the IVPA data at all wavelengths. For ultrasound pulse echo imaging, we transmitted a 10 V peak to peak Gaussian-modulated cosine wave with a center frequency of 44.5 MHz and a 50% -6 dB bandwidth relative to the peak. IVUS images were obtained by averaging the echoes from 8 transmissions per line; IVPA was not averaged (one laser pulse per wavelength per image line).

Artery measurements

The human coronary artery was placed in a TPX (TPX® Polymethylpentene) holder with 200 μm thick metal wires glued at every 1.5 mm perpendicular to the longitudinal axis to provide image registration. The holder was then placed in a water tank containing a saline solution at room temperature. The artery was tied on a cannula through which the catheter was introduced. To find sites of interest, we performed an IVUS pullback using a commercial IVUS system (Boston Scientific iLab, Atlantis SR Pro catheters), using the metal wires as reference points. The selected wires were then found using our combined IVPA/IVUS catheter.

Spatially co-registered sIVPA/IVUS cross sectional images were obtained by rotation of the catheter in 1° steps and acquiring photoacoustic and ultrasound image lines at every step. Two rotations were performed to obtain two co-registered images at 1205 and 1235 nm, and at 1680 and 1710 nm, separately. At every angle, the laser was tuned from 1205 to 1235 nm in the first measurement, and from 1680 to 1710 nm in the

second measurement, to ensure co-registration of the IVPA data per wavelength range. The ultrasound signal transmitted for pulse echo imaging, as well as the number of averaging and the average pulse energy, were the same as in the phantom measurement.

IVPA spectral data processing

The digitized spectroscopic IVPA data of the four lipid inclusions in the phantom, were band pass filtered between 10 and 70 MHz using a 100th order zero-phase forward and reverse finite impulse response (FIR) filter, and subsequently upsampled, corrected for jitter and downsampled to the original sampling frequency. Next, a Tukey window and envelope filter were applied. A correction for variations in the light energy was employed, using the amplitude of the signal close to the transducer, which is caused by the absorption of laser pulses in the ultrasound transducer and catheter tip. Depth locations of high signal intensity were chosen by selection of all peaks above a certain threshold in the 1205 and 1710 nm enveloped signal traces, respectively. Spectra at selected locations were filtered using a fourth order digital smoothing polynomial (Savitzky-Golay) filter, 32 times averaged and normalized.

sIVPA/IVUS image reconstruction

The digitized IVPA and IVUS rotational data band pass filtered and jitter corrected like the spectroscopic scans described above. The 1.2 μm wavelength range IVPA data of the artery cross section were subsequently median filtered over 5 image lines in the angular direction for extra noise reduction.

An adaptive filter was designed and applied to all rotational IVPA data to remove the artifact that was caused by the absorption of laser pulses in the ultrasound transducer and catheter tip. It presents in the IVPA image as bright rings, concealing the photoacoustic signals produced by the arterial tissue close to the catheter. A similar circular artifact in the IVUS data, caused by the 'ringing' of the transducer as a result of the transmission of ultrasound pulses, was removed by subtracting the mean in the angular direction of the affected part of the data. Both the IVPA and IVUS data were then Tukey windowed and envelope filtered. A correction for variations in the light energy between individual pulses and between the different wavelengths, using the amplitude in the ring artifact mentioned above, was applied to the IVPA data. We subsequently scan-converted the IVPA and IVUS data to Cartesian coordinates and log compressed them for display. The 'hot' and 'gray' colormaps in Matlab (R2007b) were used for the IVPA and IVUS images, respectively. To create combined IVPA/IVUS images, we overlaid the IVPA data on the IVUS images using a nonlinear red-yellow-white color scale and a linear transparency scale. All data processing was done using Matlab (R2007b).

slVPA data analysis for lipid differentiation and detection

To investigate the capability of slVPA in the two absorption bands to distinguish plaque from peri-adventitial lipids, the two 6-wavelength slVPA data sets of the lipid containing vessel phantom were processed as described above, up to scan-conversion. For each pixel in the resulting data sets, the correlation coefficient R of the PA spectrum with two reference spectra was computed. We used the PA spectra of cholesterol and peri-adventitial tissue as reference spectra for plaque and peri-adventitial lipids, respectively. Of the plaque lipid spectra (Figure 2c and 2d), in either spectral range, the cholesterol spectrum has the lowest correlation with the peri-adventitial spectrum (Figure 2b) and therefore is the most suitable to distinguish plaque from other lipids.

The 6-wavelength correlation coefficients R_x (x is lipid type; “c” for cholesterol or “pl” for peri-adventitial lipids) were median filtered over 4 degrees in the angular direction and 8 samples in the radial direction. The threshold values $R_{th,x}$ for the correlation coefficients were chosen empirically: the lowest values for which plaque lipids could still be separated from peri-adventitial lipids were selected. To create a lipid map, the lipid matching regions – those with a correlation coefficient equal to or higher than the threshold value $R_{th,x}$ – were displayed in red and overlaid on the corresponding IVUS image.

We compared the potential of slVPA at 1.2 μm and at 1.7 μm for lipid identification using two wavelengths, $\lambda_{h\omega}$ and $\lambda_{l\omega}$ (h for high lipid absorption; l for low lipid absorption) per wavelength range ω . We computed lipid maps of the phantom and artery cross section using the following algorithm: we determined the noise level at $\lambda_{h\omega}$ by sampling the PA signal inside the lumen (identified in the IVUS image) and masked out all PA signal below that level. We then calculated the relative difference $\delta_\omega = [I(\lambda_{h\omega}) - I(\lambda_{l\omega})] / I(\lambda_{h\omega})$, where $I(\lambda)$ is the PA signal amplitude at wavelength λ . δ was subsequently median filtered over 4 degrees angular by 8 samples radial. Lipids were identified by $\delta > \delta_{th}$, where δ_{th} are the threshold values determined from the analysis of the absorption spectra of pure lipids, see Figure 2c, Figure 2d and Figure 5.

Histological validation

After imaging, we cut the artery at the two wires adjacent to the imaging plane to obtain a 3 mm thick artery segment with the imaged cross-section in the middle. The segment was embedded in “optimal cutting temperature” (OCT) compound (Tissue-Tek®, Sakura Finetek Europe B.V.), frozen in liquid nitrogen cooled isopentane vapor, and stored at -80 °C until serial sectioning for staining. We performed Oil Red O (ORO) staining to identify lipids (stained red). A Hematoxylin-Eosin (H&E) stain was used to provide an overview of the artery cross section; a Resorcin-Fuchsin (RF) stain was used to demonstrate the morphology and fibrous structure of the vessel cross-sections.

Results

Lipid differentiation in phantom

We performed sIVPA measurements in the directions indicated by the white dashed lines in the photograph (top view) of the phantom in Figure 2a. The data were analyzed as described in section 2.6 and the resulting averaged normalized PA spectra of cholesterol, cholesterol oleate, cholesterol linoleate and peri-adventitial tissue in the 1.2 and 1.7 μm wavelength range are shown in Figure 2c and 2d, respectively.

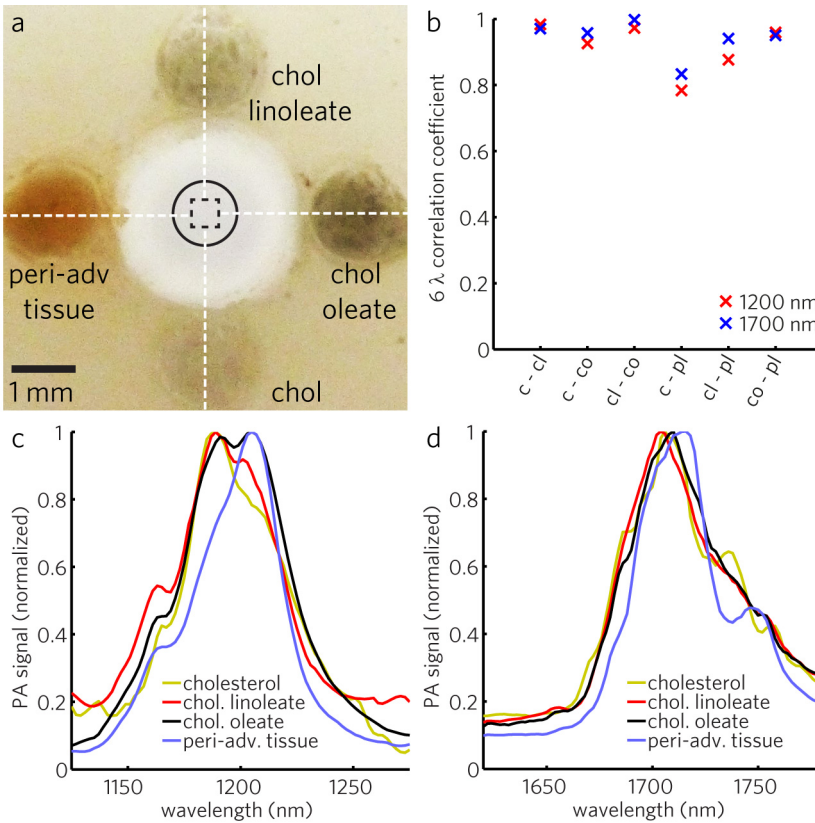


Figure 2. Lipid containing vessel phantom and IVPA spectra of lipid inclusions. a) Photograph of the phantom (top-view), filled with cholesterol (bottom), cholesterol oleate (right), cholesterol linoleate (top) and peri-adventitial tissue (left). b) 6-wavelength correlation coefficients between the spectra of the lipid inclusions. c) Average, normalized PA spectra of the four lipid inclusions in the 1.2 μm wavelength range, and d) in the 1.7 μm wavelength range. c = cholesterol; cl = cholesterol linoleate; co = cholesterol oleate; pl = peri-adventitial lipids.

While the spectra at 1.2 μm exhibit mainly differences in relative peak height, the dominant differences at 1.7 μm are shifts in the locations of the peaks between the spectra of plaque and peri-adventitial lipids.

We obtained cross sectional sIVPA/IVUS data of the lipid-containing vessel phantom at 6 wavelengths in both spectral ranges. The wavelengths are given in Table 1. The lipid maps resulting from the correlation of the data in the 1.2 μm range with the cholesterol and the peri-adventitial lipid reference spectrum are displayed in Figure 3a and 3b, respectively; The corresponding lipid maps obtained in the 1.7 μm range are shown in Figure 3c and 3d, respectively.

Table 1. Wavelengths used for 6-wavelength lipid detection

Wavelength range (μm)	Wavelengths (nm)
1.2	1185, 1195, 1205, 1215, 1225, 1235
1.7	1680, 1710, 1718, 1726, 1734, 1751

All lipid maps are overlaid on the associated, co-registered IVUS image. At 1.2 μm , the cholesterol and the two cholesterol esters, representative of plaque lipids, are all detected clearly, while the peri-adventitial tissue remained concealed (Figure 3a). At 1.7 μm , however, it was not possible to simultaneously detect the cholesterol oleate and keep the peri-adventitial tissue invisible. On the other hand, more of the cholesterol was detected than at 1.2 μm . The correlation with the peri-adventitial reference spectrum resulted in detection of the peri-adventitial tissue in the 1.2 μm wavelength range, while suppressing the other lipids (Figure 3b). In the 1.7 μm wavelength range, less of the peri-adventitial tissue was detected (Figure 3d).

Table 2 lists the threshold correlation values $R_{c,x}$ for the 6-wavelengths at 1.2 and 1.7 μm that were used to create the lipid maps in Figure 3a-3d. To be able to detect peri-adventitial lipids while suppressing plaque lipids, the correlation coefficients had to be chosen much higher for the 1.7 than for the 1.2 μm wavelength range.

Table 2. Threshold values $R_{th,x}$ and δ_{th}

Threshold variable	Wavelength range (μm)	
	1.2	1.7
$R_{th,c}$	0.87	0.88
$R_{th,p/}$	0.88	0.96
δ_{th}	0.37	0.23

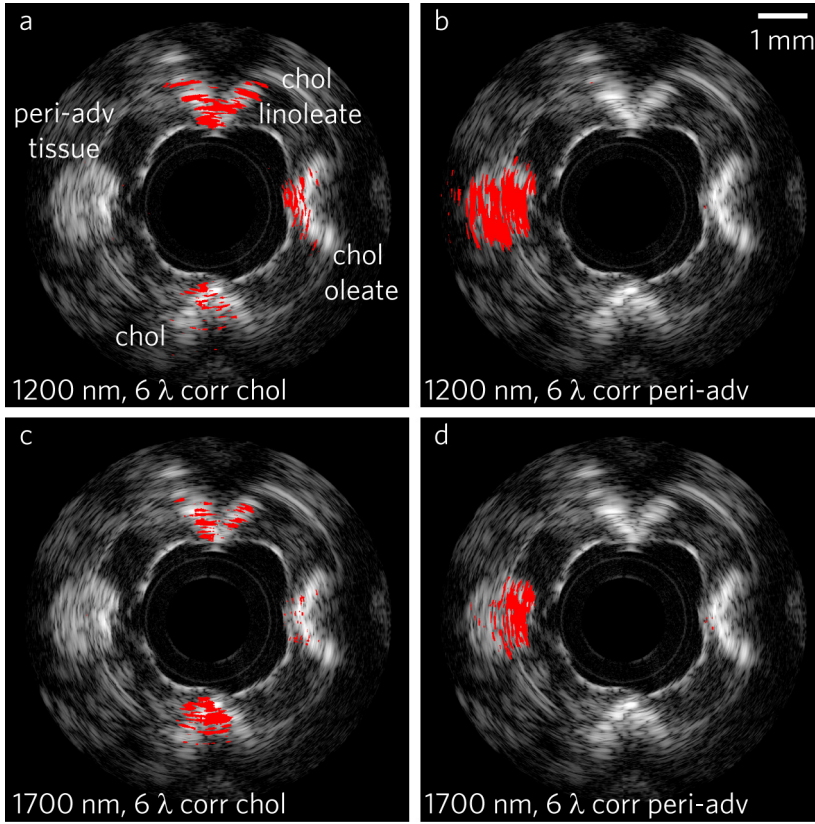


Figure 3. Lipid typing in a lipid-containing vessel phantom using sIVPA at 1.2 and 1.7 μm . a) Lipid map based on 6-wavelength correlation with the cholesterol, and b) with the peri-adventitial reference spectrum in the 1.2 μm wavelength range (1185, 1195, 1205, 1215, 1225 and 1235 nm). c) Lipid map based on the 6-wavelength correlation with the cholesterol, and d) with the peri-adventitial reference spectrum in the 1.7 μm wavelength range (1680, 1710, 1718, 1726, 1734 and 1751 nm). All lipid maps are shown overlaid on the corresponding IVUS image (dynamic range 65 dB). Plaque lipids, represented by cholesterol (bottom), cholesterol oleate (right) and cholesterol linoleate (top) are distinguished clearly from peri-adventitial tissue (left) at 1.2 μm , while lipid typing at 1.7 μm yielded an inferior result.

Lipid detection in phantom and artery

We investigated the ability of sIVPA to detect lipids using two wavelengths at 1.2 μm versus the 1.7 μm , in both the lipid containing vessel phantom and a human coronary artery ex vivo. The phantom results are shown in Figure 4. The co-registered combined IVPA/IVUS images at 1205 (high lipid absorption) and 1235 nm (low lipid absorption) and the resulting relative difference lipid map, are displayed in Figure 4a, 4b and 4c,

respectively. Figure 4d, 4e and 4f depict the corresponding high and low lipid absorption images in the 1.7 μm wavelength range, at 1710 and 1680 nm, and lipid map, respectively. In both wavelength ranges, all four lipid containing cavities exhibit an increased PA signal at λ_h compared to the PA signal at λ_l . In the 1.2 μm range IVPA images, however, a higher signal can be observed from non-lipid regions, compared to the 1.7 μm range IVPA images, due to the overall higher light fluence. Both lipid maps succeed equally well in displaying the peri-adventitial lipid region but the plaque lipids were displayed more clearly in the 1.7 μm wavelength range. The false positives in the 1.7 μm lipid map at 2 times the distance of the lipids from the catheter are the result of incomplete suppression of the pulse echo signal that is generated by absorption of the light in the transducer and catheter tip. This ultrasound signal is also visible in the 1.2 μm range but is effectively suppressed, as well as the higher PA background signal.

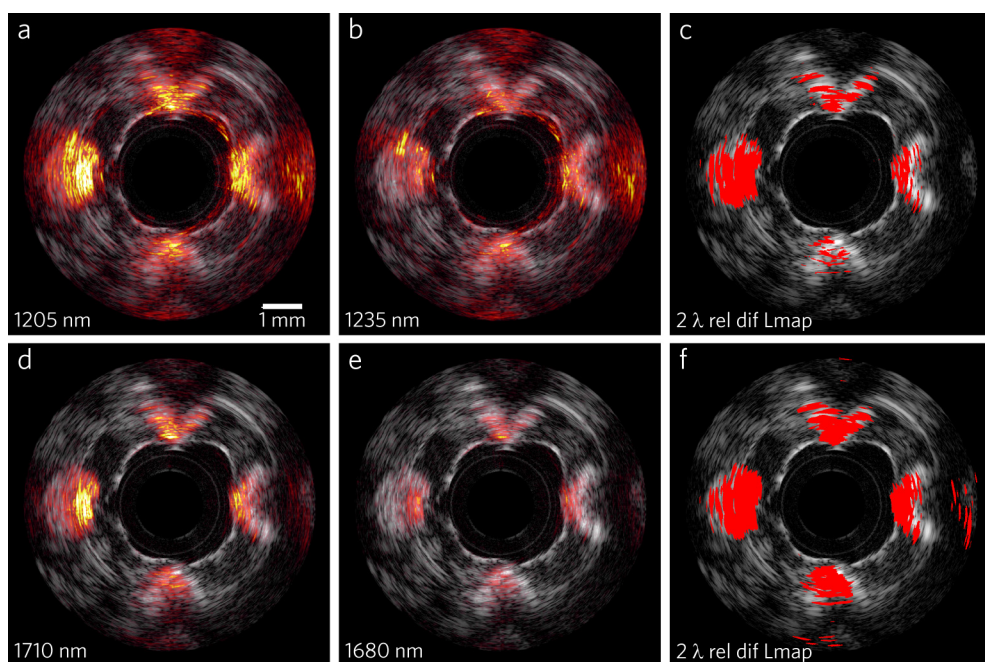


Figure 4. Lipid detection in a lipid-containing vessel phantom using sIVPA at 1.2 and 1.7 μm . a) 1205 nm and b) 1235 nm combined IVPA/IVUS images (IVPA 50 dB, IVUS 65 dB) of PVA phantom filled with cholesterol (bottom), cholesterol oleate (right), cholesterol linoleate (top) and peri-adventitial tissue (left). c) Lipid map based on 2-wavelength relative difference between the PA signal at 1205 nm and 1235 nm. d) Co-registered 1710 nm and e) 1680 nm combined IVPA/IVUS images (IVPA 50 dB, IVUS 65 dB) of the same cross section of the vessel phantom. f) Lipid map resulting from the 2-wavelength relative difference between the PA signal at 1710 nm and 1680 nm. Both lipid maps are shown overlaid on the corresponding IVUS image.

The threshold values δ_c to realize the lipid maps in Figure 4c and 4f, were chosen using the spectral data of the separate lipid compounds. The 5th to 95th percentile of the relative difference of the PA signal at high and low lipid absorption wavelengths of the individual (unaveraged) IVPA spectra measured in the lipid containing phantom were calculated (Figure 5). The relative difference of the absorption coefficient of elastin and collagen at these wavelengths, is shown as well. Threshold values were chosen as the midpoint between the lowest value found for the lipids and the highest value found for elastin and collagen (red dotted line). The resulting threshold values δ_c in both wavelength are listed in Table 2.

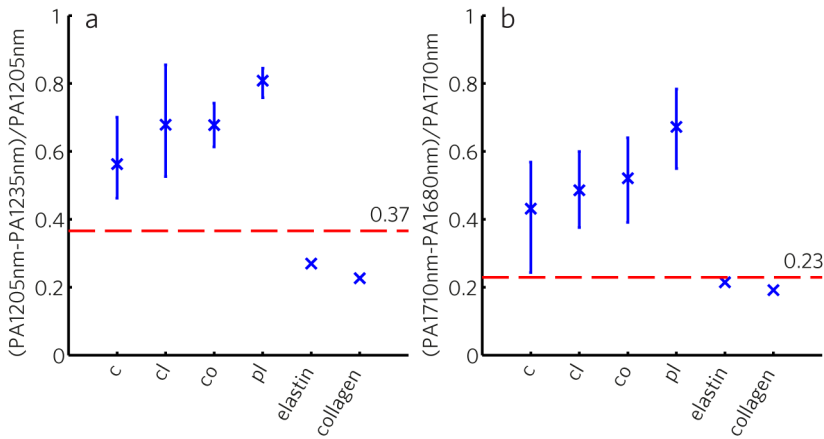


Figure 5. Relative difference of PA signal at high and low lipid absorption wavelengths of individual (unaveraged) IVPA spectra measured in the lipid containing phantom. a) 5th to 95th percentile of the relative difference of the 1205 nm and 1235 nm PA signal strength of cholesterol, cholesterol oleate, cholesterol linoleate and peri-adventitial lipids (32, 128, 160 and 96 spectra, respectively). Data for elastin and collagen are obtained from³⁸. b) 5th to 95th percentile of the relative difference of the 1205 nm and 1235 nm PA signal strength of same lipid components (same number of spectra). Elastin data obtained from⁹⁵; collagen data from⁹⁶. c = cholesterol; cl = cholesterol linoleate; co = cholesterol oleate; pl = peri-adventitial lipids.

The results of the atherosclerotic human coronary specimen (left anterior descending artery, male aged 65) measurement are shown in Figure 6. The top row, Figures 6a-6c, displays the results obtained in the 1.2 μm wavelength range; the bottom row, Figures 6d-6f, the results obtained using wavelengths around 1.7 μm . From left to right, the IVPA images at λ_H , the IVPA images at λ_L , and the 2-wavelength relative difference lipid maps are shown. All images are overlaid on the corresponding IVUS image. The IVUS images show a small lumen with an eccentric plaque at the bottom right of the vessel wall.

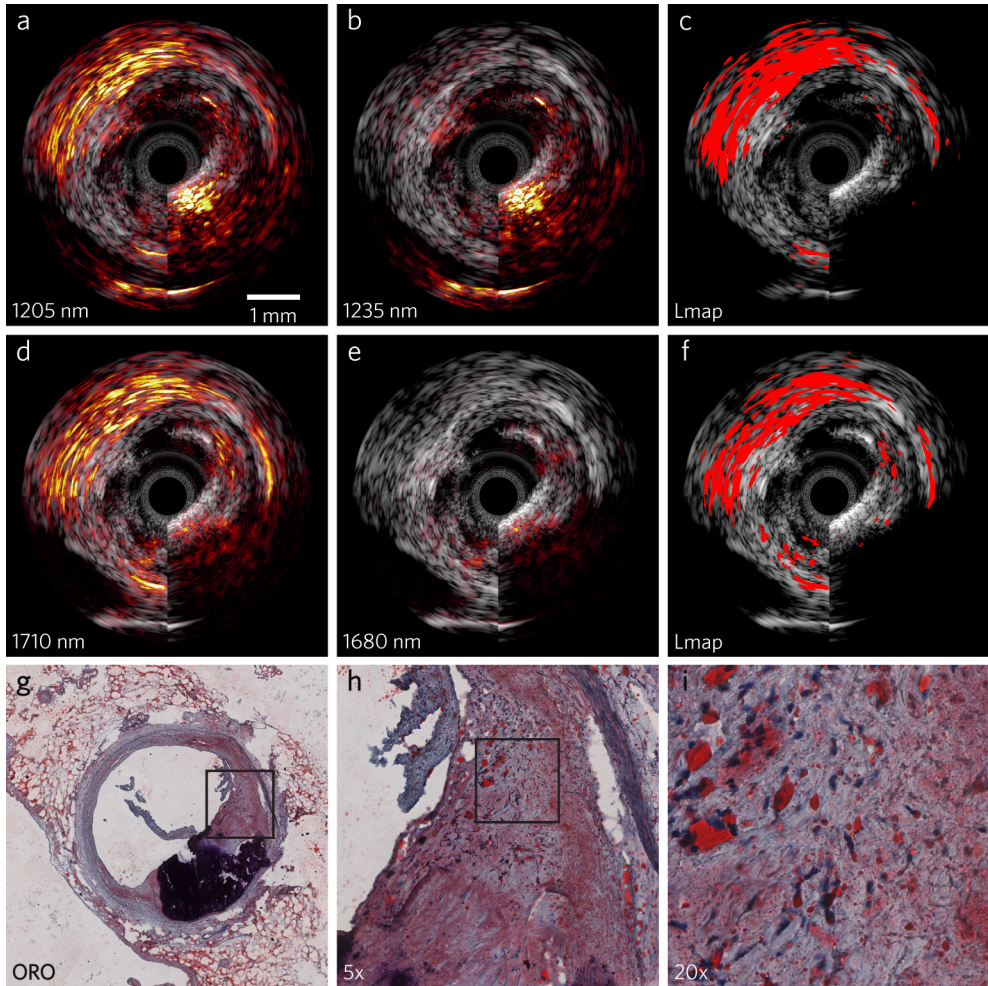


Figure 6. Lipid detection in an atherosclerotic human coronary artery using sIVPA at 1.2 and 1.7 μm . a) 1205 nm and b) 1235 nm combined IVPA/IVUS images (IVPA 25 dB, IVUS 40 dB). c) Lipid map based on 2-wavelength relative difference between the PA signal at 1205 nm and 1235 nm. d) 1710 nm and e) 1680 nm combined IVPA/IVUS images (IVPA 25 dB, IVUS 40 dB). f) Lipid map resulting from the 2-wavelength relative difference between the PA signal at 1710 nm and 1680 nm. Both lipid maps are shown overlaid on the corresponding IVUS image. g) Lipid histology stain (ORO); lipids are stained red; calcification is stained. h) 5x magnification of the part of the atherosclerotic plaque indicated as lipid rich by the lipid stains (area outlined in black in g), shows larger extracellular lipid droplets, while the lipids in all other parts of the lesion are intracellular or contained in small extracellular droplets. i) 4x magnification of area outlined in black in h).

A large calcification is present in the plaque, indicated by the shadowing in the plaque area. The ORO lipid stain, depicted in Figure 6g, confirms these findings (lipids in red; calcification black). The 1205 nm IVPA image shows a slightly enhanced signal from the lipid area in the top part of the plaque, as well as a strongly enhanced signal in the peri-adventitial region around the vessel wall, compared to the 1235 nm IVPA image. In the 1.7 μm range, the enhancement of the signal in the lipid rich plaque area is more pronounced than in the 1.2 μm range, while the signal enhancement in the peri-adventitial region is comparable. Additionally, the calcified region produces much less signal around 1.7 μm , albeit still in the same order of magnitude as the signal produced by the plaque lipids. In accordance with the differences found by visual inspection of the IVPA images, both lipid maps indicate lipids in the top part of the lesion, as well as in the peri-adventitial tissue region around the vessel wall. In the 1.7 μm lipid map however, more intraplaque lipids are detected, due to the higher signal enhancement and therefore better signal to noise ratio. The signal from the calcification is suppressed successfully in both cases. The enlargements of the ORO lipid stain (Figures 6e and 6f) of the area indicated as lipid rich in the lipid maps reveal the presence of larger extracellular lipid droplets, whereas the lipids in all other parts of the lesion are intracellular or contained in small extracellular droplets. This preferential detection is possibly caused by a higher Grüneisen coefficient, a higher concentration of the lipids or a better matching of the generated PA signal frequency to the bandwidth of the transducer. The data presented here (in Figures 3, 4 and 6) show that the maximum lipid imaging depth at 1.2 μm is approximately twice as large compared to 1.7 μm . The exact numerical value depends on the optical (scattering and absorption) and acoustic (frequency-dependent attenuation) properties of the tissue. At 1.2 μm , lipid signal was received from tissue layers in the artery wall at a depth of 5 mm.

Discussion and summary

This study assesses the lipid detection and distinction capabilities of spectroscopic intravascular photoacoustic imaging in two absorption bands, around 1.2 μm and 1.7 μm . We acquired co-registered sIVPA/IVUS data of a lipid containing vessel phantom at 6 wavelengths in either spectral window. Correlation with a cholesterol PA spectrum, as reference for atherosclerotic lipids, and with a peri-adventitial tissue reference spectrum, using 6 wavelengths from 1185 to 1235 nm, distinguishes very well between atherosclerotic lipids and peri-adventitial lipids. The same 6-wavelength correlation method applied on sIVPA data from 1680 to 1751 nm resulted in a poorer separation of in particular cholesterol oleate and peri-adventitial tissue. Applying a 2-wavelength relative difference method, we successfully detected all four lipid compounds present in the vessel phantom in both wavelength ranges, with a superior detection of all four lipids in the 1.7 μm region. In an ex vivo sIVPA/IVUS measurement of an human coronary artery,

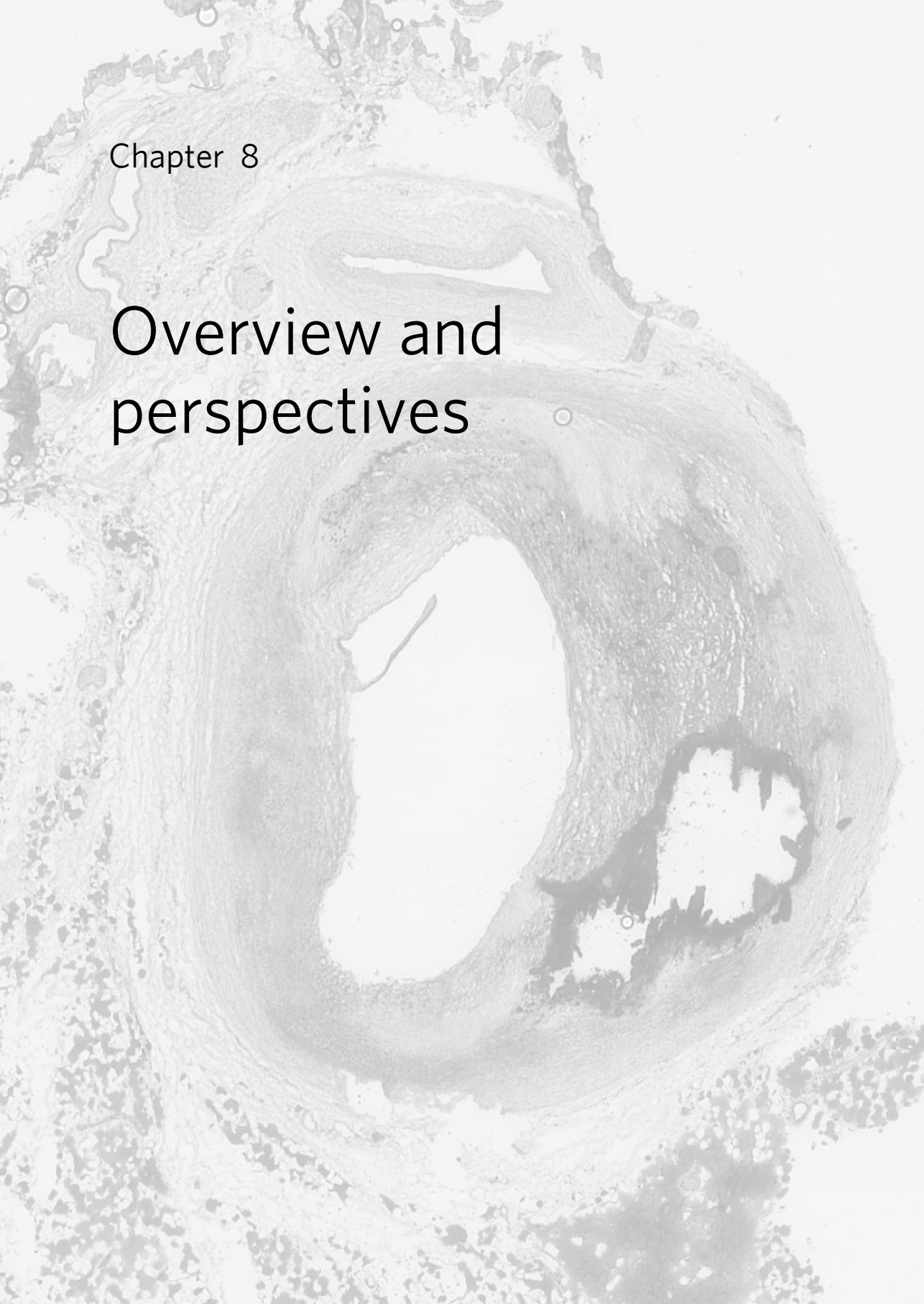
we found superior plaque lipid contrast in the 1.7 μm wavelength range, with a lower pulse energy (0.4 mJ versus 1.2 mJ at 1.2 μm) and sufficient imaging depth (for this particular vessel cross section). Low pulse energy is an advantage because it lowers the optical power that needs to be dissipated in vivo, and also reduces artifacts in IVPA imaging caused by light absorption in the catheter.

The relative difference between two wavelengths is a robust parameter to detect the lipids, also in the presence of strong water absorption in the longer wavelength band, as long as the signal received from the lipids is above the noise level. Note that a minimum of two wavelengths is required in both the 1.2 μm and the 1.7 μm wavelength range to distinguish lipids from other vessel wall constituents; the IVPA signal generated by calcium is in the order of magnitude of the signal from lipids around 1.7 μm and even higher around 1.2 μm .

Minimization of the required number of wavelengths is important for clinical application: the acquisition speed is inversely proportional to the number of PA acquisition needed to compose an image line. Light sources are expected to represent a significant fraction of the cost of an IVPA system for clinical applicability, presenting another reason to limit the number of wavelengths. We demonstrated here that two wavelengths are sufficient, in principle, to detect lipids, but not to differentiate. Noise reduction in the acquisition and more sophisticated analysis, targeted to exploit spectral differences between the various lipid tissues, may yield more insight from a two-wavelength combination.

This study is qualitative in design, exploring several analysis methods applied to the different lipid absorption bands for lipid detection and differentiation by sIVPA. A larger quantitative study will be performed in the future to determine the most favorable wavelengths and the appropriate parameters used for processing. Such a study could also establish whether the imaging depth at 1.7 μm is sufficient to image the vessel wall of larger coronary arteries, such as the left main stem, completely. A larger ex vivo study will also elucidate the representativeness of pure cholesterol, cholesterol oleate, and cholesterol linoleate for the absorption spectra of real atherosclerosis. It will provide insight into the natural variability of the absorption spectrum, which the eventual choice of wavelength combinations will have to take into account. Photoacoustic imaging seems to favor the detection of larger extracellular lipid droplets. To quantify the sensitivity of sIVPA to the different forms and sizes of intraplaque lipids, a statistical analysis of a larger data set should be performed.

In summary, we presented the lipid detection and typing capabilities of 1.2 μm and 1.7 μm sIVPA. We observed superior lipid differentiation in the shorter wavelength range in a lipid containing vessel phantom. In the longer wavelength range, however, intraplaque lipid detection was improved, both in the vessel phantom as well as in an atherosclerotic human coronary artery, with lower pulse energy.

A grayscale micrograph showing a cross-section of a blood vessel. The vessel has a thick, multi-layered wall with concentric rings of tissue. A large, clear, circular lumen is visible in the center. The surrounding tissue is dense and granular.

Chapter 8

Overview and perspectives

Intravascular photoacoustic (IVPA) imaging uses the intrinsic contrast in optical absorption between tissue types to visualize different constituents of atherosclerotic plaques. It is unique in its ability to image atherosclerotic plaque composition up to several millimeters depth and at a high depth resolution of approximately 100 μm .

IVPA is an experimental technique that is undergoing rapid development to become a clinically viable technology. IVPA has been demonstrated to distinguish calcified plaque⁴², atheroma^{40,41}, and more specifically lipids^{44,46,79} from healthy vessel wall, as well as the presence of macrophages through the use of exogenous contrast agents⁵⁰. However, many facets of real-time clinical imaging still need to be resolved. We have taken several essential steps in the direction of in vivo IVPA imaging, in terms of catheter miniaturization, lipid visualization and differentiation, wavelength selection and automated lipid detection. An overview of these accomplishments is given below. At the same time, various important aspects of the light source, catheter design, safety aspects etc., are still under investigation. These specific challenges on the road to in vivo IVPA imaging are discussed at the end of this chapter.

Contributions of this study to the field of IVPA

Practical in vivo implementation of IVPA requires the development of a dedicated catheter device. Catheter miniaturization is critical for intravascular application. Although many functioning combination catheters have been demonstrated previously, their large diameter has prevented intravascular use in human coronary arteries and they have only been tested on phantoms, rabbit aortas, and opened up human arteries. We have developed several combined optical/acoustic catheter devices that are capable of combined co-registered IVPA/IVUS imaging of human coronary arteries. With an outer diameter of 1.25 mm, we created the first fully integrated IVPA/IVUS catheter that was small enough to be inserted into human coronary arteries. We designed and built an experimental combined PA and US system to assess the imaging characteristics of the catheters using dedicated phantoms. The latest prototype has an outer diameter of 1 mm (Chapter 3).

With these small experimental catheters it was possible to image human coronary arteries of deceased patients in a laboratory setting. For this purpose, we collected fresh human coronary arteries from autopsy, showing different stages of disease. The data collected from the artery measurements were used to investigate several aspects of sIVPA imaging to progress towards clinical application. We performed histopathology of all measured arteries to corroborate our findings.

Using the prototype catheters, we demonstrated co-registered IVPA/IVUS imaging of human coronary atherosclerotic plaque. Spectroscopic IVPA (sIVPA) at different wavelengths around 1.2 μm , a lipid-specific absorption band, was performed to visualize the lipid content of an atherosclerotic lesion. IVPA spectra of a lipid rich area around a healthy vessel showed close resemblance to a reference lipid absorption spectrum, verifying the accuracy of IVPA imaging (Chapter 4).

The natural history of atherosclerosis is marked by changes in the lipid biochemistry in the diseased arterial wall. As lesions become more vulnerable, different cholesterol species accumulate in the plaque. We explored the capability of sIVPA imaging to distinguish the most important lipid components of human atherosclerotic plaques: cholesterol and the two most prominent cholesterol esters, cholesterol oleate and cholesterol linoleate. Using reference PA spectra acquired on the pure compounds, we analyzed sIVPA data from human coronary plaques ex vivo, to image plaque composition in terms of cholesterol and cholesterol ester content. In addition, we visualized the deeper lying connective tissue layers of the outer vessel wall, as well as the fatty acid containing adipose cells in the peri-adventitial tissue (Chapter 5).

To be useful in the clinic, as a research tool or to guide percutaneous coronary interventions, however, atherosclerotic lipid content information needs to be readily available without the need for observer-dependent and time-consuming image interpretation. Ideally, only the lipids present within atherosclerotic plaques in the vessel wall are displayed, while the lipids in the tissue around the vessel, which are a component of the normal coronary anatomy, remain hidden. That way, in an artery pullback, which typically contains hundreds of cross-sectional images, the cross-sections that contain plaque lipids will be obvious and can be distinguished easily, without clutter by false-positives from normal adipose tissue. For translation to *in vivo* imaging, where motion artifacts and thus imaging speed play an important role, the number of wavelengths needs to be as small as possible. Therefore, we explored methods for plaque lipid detection and differentiation using sIVPA, with the aim to minimize the number of wavelengths. We imaged a vessel phantom and human coronary arteries *ex vivo* at several wavelengths near 1.2 μm . Using as few as three wavelengths, we could detect and differentiate the lipids in the atherosclerotic plaque and peri-adventitial lipids. With two wavelengths, both plaque and peri-adventitial lipids were detected but could not be distinguished (Chapter 6).

sIVPA generally utilizes one of the two high absorption bands in the lipid absorption spectrum at 1.2 μm and 1.7 μm . Tradeoffs in terms of sensitivity, imaging depth, and possibly chemical specificity exist between the two spectral bands. We measured a lipid containing vessel phantom and an atherosclerotic human coronary artery *ex vivo* in both spectral bands to provide a direct comparison between the two wavelength ranges. We found a stronger lipid-specific signal in a human coronary atherosclerotic plaque at 1.7 μm than at 1.2 μm , even though the pulse energy was lower. The penetration depth of the excitation light at 1.7 μm remained sufficient to image medium sized coronary arteries. On the other hand, discrimination between plaque lipids and lipid deposits in peri-adventitial tissue was more successful at 1.2 μm (Chapter 7).

Towards clinical IVPA imaging of the vulnerable plaque

Combination with other intravascular modalities

IVPA is a tool for plaque composition imaging. It has limited ability to display plaque morphology, and should therefore be combined with another intravascular modality to maximize its potential for the detection of vulnerable plaques. Table 1 gives an overview of the advantages and disadvantages of the different intravascular imaging modalities and their capacity to detect the different markers of plaque vulnerability. There is no single technique that can determine plaque vulnerability completely, which is why multi-modality imaging is frequently proposed. IVPA can differentiate between plaque

components by using the differences in the optical absorption spectra of different tissues, like NIRS. However, unlike NIRS, it has depth resolution which makes it possible to know the exact spatial location of the lipids relative to the lumen border. IVPA provides optical contrast with ultrasound imaging depth. If used in combination with IVUS, IVPA can provide information on plaque composition that complements the morphological information provided by IVUS. In the future, useful combinations with other imaging modalities are likely to be explored, such as an IVPA/OCT combination.

Lipid sensitivity and specificity study

We have performed a qualitative study that demonstrated the viability of detecting arterial lipid with a limited number of wavelengths. It will be compounded in the future with a larger quantitative study to establish the optimal experimental and analysis procedures. Such a study should also include a statistical analysis to quantify the sensitivity and specificity of IVPA for lipid-rich plaque detection. The selection of wavelengths may be further optimized to improve sensitivity. Using two wavelengths only, separate depiction of atherosclerotic plaque lipids and peri-adventitial lipids was not achieved, even though PA data of the pure compounds suggest this as a possibility. In actual tissue, however, variability in optical properties and a lower signal-to-noise level preclude separation of lipid types. Our findings seem to indicate high sensitivity for extracellular lipid droplets, while intracellular lipids remain mostly undetected. Possible causes for this observation are a higher concentration of the lipids, a higher Grüneisen coefficient, which quantifies the photoacoustic conversion efficiency, or the dimensions of the lipid droplets.

IVPA of other markers of plaque vulnerability

IVPA research has primarily focused on imaging of plaque lipids^{44,46,79}. Other disease markers that have been successfully targeted are calcium and inflammatory markers, such as macrophages and matrix metalloproteinase (MMP) activity; the latter two through application of exogenous contrast agents⁹⁷. Intraplaque hemorrhage is another marker of plaque vulnerability that is a potential candidate for IVPA imaging. In a prospective study, patients whose excised carotid plaque revealed plaque hemorrhage or marked intraplaque vessel formation demonstrated an increased risk of future vascular events, independent of clinical risk factors and medication use⁹⁸. The free hemoglobin present in the hemorrhage region could provide optical contrast, primarily in the visible wavelength range⁹⁹.

Table 1. Advantages and disadvantages of each intravascular modality

	Grayscale IVUS	VH-IVUS/ iMap	Palpography	NIRS	IVOCT	IVPA
Image	Cross-section structure	Cross-section tissue type	Radial strain map (elastogram)	Lipid-core plaque map (chemogram)	Cross-section structure	Cross- section tissue type (Near-IR) light + ultrasound
Type of radiation	Ultrasound	Ultrasound	Ultrasound	Near-IR light	Near-IR light	
Axial resolution (μm)	100-200	> 250	450	N/A	10-15	100
Lateral resolution (μm)	300-500	300-500	300-500	1000	30-40	400-500
Penetration (mm)	10	5	N/A	unknown	1	5
Contrast mechanism	Acoustic scattering	Acoustic spectrum	tissue strain	Optical absorption	Optical scattering	Optical absorption
Pullback rate	0.5 mm/s	0.5 mm/s	0.5 mm/s	0.5 mm/s	20-40 mm/s	N/A
Flushing	No	No	no	no	Yes	TBD*
Current status	CS/CA	CS/CA	CS	CS/CA	CS/CA	PCS
Lumen area	++	++	-	-	++	\pm
Plaque burden	++	++	-	-	-	\pm
Positive remodeling	++	++	-	-	-	\pm
Necrotic core	\pm	++	++	++	-	++
Fibrous-cap thickness	-	-	-	-	+	-
TCFA**	-	\pm	++	-	+	\pm
Plaque rupture	+	+	-	-	++	-
Erosion	-	-	-	-	+	-
Thrombus	\pm	\pm	-	-	+	-
Inflammation	-	-	-	-	\pm	\pm
Calcium	++	++	++	-	+	-

Table 1. Subscript

Abbreviations: IVUS, intravascular ultrasound; VH, virtual histology; NIRS, near-infrared spectroscopy; IVOCT, intravascular optical coherence tomography; NIRF, near-infrared fluorescence; IVPA, intravascular photoacoustics. CA indicates clinically, commercially available; CS, clinical studies; PCS, pre-clinical studies; N/A, not applicable.

* May not be required in specific wavelength bands (e.g., the near-infrared window)

** The positive predictive value to detect “definite TCFA” (defined as agreement by both OCT and VH-IVUS) was 78% by OCT but only 46% by VH-IVUS by Sawada et al.¹⁰⁰

++, excellent; +, good; ±, possible; –, impossible.

Data derived from Kubo and Akasaka¹⁰¹, Suh et al.¹⁰², MacNeill¹⁰³ and Maehara¹⁰⁴. Palpography data derived from Schaar et al.¹⁰⁵

Imaging through blood

In order to obtain optimal photoacoustic signal strength, it is desirable to deliver as much light to the vessel wall as is possible within the physical boundaries of the instrument, and within the safety limits¹⁰⁶. Blood is a strongly scattering tissue, which can markedly reduce the light intensity at the vessel wall, even at wavelengths in the near infrared region. Several ex vivo IVPA experiments have demonstrated IVPA imaging through blood⁴⁵⁻⁴⁸ but the image quality deteriorates considerably compared to a water-filled lumen. Even when imaging at 1720 nm, at very high lipid absorption, the image quality and reliability of the atherosclerotic lipid detection by IVPA would be greatly improved by flushing. It therefore appears likely that IVPA imaging may involve flushing of the blood from the artery in the clinical setting. Blood clearing is standard practice in IVOCT imaging. Unlike IVOCT, IVPA does not rely on the complete suppression of scattering in the lumen, but only requires the delivery of sufficient power. This means that dilution, rather than complete clearing, may be good enough. The ultrasonic properties of the flush media used for OCT (iodixanol, a coronary angiography contrast agent, trade name Visipaque™ (GE Healthcare) are not precisely known, so its suitability for IVPA needs to be investigated.

Light sources

IVPA poses a set of strict requirements on the light source. Lasers used in development of the technology are powerful and versatile, but slow at pulse repetition rates of 10-50 Hz. This low pulse frequency precludes practical in vivo imaging. Particularly if flushing is used, the optimal imaging sequence will be modeled on that of Fourier domain OCT: high frame rate, high pullback speed, short pullback time of <10 s. This acquisition protocol prescribes a light source with a repetition rate of the order of 10 kHz, with wavelengths that generates relevant contrast. Such lasers are currently being developed.

Catheter miniaturization and real-time imaging system development

The smallest combined IVPA/IVUS catheter diameter built to date has a diameter of 1 mm. Current IVUS probes have an outer diameter of less than 1 mm, including the protective sheath in which they rotate. Future developments will reduce the IVPA catheter diameter to 1 mm or less for successful application in clinical practice. All-optical devices are much smaller but sacrifice IVUS functionality. An IVPA catheter operating on the principle we describe in this work may be further miniaturized through the use of a 100 μm core angle polished optical fiber with a smaller quartz cap, to produce a catheter tip with an outer diameter of 0.7 mm. The catheter tip will connect to a torque coil of the same outer diameter to create a flexible catheter that can be rotated from the proximal end. This ensures a total outer diameter of the catheter, including the protective sheath in which it rotates, of less than 1 mm. The catheter will attach to a driving unit, consisting of a translation and rotary motor, and an electrical/optical rotary joint. The current combined IVPA/IVUS imaging system is specifically designed to conduct explorative studies in a laboratory setting. Adjustments will have to be made to the system to make it suitable for real-time in vivo imaging.

Once transformed into a real-time, clinically accepted imaging modality, IVPA has the potential for becoming the next intravascular imaging revolution. It will become a powerful tool for guidance of percutaneous coronary intervention, informing the decision of which plaque to treat and length to stent with detailed composition information. IVPA will also contribute to studies of plaque vulnerability, and allow quantification of the response to different forms of intervention (device, pharmacologic, lifestyle changes) with rich chemical detail in vivo^{72,107}. It is well positioned to play a leading role in clinical studies as an imaging endpoint, to show changes in the lipid content of atherosclerotic plaques.

References

- 1 Global atlas on cardiovascular disease prevention and control. (eds. Mendis, S, Puska, P, Norrving, B) (World Health Organization, Geneva, 2011).
- 2 Falk E, Shah PK, Fuster V. Coronary plaque disruption. *Circulation*. 1995;92:657-71.
- 3 Schaar JA, Muller JE, Falk E, Virmani R, Fuster V, Serruys PW, Colombo A, Stefanadis C, Casscells WS, Moreno PR, Maseri A, van der Steen AFW. Terminology for high-risk and vulnerable coronary artery plaques. *Eur Heart J*. 2004;25:1077-82.
- 4 Virmani R, Kolodgie FD, Burke AP, Farb A, Schwartz SM. Lessons from sudden coronary death : A comprehensive morphological classification scheme for atherosclerotic lesions. *Arterioscler Thromb Vasc Biol*. 2000;20:1262-75.
- 5 Richardson PD, Davies MJ, Born GV. Influence of plaque configuration and stress distribution on fissuring of coronary atherosclerotic plaques. *Lancet*. 1989; 334:941-4.
- 6 Narula J, Nakano M, Virmani R, Kolodgie FD, Petersen R, Newcomb R, Malik S, Fuster V, Finn AV. Histopathologic Characteristics of Atherosclerotic Coronary Disease and Implications of the Findings for the Invasive and Noninvasive Detection of Vulnerable Plaques. *J Am Coll Cardiol*. 2013;61:1041-51.
- 7 Virmani R, Burke AP, Farb A, Kolodgie FD. Pathology of the vulnerable plaque. *J Am Coll Cardiol*. 2006;47:C13-C8.
- 8 Drake R, Vogl AW, Mitchell AW. *Gray's anatomy for students*, (Elsevier Health Sciences, 2009).
- 9 Serruys PW, Ormiston JA, Onuma Y, Regar E, Gonzalo N, Garcia-Garcia HM, Nieman K, Bruining N, Dorange C, Miquel-Hébert K. A bioabsorbable everolimus-eluting coronary stent system (ABSORB): 2-year outcomes and results from multiple imaging methods. *The Lancet*. 2009;373:897-910.
- 10 Piers LH, Dijkers R, Willems TP, de Smet BJ, Oudkerk M, Zijlstra F, Tio RA. Computed tomographic angiography or conventional coronary angiography in therapeutic decision-making. *Eur Heart J*. 2008;29:2902-7.
- 11 Raff GL, Gallagher MJ, O'Neill WW, Goldstein JA. Diagnostic accuracy of noninvasive coronary angiography using 64-slice spiral computed tomography. *J Am Coll Cardiol*. 2005;46:552-7.
- 12 Schroeder S, Kopp AF, Baumbach A, Meisner C, Kuettner A, Georg C, Ohnesorge B, Herdeg C, Claussen CD, Karsch KR. Noninvasive detection and evaluation of atherosclerotic coronary plaques with multislice computed tomography. *J Am Coll Cardiol*. 2001;37:1430-5.

- 13 Hoffmann U, Moselewski F, Nieman K, Jang IK, Ferencik M, Rahman AM, Cury RC, Abbara S, Joneidi-Jafari H, Achenbach S, Brady TJ. Noninvasive assessment of plaque morphology and composition in culprit and stable lesions in acute coronary syndrome and stable lesions in stable angina by multidetector computed tomography. *J Am Coll Cardiol.* 2006;47:1655-62.
- 14 Motoyama S, Kondo T, Sarai M, Sugiura A, Harigaya H, Sato T, Inoue K, Okumura M, Ishii J, Anno H, Virmani R, Ozaki Y, Hishida H, Narula J. Multislice computed tomographic characteristics of coronary lesions in acute coronary syndromes. *J Am Coll Cardiol.* 2007;50:319-26.
- 15 Motoyama S, Sarai M, Harigaya H, Anno H, Inoue K, Hara T, Naruse H, Ishii J, Hishida H, Wong ND, Virmani R, Kondo T, Ozaki Y, Narula J. Computed tomographic angiography characteristics of atherosclerotic plaques subsequently resulting in acute coronary syndrome. *J Am Coll Cardiol.* 2009;54:49-57.
- 16 Min JK, Berman DS, Dunning A, Achenbach S, Al-Mallah M, Budoff MJ, Cademartiri F, Callister TQ, Chang HJ, Cheng V, Chinnaiyan K, Chow BJ, Cury R, Delago A, Feuchtner G, Hadamitzky M, Hausleiter J, Kaufmann P, Karlsberg RP, Kim YJ, Leipsic J, Lin FY, Maffei E, Plank F, Raff G, Villines T, Labounty TM, Shaw LJ. All-cause mortality benefit of coronary revascularization vs. medical therapy in patients without known coronary artery disease undergoing coronary computed tomographic angiography: results from CONFIRM (COronary CT Angiography EvaluationN For Clinical Outcomes: An InteRnational Multicenter Registry). *Eur Heart J.* 2012;33:3088-97.
- 17 Fuster V, Kim RJ. Frontiers in cardiovascular magnetic resonance. *Circulation.* 2005;112:135-44.
- 18 Kohsaka S, Makaryus AN. Coronary angiography using noninvasive imaging techniques of cardiac CT and MRI. *Current cardiology reviews.* 2008;4:323.
- 19 Fayad ZA, Fuster V, Nikolaou K, Becker C. Computed Tomography and Magnetic Resonance Imaging for Noninvasive Coronary Angiography and Plaque Imaging: Current and Potential Future Concepts. *Circulation.* 2002;106:2026-34.
- 20 de Korte CL, Pasterkamp G, van der Steen AF, Woutman HA, Bom N. Characterization of plaque components with intravascular ultrasound elastography in human femoral and coronary arteries in vitro. *Circulation.* 2000;102:617-23.
- 21 Nissen SE, Yock P. Intravascular ultrasound - Novel pathophysiological insights and current clinical applications. *Circulation.* 2001;103:604-16.
- 22 Nair A, Kuban BD, Tuzcu EM, Schoenhagen P, Nissen SE, Vince DG. Coronary plaque classification with intravascular ultrasound radiofrequency data analysis. *Circulation.* 2002;106:2200-6.
- 23 Garcia-Garcia HM, Costa MA, Serruys PW. Imaging of coronary atherosclerosis: intravascular ultrasound. *Eur Heart J.* 2010

- 24 Thim T, Hagensen MK, Wallace-Bradley D, Granada JF, Kaluza GL, Drouet L, Paaske WP, Botker HE, Falk E. Unreliable assessment of necrotic core by Virtual Histology intravascular ultrasound in porcine coronary artery disease. *Circ Cardiovasc Imaging*. 2010;3:384-91.
- 25 Granada JF, Wallace-Bradley D, Win HK, Alviar CL, Builes A, Lev EI, Barrios R, Schulz DG, Raizner AE, Kaluza GL. In vivo plaque characterization using intravascular ultrasound-virtual histology in a porcine model of complex coronary lesions. *Arterioscler Thromb Vasc Biol*. 2007;27:387-93.
- 26 Shin ES, Garcia-Garcia HM, Ligthart JM, Witberg K, Schultz C, van der Steen AF, Serruys PW. In vivo findings of tissue characteristics using iMap IVUS and Virtual Histology IVUS. *EuroIntervention*. 2011;6:1017-9.
- 27 Tearney GJ, Waxman S, Shishkov M, Vakoc BJ, Suter MJ, Freilich MI, Desjardins AE, Oh W-Y, Bartlett LA, Rosenberg M, Bouma BE. Three-dimensional coronary artery microscopy by intracoronary optical frequency domain imaging. *J Am Coll Cardiol Img*. 2008;1:752-61.
- 28 Tearney GJ, Yabushita H, Houser SL, Aretz HT, Jang I-K, Schlendorf KH, Kauffman CR, Shishkov M, Halpern EF, Bouma BE. Quantification of macrophage content in atherosclerotic plaques by optical coherence tomography. *Circulation*. 2003;107:113-9.
- 29 Tearney GJ, Regar E, Akasaka T, Adriaenssens T, Barlis P, Bezerra HG, Bouma B, Bruining N, Cho J-m, Chowdhary S, Costa MA, de Silva R, Dijkstra J, Di Mario C, Dudeck D, Falk E, Feldman MD, Fitzgerald P, Garcia H, Gonzalo N, Granada JF, Guagliumi G, Holm NR, Honda Y, Ikeno F, Kawasaki M, Kochman J, Koltowski L, Kubo T, Kume T, Kyono H, Lam CCS, Lamouche G, Lee DP, Leon MB, Maehara A, Manfrini O, Mintz GS, Mizuno K, Morel M-a, Nadkarni S, Okura H, Otake H, Pietrasik A, Prati F, Räber L, Radu MD, Rieber J, Riga M, Rollins A, Rosenberg M, Sirbu V, Serruys PWJC, Shimada K, Shinke T, Shite J, Siegel E, Sonada S, Suter M, Takarada S, Tanaka A, Terashima M, Troels T, Uemura S, Ughi GJ, van Beusekom HMM, van der Steen AFW, van Es G-A, van Soest G, Virmani R, Waxman S, Weissman NJ, Weisz G. Consensus standards for acquisition, measurement, and reporting of intravascular optical coherence tomography studies: a report from the International Working Group for Intravascular Optical Coherence Tomography Standardization and Validation. *J Am Coll Cardiol*. 2012;59:1058-72.
- 30 van Soest G, Goderie T, Regar E, Koljenovic S, van Leenders GLJH, Gonzalo N, van Noorden S, Okamura T, Bouma BE, Tearney GJ, Oosterhuis JW, Serruys PW, van der Steen AFW. Atherosclerotic tissue characterization in vivo by optical coherence tomography attenuation imaging. *J Biomed Opt*. 2010;15:011105-9.
- 31 Garg S, Serruys PW, van der Ent M, Schultz C, Mastik F, van Soest G, van der Steen AF, Wilder MA, Muller JE, Regar E. First use in patients of a combined near infra-

- red spectroscopy and intra-vascular ultrasound catheter to identify composition and structure of coronary plaque. *EuroIntervention*. 2010;5:755-6.
- 32 Gardner CM, Tan H, Hull EL, Lissauskas JB, Sum ST, Meese TM, Jiang C, Madden SP, Caplan JD, Burke AP, Virmani R, Goldstein J, Muller JE. Detection of lipid core coronary plaques in autopsy specimens with a novel catheter-based near-infrared spectroscopy system. *JACC Cardiovasc Imaging*. 2008;1:638-48.
 - 33 Moreno PR, Lodder RA, Purushothaman KR, Charash WE, O'Connor WN, Muller JE. Detection of lipid pool, thin fibrous cap, and inflammatory cells in human aortic atherosclerotic plaques by near-infrared spectroscopy. *Circulation*. 2002;105:923-7.
 - 34 Goldstein J, Madden S, Sum S, Dixon S, Madder R, Muller J. Assessment of Plaque Composition with Near-Infrared Spectroscopy. *Current Cardiovascular Imaging Reports*. 2011;4:298-308.
 - 35 Oraevsky AA, Karabutov AA. Optoacoustic Tomography. in *Biomedical Photonics Handbook* (ed. Vo-Dinh, T) 34-1 (CRC Press Boca Raton, FL, 2003).
 - 36 Van Veen RLP, Sterenborg HJCM, Pifferi A, Torricelli A, Cubeddu R. Determination of VIS- NIR absorption coefficients of mammalian fat, with time- and spatially resolved diffuse reflectance and transmission spectroscopy. *OSA Biomedical Optics Topical Meeting*. 2004
 - 37 Tromberg BJ, Shah N, Lanning R, Cerussi A, Espinoza J, Pham T, Svaasand L, Butler J. Non-invasive in vivo characterization of breast tumors using photon migration spectroscopy. *Neoplasia*. 2000;2:26-40.
 - 38 Tsai CL, Chen JC, Wang WJ. Near-infrared absorption property of biological soft tissue constituents. *J Med Biol Eng*. 2001;21:7-14.
 - 39 Prince MR, Deutsch TF, Mathews-Roth MM, Margolis R, Parrish JA, Oseroff AR. Preferential light absorption in atheromas in vitro. Implications for laser angioplasty. *J Clin Invest*. 1986;78:295-302.
 - 40 Al Dhahir RK, Dyer PE, Zhu Z. Photoacoustic studies and selective ablation of vascular tissue using a pulsed dye laser. *Appl Phys B*. 1990;51:81-5.
 - 41 Beard PC, Mills TN. Characterization of post mortem arterial tissue using time-resolved photoacoustic spectroscopy at 436, 461 and 532 nm. *Phys Med Biol*. 1997;42:177-98.
 - 42 Crazzolara H, Vonmuench W, Rose C, Thiemann U, Haase KK, Ritter M, Karsch KR. Analysis of the acoustic response of vascular tissue irradiated by an ultraviolet-laser pulse. *J Appl Phys*. 1991;70:1847-9.
 - 43 Sethuraman S, Amirian JH, Litovsky SH, Smalling RW, Emelianov SY. Spectroscopic intravascular photoacoustic imaging to differentiate atherosclerotic plaques. *Opt Express*. 2008;16:3362-7.

- 44 Wang B, Su JL, Amirian J, Litovsky SH, Smalling R, Emelianov S. Detection of lipid in atherosclerotic vessels using ultrasound-guided spectroscopic intravascular photoacoustic imaging. *Opt Express*. 2010;18:4889-97.
- 45 Allen TJ, Beard PC. Photoacoustic characterisation of vascular tissue at NIR wavelengths. *Photons Plus Ultrasound: Imaging and Sensing* 2009. 2009;7177:71770A-9.
- 46 Allen TJ, Hall A, Dhillon AP, Owen JS, Beard PC. Spectroscopic photoacoustic imaging of lipid-rich plaques in the human aorta in the 740 to 1400 nm wavelength range. *J Biomed Opt*. 2012;17:061209-10.
- 47 Wang B, Karpouk A, Yeager D, Amirian J, Litovsky S, Smalling R, Emelianov S. Intravascular photoacoustic imaging of lipid in atherosclerotic plaques in the presence of luminal blood. *Opt Lett*. 2012;37:1244-6.
- 48 Wang B, Karpouk A, Yeager D, Amirian J, Litovsky S, Smalling R, Emelianov S. In vivo Intravascular Ultrasound-guided Photoacoustic Imaging of Lipid in Plaques Using an Animal Model of Atherosclerosis. *Ultrasound Med Biol*. 2012
- 49 Wang P, Wang P, Wang HW, Cheng JX. Mapping lipid and collagen by multispectral photoacoustic imaging of chemical bond vibration. *J Biomed Opt*. 2012;17:96010-1.
- 50 Wang B, Yantsen E, Larson T, Karpouk AB, Sethuraman S, Su JL, Sokolov K, Emelianov SY. Plasmonic intravascular photoacoustic imaging for detection of macrophages in atherosclerotic plaques. *Nano Lett*. 2009;9:2212-7.
- 51 Yeager D, Karpouk A, Wang B, Amirian J, Sokolov K, Smalling R, Emelianov S. Intravascular photoacoustic imaging of exogenously labeled atherosclerotic plaque through luminal blood. *J Biomed Opt*. 2012;17:106016-.
- 52 Razansky D, Harlaar NJ, Hillebrands JL, Taruttis A, Herzog E, Zeebregts CJ, van Dam GM, Ntziachristos V. Multispectral optoacoustic tomography of matrix metalloproteinase activity in vulnerable human carotid plaques. *Mol Imaging Biol*. 2011
- 53 Pérennès F, Beard PC, Mills TN. Intravascular photoacoustic-photothermal imaging of the arterial wall using a miniature optical fibre probe. *Horizons de l'Optique 1997 dixieme colloque de la Societe Francaise d'Optique*. 1997:A13.
- 54 Zhang EZ, Beard PC. A miniature all-optical photoacoustic imaging probe. *Photons Plus Ultrasound: Imaging and Sensing* 2011. 2011;7899:78991F-6.
- 55 Karpouk AB, Wang B, Emelianov SY. Development of a catheter for combined intravascular ultrasound and photoacoustic imaging. *Rev Sci Instrum*. 2010;81:014901-1-7.
- 56 Hsieh BY, Chen SL, Ling T, Guo LJ, Li PC. Integrated intravascular ultrasound and photoacoustic imaging scan head. *Opt Lett*. 2010;35:2892-4.
- 57 Li X, Wei W, Zhou Q, Shung KK, Chen Z. Intravascular photoacoustic imaging at 35 and 80 MHz. *J Biomed Opt*. 2012;17:106005-1.

- 58 Zhou Q, Xu X, Gottlieb EJ, Sun L, Cannata JM, Ameri H, Humayun MS, Han P, Shung KK. PMN-PT single crystal, high-frequency ultrasonic needle transducers for pulsed-wave Doppler application. *IEEE Trans Ultrason Ferroelectr Freq Control*. 2007;54:668-75.
- 59 Ziskin MC, Thickman DI, Goldenberg NJ, Lapayowker MS, Becker JM. The comet tail artifact. *J Ultrasound Med*. 1982;1:1-7.
- 60 Karpouk AB, Wang B, Emelianov SY. Integrated catheter for intravascular ultrasound and photoacoustic imaging. *Photons Plus Ultrasound: Imaging and Sensing 2010*. 2010;7564:756408-1-6.
- 61 Falk E. Plaque rupture with severe pre-existing stenosis precipitating coronary thrombosis. Characteristics of coronary atherosclerotic plaques underlying fatal occlusive thrombi. *Br Heart J*. 1983;50:127-34.
- 62 Waxman S, Ishibashi F, Muller JE. Detection and treatment of vulnerable plaques and vulnerable patients - Novel approaches to prevention of coronary events. *Circulation*. 2006;114:2390-411.
- 63 Waxman S, Freilich MI, Suter MJ, Shishkov M, Bilazarian S, Virmani R, Bouma BE, Tearney GJ. A case of lipid core plaque progression and rupture at the edge of a coronary stent: Elucidating the mechanisms of drug-eluting stent failure. *Circ Cardiovasc Interv*. 2010;3:193-6.
- 64 Nissen SE. Application of intravascular ultrasound to characterize coronary artery disease and assess the progression or regression of atherosclerosis. *Am J Cardiol*. 2002;89:24B-31B.
- 65 Palmer ND, Northridge D, Lessells A, McDicken WN, Fox KAA. In vitro analysis of coronary atheromatous lesions by intravascular ultrasound. Reproducibility and histological correlation of lesion morphology. *Eur Heart J*. 1999;20:1701-6.
- 66 Holman RT, Edmondson PR. Near-Infrared Spectra of Fatty Acids and Some Related Substances. *Anal Chem*. 1956;28:1533-8.
- 67 Madder RD, Chinnaiyan KM, Marandici AM, Goldstein JA. Features of disrupted plaques by coronary CT Angiography: correlates with invasively-proven complex lesions. *Circ Cardiovasc Imaging*. 2011;4:105-13.
- 68 Small DM. George Lyman Duff memorial lecture. Progression and regression of atherosclerotic lesions. Insights from lipid physical biochemistry. *Arterioscler Thromb Vasc Biol*. 1988;8:103-29.
- 69 Felton CV, Crook D, Davies MJ, Oliver MF. Relation of plaque lipid composition and morphology to the stability of human aortic plaques. *Arterioscler Thromb Vasc Biol*. 1997;17:1337-45.
- 70 Puato M, Faggin E, Rattazzi M, Zambon A, Cipollone F, Grego F, Ganassin L, Plebani M, Mezzetti A, Pauletto P. Atorvastatin reduces macrophage accumulation in atherosclerotic plaques : a comparison of a nonstatin-based regimen in patients undergoing carotid endarterectomy. *Stroke*. 2010;41:1163-8.

- 71 Achenbach S, Moselewski F, Ropers D, Ferencik M, Hoffmann U, MacNeill B, Pohle K, Baum U, Anders K, Jang IK, Daniel WG, Brady TJ. Detection of calcified and noncalcified coronary atherosclerotic plaque by contrast-enhanced, submillimeter multidetector spiral computed tomography : a segment-based comparison with intravascular ultrasound. *Circulation*. 2004;109:14-7.
- 72 Serruys PW, Garcia-Garcia HM, Buszman P, Erne P, Verheye S, Aschermann M, Duckers H, Bleie O, Dudek D, Botker HE, von Birgelen C, D'Amico D, Hutchinson T, Zambanini A, Mastik F, van Es GA, van der Steen AF, Vince DG, Ganz P, Hamm CW, Wijns W, Zalewski A. Effects of the direct lipoprotein-associated phospholipase A(2) inhibitor darapladib on human coronary atherosclerotic plaque. *Circulation*. 2008;118:1172-82.
- 73 Nozue T, Yamamoto S, Tohyama S, Umezawa S, Kunishima T, Sato A, Miyake S, Takeyama Y, Morino Y, Yamauchi T, Muramatsu T, Hibi K, Sozu T, Terashima M, Michishita I. Statin treatment for coronary artery plaque composition based on intravascular ultrasound radiofrequency data analysis. *Am Heart J*. 2012;163:191-9.
- 74 Nissen SE, Nicholls SJ, Sipahi I, Libby P, Raichlen JS, Ballantyne CM, Davignon J, Erbel R, Fruchart JC, Tardif JC, Schoenhagen P, Crowe T, Cain V, Wolski K, Goormastic M, Tuzcu EM. Effect of very high-intensity statin therapy on regression of coronary atherosclerosis: the ASTEROID trial. *J Am Med Assoc*. 2006;295:1556-65.
- 75 Stone GW, Maehara A, Lansky AJ, de Bruyne B, Cristea E, Mintz GS, Mehran R, McPherson J, Farhat N, Marso SP, Parise H, Templin B, White R, Zhang Z, Serruys PW. A prospective natural-history study of coronary atherosclerosis. *N Engl J Med*. 2011;364:226-35.
- 76 Libby P, Sasiela W. Plaque stabilization: Can we turn theory into evidence? *Am J Cardiol*. 2006;98:26P-33P.
- 77 Klein LW. Atherosclerosis regression, vascular remodeling, and plaque stabilization. *J Am Coll Cardiol*. 2007;49:271-3.
- 78 Beard P. Biomedical photoacoustic imaging. *Interface Focus*. 2011;1:602-31.
- 79 Jansen K, van der Steen AFW, van Beusekom HMM, Oosterhuis JW, van Soest G. Intravascular photoacoustic imaging of human coronary atherosclerosis. *Opt Lett*. 2011;36:597-9.
- 80 Jansen K, Springeling G, Lancee C, Beurskens R, Mastik F, van der Steen AFW, van Soest G. An intravascular photoacoustic imaging catheter. *International Ultrasonics Symposium (IUS)*, 2010 IEEE. 2010:378-81.
- 81 Weyer LG, Lo SC. Spectra-structure correlations in the near-infrared. in *Handbook of Vibrational Spectroscopy*, Vol. 3 (ed. Tabata, M) 1817-37 (John Wiley & Sons, Chichester, 2002).

- 82 Katz SS, Shipley GG, Small DM. Physical chemistry of the lipids of human atherosclerotic lesions. Demonstration of a lesion intermediate between fatty streaks and advanced plaques. *J Clin Invest.* 1976;58:200-11.
- 83 Suarna C, Dean RT, May J, Stocker R. Human atherosclerotic plaque contains both oxidized lipids and relatively large amounts of α -tocopherol and ascorbate. *Arterioscler Thromb Vasc Biol.* 1995;15:1616-24.
- 84 Waxman S, Dixon SR, L'Allier P, Moses JW, Petersen JL, Cutlip D, Tardif JC, Nesto RW, Muller JE, Hendricks MJ, Sum ST, Gardner CM, Goldstein JA, Stone GW, Krucoff MW. In vivo validation of a catheter-based near-infrared spectroscopy system for detection of lipid core coronary plaques initial results of the SPECTACL study. *JACC Cardiovasc Imaging.* 2009;2:858-68.
- 85 de Korte CL, van der Steen AFW, Cespedes EI, Pasterkamp G, Carlier SG, Mastik F, Schoneveld AH, Serruys PW, Bom N. Characterization of plaque components and vulnerability with intravascular ultrasound elastography. *Phys Med Biol.* 2000;45:1465-75.
- 86 Gardner CM, Lissauskas J, Hull EL, Tan H, Sum S, Meese T, Jiang C, Madden S, Caplan J, Muller JE. A catheter-based near-infrared scanning spectroscopy system for imaging lipid-rich plaques in human coronary arteries in vivo. *Proc. SPIE.* 2007;6765:67650G-8.
- 87 Razansky D, Vinegoni C, Ntziachristos V. Multispectral photoacoustic imaging of fluorochromes in small animals. *Opt Lett.* 2007;32:2891-3.
- 88 Laufer J, Delpy D, Elwell C, Beard P. Quantitative spatially resolved measurement of tissue chromophore concentrations using photoacoustic spectroscopy: application to the measurement of blood oxygenation and haemoglobin concentration. *Phys Med Biol.* 2007;52:141-68.
- 89 Wang H-W, Chai N, Wang P, Hu S, Dou W, Umulis D, Wang LV, Sturek M, Lucht R, Cheng J-X. Label-Free Bond-Selective Imaging by Listening to Vibrationally Excited Molecules. *Physical Review Letters.* 2011;106:238106.
- 90 Lundberg B. Chemical-Composition and Physical State of Lipid Deposits in Atherosclerosis. *Atherosclerosis.* 1985;56:93-110.
- 91 Stegemann C, Drozdov I, Shalhoub J, Humphries J, Ladroue C, Didangelos A, Baumert M, Allen M, Davies AH, Monaco C, Smith A, Xu Q, Mayr M. Comparative lipidomics profiling of human atherosclerotic plaques. *Circ Cardiovasc Genet.* 2011;4:232-42.
- 92 Glatz J, Deliollanis NC, Buehler A, Razansky D, Ntziachristos V. Blind source unmixing in multi-spectral optoacoustic tomography. *Opt Express.* 2011;19:3175-84.
- 93 Rose FW. Quantitative analysis, with respect to the component structural groups, of the infrared (1 to 2 μ) molal absorptive indices of 55 hydrocarbons. *J. Res. Natl. Bur. Stand.* 1938;20:129.

- 94 Anderson RR, Farinelli W, Laubach H, Manstein D, Yaroslavsky AN, Gubeli J, Jordan K, Neil GR, Shinn M, Chandler W, Williams GP, Benson SV, Douglas DR, Dylla HF. Selective photothermolysis of lipid-rich tissues: A free electron laser study. *Lasers Surg Med.* 2006;38:913-9.
- 95 Nilsson AMK, Heinrich D, Olajos J, Andersson-Engels S. Near infrared diffuse reflection and laser-induced fluorescence spectroscopy for myocardial tissue characterisation. *Spectrochimica Acta Part A: Molecular and Biomolecular Spectroscopy.* 1997;53:1901-12.
- 96 Caplan JD, Waxman S, Nesto RW, Muller JE. Near-infrared spectroscopy for the detection of vulnerable coronary artery plaques. *J Am Coll Cardiol.* 2006;47:C92-6.
- 97 Jansen K, van Soest G, van der Steen T. Photoacoustic Imaging of Coronary Arteries: current status and potential clinical application. in *Coronary atherosclerosis: current management and treatment* (eds. Arampatzis, C, McFadden, EP, Michalis, LK, Virmani, R, Serruys, PW) 166-74 (Informa Healthcare, London, UK, 2012).
- 98 Hellings WE, Peeters W, Moll FL, Piers SR, van Setten J, Van der Spek PJ, de Vries JP, Seldenrijk KA, De Bruin PC, Vink A, Velema E, de Kleijn DP, Pasterkamp G. Composition of carotid atherosclerotic plaque is associated with cardiovascular outcome: a prognostic study. *Circulation.* 2010;121:1941-50.
- 99 Roggan A, Friebel M, Dörschel K, Hahn A, Müller G. Optical properties of circulating human blood in the wavelength range 400-2500 nm. *J Biomed Opt.* 1999;4:36-46.
- 100 Sawada T, Shite J, Garcia-Garcia HM, Shinke T, Watanabe S, Otake H, Matsumoto D, Tanino Y, Ogasawara D, Kawamori H, Kato H, Miyoshi N, Yokoyama M, Serruys PW, Hirata K-i. Feasibility of combined use of intravascular ultrasound radiofrequency data analysis and optical coherence tomography for detecting thin-cap fibroatheroma. *Eur Heart J.* 2008;29:1136-46.
- 101 Kubo T, Akasaka T. What is the optimal imaging tool for coronary atherosclerosis? in *Coronary atherosclerosis: current management and treatment* (eds. Arampatzis, C, McFadden, EP, Michalis, LK, Virmani, R, Serruys, PW) 250-8 (Informa Healthcare, London, UK, 2012).
- 102 Suh WM, Seto AH, Margey RJP, Cruz-Gonzalez I, Jang I-K. Intravascular Detection of the Vulnerable Plaque. *Circ Cardiovasc Imaging.* 2011;4:169-78.
- 103 MacNeill BD, Lowe HC, Takano M, Fuster V, Jang IK. Intravascular modalities for detection of vulnerable plaque - Current status. *Arterioscler Thromb Vasc Biol.* 2003;23:1333-42.
- 104 Maehara A, Mintz GS, Weissman NJ. Advances in intravascular imaging. *Circ Cardiovasc Interv.* 2009;2:482-90.
- 105 Schaar JA, van der Steen AF, Mastik F, Baldewsing RA, Serruys PW. Intravascular palpography for vulnerable plaque assessment. *J Am Coll Cardiol.* 2006;47:C86-91.

- 106 A.N.S.I. ANSI Z136.3 - American national standard for the safe use of lasers in health care. 2011
- 107 Van Mieghem CA, McFadden EP, de Feyter PJ, Bruining N, Schaar JA, Mollet NR, Cademartiri F, Goedhart D, de Winter S, Granillo GR, Valgimigli M, Mastik F, van der Steen AF, van der Giessen WJ, Sianos G, Backx B, Morel MA, van Es GA, Zalewski A, Serruys PW. Noninvasive detection of subclinical coronary atherosclerosis coupled with assessment of changes in plaque characteristics using novel invasive imaging modalities: the Integrated Biomarker and Imaging Study (IBIS). *J Am Coll Cardiol.* 2006;47:1134-42.

Summary

Cardiovascular diseases (CVDs) remain the largest cause of death worldwide. Of the 17 million deaths from CVDs in 2008, 7.3 million were caused by heart attacks. While in high-income countries deaths from CVDs have been declining over the past decades, low- and middle-income countries have seen a sharp increase. A large percentage of these deaths occurred before the age of 60. These premature deaths from CVDs reduce productivity and limit economic growth. Additionally, the health problems associated with CVDs pose a tremendous socio-economic burden on societies and can cause major suffering for those affected.

Although CVDs are preventable to a large extent, risk factors like older age and family history cannot be taken away. Therefore, heart attacks can never be entirely eliminated and percutaneous coronary interventions will continue to save the lives of many experiencing a heart attack. During this procedure, the clogged coronary artery is reopened and a stent is placed to keep it from closing again. Unplanned repeat interventions are often needed, however, and in half of the cases the symptoms are caused by restenosis of the treated lesion. This fact illustrates the necessity for improved intervention procedures and thus a better understanding of the underlying disease itself, called atherosclerosis.

The knowledge of the natural history of atherosclerosis and its causal relationship to cardiovascular events has increased enormously over the last decades. Was at one point calcification of the arteries believed to be the main wrongdoer, the current paradigm states that the rupture of a so-called vulnerable plaque lies at the origin of most heart attacks. The vulnerability of an atherosclerotic plaque – its susceptibility to rupture – is known to be related to the composition of the plaque, the distribution of mechanical stress within it, and the presence and extent of associated inflammation. One of the most common types of vulnerable plaques is the thin-cap fibroatheroma (TCFA). These lesions are characterized by a thin fibrous cap, weakened by the presence of macrophages (scavenger cells), covering a lipid-rich necrotic core. The necrotic core is the result of cell death inside a lesion by the accumulation of cholesterol species. It contains cell debris, cholesterol crystals and extracellular droplets of cholesterol esters. A concurring degradation of the supporting structure in the necrotic core enables its content to freely flow into the bloodstream upon rupture of the cap due to high stresses (high blood pressure). This necrotic core material is thrombogenic, which means that a blood clot will be formed upon contact with the blood and the artery can become clogged. When this happens in a coronary artery, the result will be a heart attack.

The development, up to rupture, of vulnerable atherosclerotic plaques is still only partially understood and their identification is a central issue in cardiac imaging. Intravascular imaging techniques play a major role in the study of these lesions, but

established techniques, such as intravascular ultrasound (IVUS) and optical coherence tomography (OCT), are unable to image plaque composition. They cannot positively identify and quantify lipid content, or distinguish between lipid types present in atherosclerotic plaques. To meet the need for plaque composition imaging in order to determine plaque vulnerability, we have developed a novel technique called intravascular photoacoustic imaging (IVPA). IVPA is a tool for plaque composition imaging that adds highly detailed chemical information to existing diagnostic techniques for coronary atherosclerosis.

IVPA relies on the detection of acoustic waves generated by the absorption of short (nanosecond) light pulses. The dissipation of the absorbed optical energy causes instantaneous local thermal expansion of the tissue, which generates a broadband acoustic wave. The acoustic signal can be detected using an ultrasound transducer (microphone) such as employed in IVUS. The distance between an optical absorber and catheter can be inferred from the elapsed time between the optical excitation and the detection of the acoustic signal, analogous to counting the time between seeing a lightning flash and hearing its thunder. In this way, depth resolution is provided. IVPA is special in this regard; other chemical diagnostic methods such as Raman spectroscopy and near-infrared absorption spectroscopy lack this ability to resolve depth. In IVPA, a cross-sectional image is created by rotation of a IVPA catheter inside the vessel. At every angle, a light pulse is sent and the acoustic signal generated in the vessel wall is recorded. A coronary artery can be investigated by performing a 'pullback': while rotating, the catheter is pulled back through the artery. IVPA image contrast depends on differences in optical absorption at the excitation wavelengths. Greater optical absorption results in greater thermal expansion and hence a stronger acoustic signal. Plaque composition can be probed if the optical absorption for the different constituents differs. Every biological molecule has an absorption spectrum, acting as a chemical fingerprint. By selecting the excitation wavelength(s) for maximum absorption contrast between relevant vessel wall components, such as collagen, calcified tissue, and lipid material, IVPA can identify plaque composition.

To date, lipids and calcification have been the primary targets of IVPA imaging, using endogenous contrast provided by the tissue absorption spectra. Considerable work has also been done on visualizing macrophages and matrix metalloproteinase activity, an indicator of plaque instability, using exogenous absorbers. However, many facets of real-time clinical imaging still need to be resolved. We have taken several essential steps in the direction of in vivo IVPA imaging.

Practical in vivo implementation of IVPA requires the development of a dedicated catheter device that is. Although many functioning combined IVPA/IVUS catheters have been demonstrated previously, their large diameter has prevented intravascular use in human coronary arteries. With an outer diameter of 1.25 mm, we created the first fully integrated IVPA/IVUS catheter that was small enough to be inserted into human

coronary arteries. An experimental combined PA and US system was built to assess the imaging characteristics of the catheters using dedicated phantoms (test models). The latest prototype has an outer diameter of 1 mm.

With these small experimental catheters it was possible to image human coronary arteries of deceased patients in a laboratory setting. For this purpose, we collected fresh human coronary arteries from autopsy, showing different stages of disease. Histopathology was performed on all measured arteries to corroborate our findings.

The data collected from the artery measurements were used to investigate several aspects of IVPA imaging to progress towards clinical application. Firstly, we demonstrated co-registered IVPA/IVUS imaging of lipids in human atherosclerotic coronary arteries. Spectroscopic IVPA (sIVPA) at different wavelengths around 1.2 μm , a lipid-specific absorption band, was performed to visualize the lipid content of an atherosclerotic lesion.

As lesions become more vulnerable, different cholesterol species accumulate in the plaque. We showed that IVPA can be used to distinguish between the most important lipid components of human atherosclerotic plaques, which can be used to study the development of atherosclerotic lesions.

To be useful in the clinic, as a research tool or to guide percutaneous coronary interventions, however, atherosclerotic lipid content information needs to be readily available without the need for observer-dependent and time-consuming image interpretation. We created methods to automatically detect and distinguish lipid types using as few as three wavelengths, making them applicable to an in vivo setting. These lipid detection methods successfully detected atherosclerotic lesion lipid content based on spectroscopic intravascular photoacoustic imaging data, in a semi-automated fashion and with high resolution.

sIVPA generally utilizes one of the two high absorption bands in the lipid absorption spectrum at 1.2 μm and 1.7 μm . Tradeoffs in terms of sensitivity, imaging depth, and possibly chemical specificity exist between the two spectral bands. We provided a direct comparison of sIVPA of human coronary arteries in these two spectral bands and found a superior atherosclerotic lipid detection performance at 1.7 μm , discrimination between plaque lipids and lipid deposits in peri-adventitial tissue was more successful at 1.2 μm .

The work presented in this thesis signifies several essential steps towards in vivo clinical IVPA imaging. Although many facets of real-time clinical imaging still need to be resolved, the contributions of this study to the field of IVPA, have moved the development of a real-time in vivo IVPA/IVUS system capable of imaging the lipid content of atherosclerotic plaques in clear view.

Samenvatting

Cardiovasculaire aandoeningen vormen wereldwijd doodsoorzaak nummer één. Van de 17 miljoen sterfgevallen die ze in 2008 veroorzaakten, waren er 7.3 miljoen het gevolg van een hartinfarct. Veel mensen overlijden al voor hun 60^{ste} levensjaar aan de gevolgen van cardiovasculaire aandoeningen. Deze vroegtijdige sterfte veroorzaakt een productiviteitsverlies en beperking van de economische groei. Bovendien vormen de bijbehorende gezondheidsproblemen een zware socio-economische belasting voor samenlevingen en de getroffen zelf.

Cardiovasculaire aandoeningen zijn voor een groot gedeelte te voorkomen door een gezonde levensstijl, maar risicofactoren als leeftijd en aanleg kunnen niet weggenomen worden. Hartinfarcten zullen dan ook nooit helemaal geëlimineerd kunnen worden en percutane coronaire interventies zullen de levens blijven redden van velen die een hartinfarct ondervinden. Tijdens deze dotterprocedure wordt de verstopte kransslagader geopend en wordt er een stent geplaatst om het vat open te houden. De symptomen komen helaas vaak terug en ongeplande herhaling van de behandeling is dan ook regelmatig nodig. In ongeveer de helft van de gevallen worden de symptomen veroorzaakt door een vernauwing op de behandelde locatie. Dit feit illustreert de noodzaak voor verbeterde interventieprocedures, waarvoor een beter begrip van de onderliggende aandoening, atherosclerose, nodig is.

Atherosclerose is een ontstekingsproces dat gekarakteriseerd wordt door de ophoping van vet, macrofagen, bindweefsel, gladde spiercellen en calcium in de vaatwand. Zo'n ophoping wordt een atherosclerotische plaque genoemd. De kennis over de ontwikkeling van atherosclerose en het oorzakelijk verband met het ontstaan van hartinfarcten is enorm toegenomen gedurende de laatste decennia. Werd op een bepaald moment nog gedacht dat calcificatie van de kransslagaders de belangrijkste boosdoener was, inmiddels weten we dat het scheuren van een kwetsbare plaque de oorzaak is van veruit het grootste deel van alle hartinfarcten. De kwetsbaarheid van een plaque wordt bepaald door de samenstelling, de verdeling van de mechanische belasting en de mate van ontsteking in de plaque. Het merendeel van deze kwetsbare plaques bestaat uit een vetrijke necrotische kern, bedekt met een dunne fibreuze kap, die verzwakt is door de aanwezigheid van macrofagen (afweercellen die dood celmateriaal en vet opruimen). De necrotische kern bestaat uit dood celmateriaal, cholesterol kristallen en druppels vloeibare cholesterolesters. Tijdens het ontstaan van deze necrotische kern vindt er een afbraak van de ondersteunende structuur plaats, waardoor bij scheuring van de kap als gevolg van hoge belasting (hoge bloeddruk) de inhoud vrij de bloedstroom in kan vloeien. Op het moment dat de inhoud van de plaque in contact komt met het bloed ontstaat er een bloedstolsel dat het vat kan afsluiten. Als dit in een kransslagader gebeurt, is een hartinfarct het gevolg.

De ontwikkeling van kwetsbare plaques tot aan het moment van scheuren, wordt nog maar gedeeltelijk begrepen en de identificatie van kwetsbare plaques is een centraal thema binnen de cardiologische beeldvorming. Intravasculaire technieken spelen een belangrijke rol bij het onderzoek naar deze plaques maar bestaande diagnostische technieken, zoals intravasculair ultrageluid (IVUS) en optische coherentie tomografie (OCT), kunnen de samenstelling van plaques niet in beeld brengen. Wij hebben een nieuwe techniek ontwikkeld, intravasculaire fotoakoestiek (IVPA), die plaque samenstelling in beeld kan brengen door gebruik te maken van het optische contrast tussen weefsels.

IVPA berust op de detectie van akoestische signalen die gegenereerd worden door de absorptie van korte (nanoseconde) lichtpulsen. De geabsorbeerde optische energie wordt omgezet tot warmte en veroorzaakt een kortstondige thermische uitzetting van het weefsel, wat vervolgens een akoestisch signaal genereert. Het akoestisch signaal kan gedetecteerd worden met een ultrageluid transducer (zender-ontvanger) zoals ook in IVUS gebruikt wordt. De afstand tussen het optisch absorberend weefsel en de transducer kan afgeleid worden uit de tijd tussen het plaatsvinden van de lichtpuls en het ontvangen van het akoestische signaal. Dit is vergelijkbaar met het bepalen van de afstand van een bliksemflits door middel van het tellen van de tijd tot je de donder hoort. Op deze manier wordt diepteresolutie gecreëerd, zodat 3D plaatjes van de vaatwand gemaakt kunnen worden. IVPA is bijzonder in dit opzicht: andere diagnostische methodes die de plaque samenstelling kunnen meten, zoals Raman spectroscopie en nabij-infrarood absorptie spectroscopie, hebben geen diepteresolutie. In IVPA wordt een dwarsdoorsnede-afbeelding van een vat gemaakt door middel van de rotatie van een IVPA katheter binnen in het vat. In iedere richting wordt een lichtpuls verzonden en het gegenereerde akoestisch signaal opgenomen. Een kransslagader kan in zijn geheel in beeld gebracht worden door de katheter al roterend door het vat te verplaatsen. Het contrast in IVPA beelden hangt af van de verschillen in de absorptie van het licht bij de golflengte die gebruikt wordt. Meer optische absorptie zorgt voor grotere thermische expansie en dus een sterker akoestisch signaal. Plaque samenstelling kan bepaald worden wanneer de optische absorptie van de aanwezige bestanddelen van elkaar verschilt. Elk biologisch molecuul heeft zijn eigen absorptiespectrum dat als chemische vingerafdruk dient. Door lichtgolflengtes te kiezen die maximaal absorptiecontrast tussen de verschillende weefseltypen geven, kan met IVPA de plaque samenstelling in beeld gebracht worden.

De nadruk bij IVPA onderzoek heeft tot nu vooral gelegen op het visualiseren van vetten en calcium in atherosclerotische plaques. Ook macrofagen en andere ontstekingsfactoren zijn met IVPA in beeld gebracht. Veel aspecten van de klinische real-time implementatie IVPA zijn echter nog onbekend. Het doel van dit onderzoeksproject was het nemen van verscheidene essentiële stappen op de weg naar de klinische toepassing van IVPA.

Voor de praktische uitvoering van IVPA is de ontwikkeling van een speciaal katheter noodzakelijk. Hoewel al verscheidene goed functionerende combinatie IVPA/IVUS katheters geproduceerd zijn, verhinderde hun grote omvang intravasculair gebruik in menselijke kransslagaders. Wij hebben de eerste IVPA/IVUS katheter vervaardigd die, met een buitendiameter van 1.25 mm, klein genoeg is om in menselijke kransslagaders in te brengen. Verdere miniaturisatie heeft een prototype katheter opgeleverd met buitendiameter van slechts 1 mm. Met deze katheters, in combinatie met een zelfgebouwd experimenteel beeldvormingssysteem, hebben we intravasculaire metingen verricht in menselijke kransslagaders van overleden patiënten. We hebben histopathologie van de gemeten vaten gebruikt als controlemeting.

Met de data van deze experimenten hebben we verschillende aspecten van de klinische applicatie van IVPA onderzocht. Allereerst hebben we het vet in een atherosclerotische plaque in beeld gebracht, door gebruik van licht van verschillende golflengten rond 1.2 μm , waar zich een grote piek in het absorptiespectrum van vetten bevindt.

Naarmate plaques kwetsbaarder worden, verandert ook de samenstelling van de aanwezige vetten. Wij hebben aangetoond dat met IVPA de belangrijkste vetcomponenten van menselijke plaques in beeld gebracht kunnen worden. Deze mogelijkheid kan gebruikt worden om de ontwikkeling van atherosclerotische plaques te bestuderen.

Voor de klinische toepassing van IVPA als onderzoeksinstrument of als hulpmiddel bij dotterprocedures, moet de informatie over de vetinhoud van plaques direct beschikbaar zijn, zonder dat waarnemer-afhankelijke en tijdrovende beeldinterpretaties nodig zijn. Wij hebben methodes ontwikkeld waarmee de vetten automatisch opgespoord kunnen worden en waarmee bovendien vetten in plaques van andere in de vaatwand aanwezige vetten onderscheiden kunnen worden.

IVPA gebruikt doorgaans licht met een golflengte van rond de 1.2 μm of 1.7 μm . Tussen deze twee golflengtegebieden zien we verschillen in gevoeligheid voor vetten, de diepte waarop we de vetten nog kunnen zien en de mogelijkheid om verschillende vetten van elkaar te onderscheiden. We hebben een directe vergelijking gemaakt door het meten van menselijke kransslagaders in beide golflengtegebieden en vonden een superieure vetdetectie met IPVA rond 1.7 μm , terwijl plaque vetten beter van andere vetten te onderscheiden waren met IVPA rond 1.2 μm .

Het werk dat in dit proefschrift gepresenteerd wordt, vertegenwoordigt verscheidene essentiële stappen in de richting van de klinische toepassing van IVPA. Hoewel veel facetten van klinisch gebruik nog uitgewerkt moeten worden, heeft dit werk de ontwikkeling van een real-time klinisch IVPA/IVUS systeem waarmee atherosclerotische vetten automatisch gedetecteerd kunnen worden aanzienlijk dichterbij gebracht.

Acknowledgements

I remember clearly the phone conversation I had with my very good friend Saskia, some five and a half years ago. I was trying to arrange a smooth exit from Texas, where I had resided for nearly five years, and at the same time was planning my 'come back' to the Netherlands. Honestly though, I didn't have a clue as to what it would look like. I only knew I was bringing back two dogs, two bikes, a chair and a couple of boxes filled with paperwork. During that last summer in Texas, I was moving from one house to the next, taking care of people's dogs or roses or whatever needed taking care of. Seated in the study of one of these temporary homes, I was on the phone with Saskia, going through my options. She pointed this website out to me, academictransfer.com, and while we were still talking, my eye fell on a PhD position that attracted my attention. I sent out a letter of interest immediately and had my first job interview over the phone not long after that, from my last Texas home. The second job interview took place one day after my arrival back in the Netherlands and after still another interview I was called by Ton van der Steen who told me I'd gotten the job.

Therefore, since this story started with you, Saskia, I would like to begin my list of acknowledgements by thanking you. With your never ending optimism and unlimited enthusiasm, you were able to cheer me up and motivate me enough to apply for this job during these hard and sometimes desperate times.

Nicole and Kees, I thank you for inviting me - and the dogs! - to stay with you in Eindhoven on my return from the States. You gave me the much needed base from which I could organize my life again. Nicole, your loyal and considerate friendship has been a much appreciated support and solace. I look forward to our snow walking adventure in the Vogues coming winter.

Ton, Gijs, Nico, thank you for having confidence in my abilities or at least being willing to give me the opportunity to show them, despite my lack of experience in the field of biomedical sciences and my less than easy to interpret cv. Ton, you have been the best boss I have ever had the pleasure to work for (with)! Your kindheartedness and generosity have made me feel very welcome from the start and gave me the confidence to start this project on unknown territory and see it through to the end. You've also shown me what it takes to be the leader of a successful research group.

Gijs, your guidance has been indispensable. I was lucky enough to be your first PhD student and therefore receive your undivided attention for the first period of my promotion time. Without your help and seemingly unlimited knowledge and comprehension of just about any subject matter, I wouldn't have known where to begin. Photoacoustics was an enigma to me and even though you would sometimes get a bit impatient with my ignorance, you gave me the liberty and trust to figure out things for myself. When I landed my new job a little sooner than ideally desirable, you supported

me every step of the hurried way to make sure my PhD would come to a good end. Thank you for your guidance, support, trust and, not least of all, good company. You told me once you wanted to make sure I would 'land well' after my PhD and I think we both agree I did. I am very happy to have gotten to know you and your lovely wife, Suze, and kids, Jasper and Loekie and hope to keep in touch!

Pieter, it pains me to know that I will never have a colleague like you again! How often in your life do you get a colleague that sings every (every!!) day, writes you in his self-made lyrics, is always cheerful and enthusiastic, is interested in your work and wellbeing, will give you his worthy advice, wants to work together with you, alternately teases and engages you in good conversation and keeps you the best possible company at conferences. To top it all off, you and your beautiful wife Grethe have taken care of my dogs on numerous occasions and continue to do so, even now we don't see each other on a regular basis anymore, and even though you hate the hair! Thank you for being my friend Pieter, you are one of the most colorful people I know.

Min, I have to admit that when you just arrived, I didn't know what to do with you. I was so used to working by myself and most of the time completely independently and suddenly I had somebody that looked over my shoulder with everything I did. It took me one week to realize you weren't going to go away and that we were going to work together from then on. Ever since that moment of realization, I've been so happy to have you on my team! You are an eager and quick learner and your input and help has been invaluable. With your knowledge of image processing you solved one of the biggest problems I was dealing with during the project: you got rid of the rings! But more importantly, you've become a dear friend and your good company has made my work so much more enjoyable. I'm happy and proud that you will be continuing the project and hope to see much more of you, Han and Tessie.

Next, I get to the other members of the 'laser lab'/'cave'/22nd floor, of course. Tianshi and Muthu, I would like to thank you for your kindness and friendliness, invitations to your home (Muthu, it will happen!), discussions on feminist issues, and bringing the Asian vibe, and food, to our little annex on the 22nd floor. With every new arrival, our lab was getting more Asianized and with that, more and more enjoyable. Thank you for good times, in and out of the lab!

Next, I would like to thank Geert, who has been one of the driving forces behind the project. He built every catheter that I used and almost every part of the setup that I needed to use them with. Geert, it's thanks to your handiness and skills and not in the least your interest for the project that I was able to produce those price-winning images; you consistently told me you did not have time to satisfy my often last-minute requests but invariably managed to do them anyway. Thank you for all your help and the ever enjoyable times we spent working together!

Ali, we started and finished approximately at the same time and got to spend quite some time together, mostly revolving around coronary arteries: coronary collection from

the morgue, coronary imaging, coronary freezing and coronary searches. I've always enjoyed these times we spent working together. I wish you an enjoyable and successful time in Atlanta!

Robert, I would like to thank you for your help with all the electrical issues on, and off, the project. For helping me with painting the walls of my house and sharing your knowledge about gas heaters, earth spikes and circuit breakers, and always thinking of my dogs when you make pea or ox tail soup!

I want to express my appreciation for all the help I received on the project from so many people: Heleen van Beusekom, Gerrit van Dijk, Jaap Slooff and Jaap Bogers, Marguerite Schipper, all the autopsy assistants - in particular Ariadne Ooms and Britt Blokker - Rorry van Haeren, Kim Kuijt - van Gaalen, Richard van Duin, Michiel Manten, Monique Mulder and Adrie Verhoeven, Karin Witberg and Jurgen Ligthart, Annemarie Visscher and Antony van Dijk, Wijnand den Dekker, Anouk van Dijk and Stijn van den Oord, and Peter Burgers and Theo Luider. I enjoyed working together with you and even though our joint efforts have not always generated publishable results, your contributions have been invariably insightful and highly appreciated.

Guillaume, Marcia, Telli, Enrico, thank you for all the good times we shared. You were good company in the lab and on many outings, including our 'extra labuitje' to Paris. I hope we will meet again soon, preferably in one of the world's nicest cities, like Paris or Lille.

Special thanks go out to the lab's permanent team: Frits, Gerard, Charles, Jan, Hans Verdoes, Hans Bosch and especially Mieke en Gracia. Without all of your efforts and dedication, none of the PhD student's work would ever see the light of day. Mieke, Gracia, I would like to thank you especially for your dedication, helpfulness and kindness. Your presence has always illuminated the lab!

I would also like to thank Varya, Alex, Ilya, Ying, Zeynettin, Jacopo, Kim, Lambert, Frank, Jolanda, Esther, Egon, Sandra, Rick and all the other members and former members of the Biomedical Engineering team for being great colleagues and making my time in the group a very enjoyable one.

I thank the people of ICIN - Netherlands Heart Institute for welcoming me in their team and supporting me at a distance.

To my very kind and supportive neighbors, Liesbeth en Rogier, Maaïke, Maaïke en Wouter, Arnoud, and ex-neighbor Marcel I would like to say: thank you for your good company and the occasional burden relieve, such as dog walking and cooking. It's very true what they say: een goede buur is beter dan een verre vriend! I would like to add to that: Zonder Noorden geen thuis!

Then, obviously, my dear friends, who stood by me, supported me and have given me so much joy throughout the Eindhoven decade, the Texas years and during my time in Rotterdam: Claudia, Erik and Dieuwertje, who's house, tent and hearts are always open for me and whomever I choose to bring - mostly the dogs and David; Anne, with whom

I spent so much of my Eindhoven study time, including a thrilling and adventurous time in Thailand (apparently we were together so much that people were unable to keep us apart, even though we don't look alike); Saskia, who I've mentioned already but whose bubbling personality deserves another mention; Bregje, Tamara, Stefan, Claartje, Suzanne, Roosje, Mark B., Mark F., other circuit 500 members, Alain, my Rotterdam bff and movie buddy, and many more: you've all been there for me and stayed in touch despite the long distance. Many of you even managed to come and visit me in Texas! Thank you all for everything!

Bruno, Jacqueline, Poutchett, Marie, Hadrien: je tiens à vous remercier de m'avoir accueilli si chaleureusement dans votre famille. J'apprécie les moments que je passe avec vous à Paris, à Rotterdam où ailleurs !

Cindy, Frank and Charley, Erwin, Magda, Jaya and Binh, Arwen and Bregit, lieve familie, it is so nice to be close to you again! Thank you for all your love and support, far away and close by. Cindy, we were so close growing up, you were my best friend and partner in crime. We have since gone our own separate ways that necessarily enlarged the distance between us. I'm happy that we now live in the same city and get to spend more time together again. Our weekly yoga outings have been very enjoyable and I miss them already! Erwin, the best brother a girl can have. We've had so many good times together: living together, playing soccer, running, making plans for our future businesses. You even came to visit me twice in Texas, or was it three times? We would talk about you moving there too so we could go mountain biking, wakeboarding and, of course, start a business together! Instead I moved back home and you married Magda, who's company I enjoy enormously, and got two wonderful daughters. Jaya and Binh, you've lightened up my life! Jaya, I hope we always stay such close friends and have so much fun together, and Binh, I hope you always keep that gorgeous and mischievous sparkle in your eyes.

Arwen, I would like to thank you especially for your help on the shaping of this thesis. Without it, it wouldn't have looked half as nice!

Bregit, my big sister. When we were little, you always took me by the hand and I just followed you wherever you would go. You've always been so wonderfully sane and mature; I guess we've been opposites in almost every possible way but despite, or maybe because of that, we've always been close and have had a lot of good times together. I would like to thank you especially, for all help you've given me upon my return from Texas with just about anything: finding a good place to live for me and my dogs, finding the furniture to put in it, coming to walk my dogs and cook for me whenever I was sick, and not to forget all the moral support that I needed so badly just after coming back to the Netherlands.

Papa en mama, you have been there for me always and your loving care and encouragement have gotten me through so many things in life. You surely taught me to hold on and keep going when the going gets rough. I know I certainly haven't been easy

to handle those pubescent years and I've not always made it easy for you to keep believing in me but I hope I made you proud at times too. Thank you for your immense support when I was far away from home and needing it so much. Your determination to visit me yearly meant so much to me! And thank you also for your continued support now that I'm closer to home again. I'm very happy to be able to see you much more often than the two times a year!

Pavlov en Harriet, my Texan mums: you've provided me with an unlimited supply of love and good company, warm welcomes when I come home, earfuls of howling, and a countless number of good walks in the countryside; I hope you will continue to do so until...forever.

Finally, of course, David. You're my new found happiness. I simply don't know what else to say, except: thank you bébé, for being by my side (or, at least, just a train trip away). I love you.

Curriculum Vitae



Krista Jansen was born in Sint-Oedenrode on July 25, 1974. She received her primary education at de Havelt, Handel after which she followed her secondary education went at the Macropedius College, Gemert.

She earned a Master of Science degree in International Technological Development at the University of Technology Eindhoven in December 2001. During her studies, she was active in many student clubs, such as Mechanical Engineering for Society (WenS), Eindhoven Student Syndicate (ESVB), Environmental Platform (Milieuplatform), and Pusphaira, the student soccer team. She also spent a semester studying at Worcester Polytechnic Institute, Massachusetts and carried out an extracurricular internship in Khok Mo, Thailand, on industrial development of rural areas. She conducted her final project in Bandung, Indonesia, on the performance of the Indonesian oil refining industry. Health problems unfortunately prevented her from pursuing her dream: technology transfer and management in development countries. Undauntedly, she embarked on a string of adventures closer to home (bicycle messenger, bartender, waitress, assembly employee at DAF trucks, mail and pizza deliverer, among others), culminating in a management traineeship at Prorail, the Dutch railroad company.

She emigrated to Denton, Texas to live with her boyfriend and tried her luck working as a middle and high school teacher but decided soon to start studying again and obtained her Master of Science degree in Physics in December 2007 at the University of North Texas. She worked as a physics teacher at the same university for a semester before returning to the Netherlands in September 2008, where she joined the Thorax Center Department of Biomedical Engineering of the Erasmus University Medical Center in Rotterdam to carry out her PhD work on 'Intravascular photoacoustics' under the supervision of Gijs van Soest and Antonius F. W. van der Steen.

As of August 2013, she is working at the Audiology Center of VU University Medical Center Amsterdam as a medical physicist-audiologist in training.

Publications

Articles

K. Jansen, A.F.W. van der Steen, H.H.M. van Beusekom, J.W. Oosterhuis, G. van Soest, **Intravascular photoacoustic imaging of human coronary atherosclerosis**, *Optics Letters* 36(5):597-9 (2011).

D. Maresca, K. Jansen, G. Renaud, G. van Soest, X. Li, Q. Zhou, N. de Jong, K.K. Shung, A.F.W. van der Steen, **Intravascular ultrasound chirp imaging**, *Applied Physics Letters*, 100 043703-043703 (2012).

K. Jansen, M. Wu, A.F.W. van der Steen, G. van Soest, **Lipid detection in atherosclerotic human coronaries by spectroscopic intravascular photoacoustic imaging**, *Optics Express*, 21 21472-21484 (2013).

K. Jansen, M. Wu, A.F.W. van der Steen, G. van Soest, **Intravascular photoacoustic imaging: a new tool for vulnerable plaque identification**, *UMB, in print*.

K. Jansen, M. Wu, A.F.W. van der Steen, G. van Soest, **Comparison of spectroscopic photoacoustic imaging of human coronary atherosclerosis in two spectral bands**, *submitted*.

K. Jansen, A.F.W. van der Steen, M. Wu, H.M.M. van Beusekom, G. Springeling, X. Li, Q. Zhou, K.K. Shung, D.P.V. de Kleijn, G. van Soest, **Spectroscopic intravascular photoacoustic imaging of lipids in atherosclerosis**, *submitted*.

D. Maresca; I. Skachkov; G. Renaud; K. Jansen; G. van Soest; N. de Jong; A.F.W. van der Steen, **Imaging microvasculature with contrast-enhanced ultraharmonic ultrasound**, *submitted*.

Book chapter

K. Jansen, G. van Soest, A.F.W. van der Steen, **Photoacoustic imaging of coronary arteries: current status and potential clinical application**, in: C. Arampatzis, E.P. McFadden, L.K. Michalis, R. Virmani, P.W. Serruys (Eds.) *Coronary atherosclerosis: current management and treatment*, Informa Healthcare, London, UK, pp. 166-174 (2012).

Conference presentations

K. Jansen, G. Springeling, C. Lancee, R. Beurskens, F. Mastik, A.F.W. van der Steen, G. van Soest, **An intravascular photoacoustic imaging catheter**, *Proceedings of the 2010 IEEE International Ultrasonics Symposium (IUS)*, 378-381 (2010).

A.F.W. van der Steen, G. van Soest, M. Emmer, D. Maresca, K. Jansen, F. Mastik, P.W. Serruys, E. Regar, **Intravascular ultrasound: Assessment of atherosclerosis**, *Proceedings of the 2010 IEEE International Symposium on Biomedical Imaging: From Nano to Macro*, 281-281 (2010).

K. Jansen, A.F.W. van der Steen, G. Springeling, H.M.M. van Beusekom, J.W. Oosterhuis, G. van Soest, **Intravascular photoacoustic imaging of human coronary atherosclerosis**, *2011 SPIE Photonics West conference, Bios - Proceedings of SPIE 7899, Photons Plus Ultrasound: Imaging and Sensing 2011*, 789904-789907 (2011).

D. Maresca, K. Jansen, G. Renaud, W. Den Dekker, G. van Soest, X. Li, Q. Zhou, J. Cannata, K.K. Shung, A.F.W. van der Steen, **Intravascular ultrasound chirp imaging**, *Proceedings of the 2011 IEEE International Ultrasonics Symposium (IUS)*, 2110-2113 (2011).

K. Jansen, A.F.W. van der Steen, H.M.M. van Beusekom, J.W. Oosterhuis, G. van Soest, **Intravascular photoacoustic imaging of human coronary atherosclerosis**, *SPIE/OSA European Conferences on Biomedical Optics (ECBO) 2011, Conference 8090: Novel Biophotonic Techniques and Applications*, 8090-18 (2011).

K. Jansen, A.F.W. van der Steen, H.M.M. van Beusekom, J.W. Oosterhuis, G. Springeling, F. Mastik, G. van Soest, **Automatic lipid detection in human coronary atherosclerosis using spectroscopic intravascular photoacoustic imaging**, *2012 SPIE Photonics West conference, Bios, Proceedings of SPIE Vol. 8207: Diagnostic and Therapeutic Applications of Light in Cardiology*, 8207E-93 (2012).

K. Jansen, A.F.W. van der Steen, H.M.M. van Beusekom, J.W. Oosterhuis, G. Springeling, G. van Soest, **Intravascular photoacoustic imaging of lipids in human coronary atherosclerosis**, *EuroPCR* (2012).

K. Jansen, A.F.W. van der Steen, H.M.M. van Beusekom, G. Springeling, M. Wu, F. Mastik, G. van Soest, **Automatic lipid detection in human coronary atherosclerosis using spectroscopic intravascular photoacoustic imaging**, *Proceedings of the 2012 IEEE International Ultrasonics Symposium (IUS)*, 32-35 (2012).

K. Jansen, A.F.W. van der Steen, G. Springeling, M. Wu, A.J.M. Verhoeven, M.T. Mulder, X. Li, Q. Zhou, K.K. Shung, D.P.V. de Kleijn, G. van Soest, **Differentiating lipid types using intravascular photoacoustic spectroscopy**, *2013 SPIE Photonics West conference, Bios, Proceedings of SPIE Vol. 8581: Photons plus Ultrasound: Imaging and Sensing 2013*, 8581-10 (2013).

K. Jansen, A.F.W. van der Steen, H.M.M. van Beusekom, M. Wu, G. Springeling, G. van Soest, **Spectroscopic Intravascular Photoacoustic Imaging Visualizes Cholesterol Species In Human Coronary Atherosclerosis**, *SPIE/OSA European Conferences on Biomedical Optics (ECBO) 2013, Opto-Acoustic Methods & Applications: Novel Applications II*, ES4B.5 (2013).

Invited talks

K. Jansen, A.F.W. van der Steen, G. Springeling, H.M.M. van Beusekom, J.W. Oosterhuis, G. van Soest, **Intravascular photoacoustic imaging of coronary atherosclerosis**, *Optics in Cardiology*, Rotterdam, The Netherlands (2011).

K. Jansen, A.F.W. van der Steen, G. Springeling, H.M.M. van Beusekom, J.W. Oosterhuis, G. van Soest, **Intravascular photoacoustic imaging of coronary atherosclerosis**, *Sound Light – Photons for Health symposium*, Twente University of Technology, Enschede, The Netherlands (2011).

K. Jansen, A.F.W. van der Steen, M. Wu, H.M.M. van Beusekom, G. Springeling, T.M. Luider, P.C. Burgers, D.P.V. de Kleijn, G. van Soest, **Intravascular photoacoustic spectroscopy**, *Optics in Cardiology*, Rotterdam, The Netherlands (2013).

Awards

Poster Award

A hybrid photoacoustic and ultrasonic catheter for intravascular imaging, *Gordon Research Conference, Lasers in Medicine and Biology*, Holderness School New Hampshire, Gordon, NH, USA, (2010).

Best Oral Paper Award, 1st Prize

K. Jansen, A.F.W. van der Steen, G. Springeling, H.M.M. van Beusekom, J.W. Oosterhuis, G. van Soest, **Intravascular photoacoustic imaging of human coronary atherosclerosis**, *2011 SPIE Photonics West conference, Bios - Proceedings of SPIE 7899, Photons Plus Ultrasound: Imaging and Sensing 2011*, 789904-789907 (2011).

Toptica Best Student Paper Award, 1st Prize

K. Jansen, A.F.W. van der Steen, H.M.M. van Beusekom, J.W. Oosterhuis, G. van Soest, **Intravascular photoacoustic imaging of human coronary atherosclerosis**, *SPIE/OSA European Conferences on Biomedical Optics (ECBO) 2011, Conference 8090: Novel Biophotonic Techniques and Applications*, Munich, Germany, 8090-18 (2011).

PhD Portfolio

International conference attendance	Date	ECTS
Biomechanics in Vascular Biology and Cardiovascular Disease symposium, Rotterdam, The Netherlands	04/2009	0.60
Fotonica evenement 2009, Nieuwegein, The Netherlands	04/2009	0.30
European Conference on Biomedical Optics 2009, Munich	06/2009	1.20
Vulnerable Plaque Meeting 2009 Vougliagmeni, Athens, Greece	06/2009	0.90
2009 IEEE International Ultrasonics Symposium (IUS), Rome, Italy	09/2009	1.20
15th European Symposium on Ultrasound Contrast Imaging, Rotterdam, The Netherlands	01/2010	0.60
Vulnerable Plaque Meeting 2010, Cascais, Portugal	06/2010	1.20
Lasers In Medicine & Biology, 2010, Gordon Research Conferences, Holderness, USA	07/2010	1.80
2010 IEEE International Ultrasonics Symposium, San Diego, CA, USA	10/2010	1.20
2011 BiOS, SPIE Photonics West, San Francisco, USA	01/2011	1.80
European Conference on Biomedical Optics 2011, Munich	05/2011	1.50
2011 Optics in Cardiology, Rotterdam, The Netherlands	12/2011	0.60
2012 BiOS, SPIE Photonics West, San Francisco, USA	01/2012	1.80
EuroPCR 2012, Palais des Congrès, Paris, France	05/2012	0.90
Lasers In Medicine & Biology, 2012, Gordon Research Conferences, Holderness, USA	07/2012	1.80
2012 IEEE International Ultrasonics Symposium, Dresden, Germany	10/2012	1.20
2013 BiOS, SPIE Photonics West, San Francisco, USA	02/2013	1.80
2013 Optics in Cardiology, Rotterdam, The Netherlands	03/2013	1.00

Conference presentations	Date	ECTS
Oral presentation - 2010 Dutch Society for Medical Ultrasound meeting	05/2010	1.00
Poster presentation - 2010 Lasers In Medicine & Biology, Gordon Research Conferences (GRC)	07/2010	1.00
Oral presentation - 2010 IEEE International Ultrasonics Symposium	10/2010	1.90
Oral presentation - 2011 BiOS, SPIE Photonics West conference	01/2011	1.90
Oral presentation - 2011 European Conference on Biomedical Optics	05/2011	1.90
Oral presentation - SoundLight -- Photons for Health symposium	11/2011	0.70
Oral presentation - 2010 Optics in Cardiology symposium	12/2011	1.00
Oral presentation - 2012 BiOS, SPIE Photonics West conference	01/2012	1.90
Oral presentation - EuroPCR 2012	05/2012	0.70
Poster presentation - Lasers In Medicine & Biology, GRC	07/2012	1.60
Oral presentation - 2012 IEEE International Ultrasonics Symposium	10/2012	1.90
Oral presentation - 2013 BiOS, SPIE Photonics West conference	02/2013	1.90
Oral presentation - 2013 Optics in Cardiology symposium	03/2013	1.80

Courses	Date	ECTS
Piezoelectric Ultrasound Transducer Fundamentals, 2009 IEEE IUS	09/2009	0.15
Time Reversal Acoustics, 2009 IEEE IUS	09/2009	0.15
Pathophysiology of ischemic heart disease, COEUR postgraduate school	10/2009	1.50
Medical Imaging-1: Principles, Radiology & Ultrasounds, 2009 ESMP	10/2009	1.80
Medical Imaging-2: Magnetic Resonance, PET & SPECT, 2009 ESMP	10/2009	1.80
4 th Animal Imaging Workshop, AMIE postgraduate school	02/2010	0.75
Photo-acoustic Imaging and Sensing, 2010 IEEE IUS	10/2010	0.15
Estimation and Imaging of Tissue Motion and Blood Velocity, 2010 IEEE IUS	10/2010	0.15
Tissue Optics, 2011 BiOS, SPIE Photonics West	01/2011	0.15
Photoshop and Illustrator Workshop, MolMed postgraduate school	02/2011	0.30
In-Design Workshop, MolMed postgraduate school	05/2011	0.20
ICIN-Netherlands Heart Institute PhD Student Masterclass	09/2011	0.55
Ultrafast Ultrasound Imaging: Principles and Applications, 2012 IEEE IUS	10/2012	0.15
Minicursus Methodologie van Patiëntgebonden Onderzoek en Voorbereiding van Subsidieaanvragen, congresbureau, Erasmus MC	02/2012	0.30

Research Seminars	Date	ECTS
Dutch Society for Medical Ultrasound meeting, Rotterdam, The Netherlands	05/2009	0.15
Dutch Society for Medical Ultrasound meeting, Twente, The Netherlands	04/2010	0.15
STW Year Congress 2010, Nieuwegein	10/2010	0.30
COEUR Research Seminar: Imaging of Atherosclerosis	12/2010	0.40
Symposium: Acute Myocardial Infarction: the next decade, Erasmus MC, Rotterdam	12/2010	0.30
COEUR Research Seminar: Detection of early atherosclerosis	03/2011	0.40
COEUR Research Seminar: The First Erasmus MC Meeting of the Interdisciplinary Working Group on Healthy Aging	04/2011	0.15
COEUR PhD-day 2011	04/2011	0.40
SoundLight - Photons for Health, symposium University of Twente	11/2011	0.30
COEUR Research Seminar: Biomarkers in Cardiovascular Disease	09/2012	0.40
COEUR lecture: Human Smooth Muscle Cell Heterogeneity-from bedside to CALM(odulin)	10/2012	0.10

Total ECTs: 51.75